Mobilization and Displacement of Residual Oil by means of Chemical Enhanced Oil Recovery Processes

Al Saadi, Faisal

DOI
10.4233/uuid:cf7fe485-1ef1-426a-bfa1-7925ef11394c

Publication date
2019

Document Version
Final published version

Citation (APA)
Al Saadi, F. (2019). *Mobilization and Displacement of Residual Oil by means of Chemical Enhanced Oil Recovery Processes*. [Dissertation (TU Delft), Delft University of Technology].
https://doi.org/10.4233/uuid:cf7fe485-1ef1-426a-bfa1-7925ef11394c

Important note
To cite this publication, please use the final published version (if applicable).
Please check the document version above.

Mobilization and Displacement of Residual Oil by means of Chemical Enhanced Oil Recovery Processes

Dissertation

for the purpose of obtaining the degree of doctor

at Delft University of Technology

by the authority of the Rector Magnificus, Prof.dr.ir. T.H.J.J. van der Hagen,

chair of the Board for Doctorates

to be defended publicly on

Wednesday 30, October 2019 at 12:30 o'clock

by

Faisal Salim Hamed AL SAADI

Master of Science in Petroleum Engineering, Heriot-Watt University, United Kingdom

Born in Rustaq, Sultanate of Oman

This dissertation has been approved by the promotors:

Prof. Ir. C.P.J.W. van Kruijsdijk

Dr. K-H.A.A. Wolf

Composition of the doctoral committee:

Rector Magnificus,	chairperson
Prof. Ir. C.P.J.W. van Kruijsdijk,	Delft University of Technology, promotor
Dr. K-H.A.A. Wolf,	Delft University of Technology, promotor

Independent members:

Dr.ir. D.W. van Batenburg	Shell Global Solutions International
Prof.dr.ir. T.J. Heimovaara	Delft University of Technology
Prof.dr. C.J. Spiers	U-Utrecht
Prof.dr.ir. H.E.J.G. Schlangen	Delft University of Technology
Prof.Dr. K.K. Mohanty	University of Texas at Austin
Prof.dr. W.R. Rossen	Delft University of Technology, reserve member

Propositions

Accompanying the thesis:

Mobilization and Displacement of Residual Oil by means of Chemical Enhanced Oil Recovery Processes

1- Fontainebleau sandstone reveals homogeneity in its texture and mineralogy due to its pure composition. However, in low porosity ($\varphi < 0.08$) samples, quartz overgrowth has a significant impact on fluid flow by reducing pore-throat diameter. The tortuosity increases because the pore throat cementation has a considerable larger spatial effect than pore lining type of cementation which results in reducing the average coordination number.

2- We must question the scientific conclusions that are drawn based on two or three experiments, while the reproducibility is not confirmed. In the worst case, a significant fraction of the literature will disappear. Hence, experiments must be reproducible, so as to distinguish between data that provide meaningful insights into the dynamics of the build-up of oil banks and those that represent statistical anomalies or flaws in an experimental design.

3- In the literature, there is no clear definition or urgency of building the oil bank. We define the oil bank as a continuous volume of mobilized oil that forms from the coalescence of mobilised oil ganglia. Once developed, the dimensions of the oil bank extend during its movement through a porous medium.

4- Building a stable oil bank supports the efficiency of the chemical enhanced oil recovery (EOR) process, as oil in microemulsion form is minimised. This is of significant advantage to the surface facility in the producing field, as oil in emulsion can interfere with the facility's process.

5- Surfactant flooding without polymer must not be pursued as a chemical-enhanced oil recovery process for oil-field application.

6- In the surfactant-polymer-enhanced oil recovery method, residual oil can be produced without the need for building an oil bank.

7- The mobility of oil is greater (i.e. oil production is accelerated) when it is produced from a connected oil bank rather than from a dispersed flow as an emulsion. This has a positive impact on the revenue (net present value) of the chemical EOR process.

8- Core-flow experiments are an easy way of excluding successful chemical EOR methods.

9- There is no (and there will be no) final conclusions in the scientific world. "All Knowledge is provisional, temporary, capable of refutation at any moment, "KarlPopper"

10- A PhD thesis addressing the topic of fluid flow in porous media without a chapter on the characterisation of the porous media is like a tree without roots.

11- The Netherlands, and specifically Amsterdam, is an example of a multicultural society. The entire world will one day be represented by multicultural societies in which everyone's culture is accepted without one feeling like one's own has been compromised.

These propositions are regarded as opposable and defendable, and have been approved as such by promotors, Prof. Ir. C.P.J.W. van Kruijsdijk and Dr. K-H.A.A. Wolf.

Stellingen

Bijgaand het proefschrift:

Mobilization and Displacement of Residual Oil by means of Chemical Enhanced Oil Recovery Processes

(Or in dutch)

De dynamiek van de opbouw van een oliebank bij injectie van oppervlakte-actieve-stoffen en polymeer

1- De Fontainebleau zandsteen toont homogeniteit in zijn textuur en mineralogie dankzij zijn pure samenstelling. Maar, bij lage porositeit ($\varphi < 0.08$) heeft kwartsgroei een significante invloed op de stroming van vloeistoffen vanwege diens afname in diameter van de vernauwingen in het porienetwerk. De tortuositeit in het porienetwerk neemt toe aangezien de cementatie in de vernauwingen een aanzienlijk grotere invloed heeft op de ruimtelijke ordening dan cementatie elders in het porienetwerk, wat een afname in het gemiddelde coördinatiegetal als gevolg heeft.

2- Wetenschappelijke conclusies die gebaseerd zijn op slechts twee of drie experimenten en waarvan de reproduceerbaarheid niet vastgesteld is moeten in twijfel getrokken worden. In het slechtste geval zal er een aanzienlijk deel van de literatuur verwijderd worden. Gezien dit feit dienen experimenten herhaalbaar te zijn, zodat er onderscheid gemaakt kan worden tussen data die inzicht geeft in de dynamiek van de opbouw van een oliebank en data die statistisch gezien niet relevant is of te wijten is aan tekortkomingen in de experimentele opzet.

3- In bestaande literatuur is er geen duidelijke definitie of een drang naar de opbouw van een oliebank. Een oliebank is gedefinieerd als een continu lichaam van gemobiliseerde olie dat gevormd wordt nadat gemobiliseerde oliedruppels samenkomen. Nadat deze gevormd is zal de oliebank in omvang toenemen terwijl deze getransporteerd wordt door het poreus medium.

4- De opbouw van een oliebank vergroot de efficiëntie van het proces van “chemical enhanced oil recovery” (EOR), aangezien de hoeveelheid olie in micro-emulsie geminimaliseerd wordt. Dit is in de praktijk zeer voordelig voor de faciliteiten in een olieveld, gezien het feit dat olie in de vorm van emulsies het proces verstoord.

5- Het injecteren van oppervlakte-actieve-stoffen (surfactants) zonder polymeer in oplossing dient niet nagestreefd te worden bij een EOR-proces in een olieveld.

6- In het proces van surfactant-polymer-EOR kan er residuale olie geproduceerd worden zonder de opbouw van een oliebank.

7- De mobiliteit van de olie is gunstiger, oftewel olieproductie wordt versneld, als deze geproduceerd wordt in de vorm van een oliebank in plaats van transport in een emulsie. Dit heeft een positieve invloed op de omzet (netto contante waarde) van het EOR-proces.

8- Core-flowexperimenten zijn een makkelijk middel om succesvolle EOR-methodes uit te sluiten.

9- In de wetenschappelijke wereld bestaan er geen onweerlegbare conclusies (en deze zullen ook nooit bestaan). “All Knowledge is provisional, temporary, capable of refutation at any moment”, -Karl Popper; vrij vertaald: Alle kennis is tijdelijk en kan op elk moment weerlegd worden.

10- Een proefschrift in het kader van stroming van vloeistoffen door een poreus medium, zonder een hoofdstuk over de karakterisatie van dat poreus medium, is als een boom zonder wortels.

11- Nederland, met name Amsterdam, is een voorbeeld van een multiculturele samenleving. De hele wereld zal ooit vertegenwoordigd worden door multiculturele samenlevingen waarin iedereens cultuur wordt geaccepteerd zonder dat iemand het gevoel heeft dat zijn of haar cultuur niet gerespecteerd wordt.

Deze stellingen worden gezien als geldig en verdedigbaar en zijn goedgekeurd door begeleiders

Prof. Ir. C.P.J.W. van Kruijsdijk en Dr. K.H.A.A. Wolf.

Table of Contents

Summary

Dynamics of building an oil bank by Surfactant Polymer Injection

Enhanced oil recovery (EOR) seeks to improve the recovery of oil from existing mature oil fields. It targets the oil left behind after conventional recovery by natural reservoir drive and water injection. The injection of surfactant polymer chemicals can enhance oil recovery by reducing the interfacial tension, allowing more oil to be released from its host rock and improving the flood conformance.

In this study, the principles and parameters of chemical surfactant polymer EOR mechanisms, which mobilise, displace and transport residual oil (i.e. build an effective oil bank) after water injection were investigated. The current understanding of when, and under what conditions, an oil bank is formed and maintained is limited. This is relevant in core-flow experiments that need to be appropriately interpreted and scaled, from the centimetre to the field scale, in various steps. Various factors that influence the dynamics of building a stable oil bank were evaluated, using an extensive core-flow experimental study with the aid of computed tomography scanning.

A porous medium was characterised because its properties significantly influence the displacement and transport of fluids. Such characterisations of rocks help us to understand the impact of the pore–grain framework, petrophysical properties and the micrometre- to metre-scale aspects of fluid transport processes. A porous medium was chosen that displayed consistent and homogeneous properties. The aim was to obtain a reproducible core-flow experiment. The Fontainebleau Sandstone met these preconditions. It has a homogeneous texture and mineralogy, due to the purity of its composition. It contains virtually no clay minerals, with only accessory clay being found. This has no impact on fluid flow behaviour during core-flow experiments. This was meant to ensure maximal reproducibility and comparison of the fluid-flow experimental results (Chapter 2).

Two experimental setups (microfluidic and core-flow) were developed to investigate the dynamics of oil mobilisation and transport in a porous medium. The aim was to quantitatively compare a large number of core-flow results and determine any differentiation. This approach required the experimental reproducibility and validation of the variance of the results under the same input conditions (i.e. temperature, pore pressure, chemicals, pore volumes, etc.), using the same rock sample; in several published studies, certain conclusions have been drawn based on only two or three experiments, and the reproducibility of the data have not been confirmed. The main question was whether the mechanism of a physical process worked in the same way or if the same experiment gave different results when repeated. In the multiple experiments used here, by ensuring reproducibility, the data that provided accurate insights into the dynamics of oil bank build-up could be distinguished from results that were statistically insignificant. As the

experiments were replicated, we could ensure there would be no anomalies between differently designed experiments (Chapter 3).

After characterising the porous medium (the Fontainebleau Sandstone), and testing the robustness of our experimental setup, we investigated various factors that can influence the dynamics of building a stable oil bank. The effect of pore volume and the heterogeneity of the porous medium were evaluated, along with the impact of surfactant phase behaviour, the micro-emulsion viscosity and the polymer requirement for favourable mobility conditions. In addition, the process of building the oil bank at the microscopic (pore) scale was visualised, which provided insights into what occurs at that scale and how oil droplets mobilise, coalesce and advance in front of the chemical flood during the displacement process (Chapter 4).

Finally, a summary and the conclusions of the research are presented. The oil bank was defined as a continuous volume of mobilised oil that forms from the coalescence of mobilised oil ganglia. Once developed, the dimensions of the oil bank extend during its transport through the porous medium. Building a stable oil bank supports the efficiency of the chemical EOR process, during which most of the residual oil is mobilised, amassed and transported in front of the chemical flood. Such oil is produced mostly using brine, and oil existing as a micro-emulsion is minimised. This provides a significant advantage to the surface facility in the producing field because oil in the form of an emulsion can interfere with the facility's process. The mobility of the oil is greater (i.e. oil production is accelerated) when it is produced as a connected oil bank rather than as a dispersed flow as an emulsion. This has a positive impact on the revenue (net present value) of the chemical EOR process. The results show a positive correlation between sample size and oil bank characteristics, based on pore volume and matrix homogeneity. In addition, the experiments showed that, even under the same laboratory conditions, there is variability among identical experiments on the same core. Without replicability, only the larger differences between different core-floods are significant. This is often overlooked in core-flood studies.

Samenvatting

Enhanced oil recovery (EOR) tracht de productie van olie uit bestaande lang in gebruik genomen olievelden te verbeteren. EOR richt zich op de olie die achtergebleven is na conventionele manieren van olieproductie, zoals het natuurlijke depletie mechanisme of water injectie. Het injecteren van oplossingen van oppervlakte-actieve stof en polymeer (surfactant polymer) wordt de oppervlaktespanning verlaagd waardoor meer olie door het reservoir wordt vrijgelaten en waarmee de conformiteit van het front van de vloed verbeterd wordt.

In dit onderzoek worden de effecten geëvalueerd van de principes en relevante parameters van surfactant polymer EOR, die invloed hebben op de creatie van een effectieve oliebank, oftewel het mobiliseren, verplaatsen en transporteren van de residuale olie na injectie van water. Er bestaat momenteel slechts een beperkt beeld van de specifieke omstandigheden waarin een oliebank wordt gevormd en hoe deze zich daarna ontwikkeld. Dit is relevant voor core-flow experimenten die adequate dienen te worden geïnterpreteerd en stapsgewijs worden opgeschaald van centimeterschaal naar reservoir schaal. Met behulp van een extensieve reeks core-flow experimenten en computertomografie werden de factoren onderzocht die invloed hebben op de dynamiek van het vormen van een stabiele oliebank.

Een poreus medium werd gekarakteriseerd gezien het feit dat zijn fysieke eigenschappen een significante invloed hebben op het mobiliseren en transporteren van vloeistoffen. Een dergelijke karakterisatie geeft enig inzicht in de effecten van het porienetwerk, de petrofysische eigenschappen en het aspect van micrometer- tot meterschaal van het transport van vloeistoffen. Er werd een poreus medium gekozen dat een grote mate van consistentie en homogeniteit vertoonde, omwille van het verkrijgen van vergelijkbare resultaten uit core-flow experimenten. De Fontainebleau zandsteen voldeed aan deze voorwaardes; het heeft een grote mate van homogeniteit wat betreft de textuur en mineralogie vanwege de puurheid in compositie. Het bevat vrijwel geen kleimineralen met alleen wat incidentele kleideeltjes die geen invloed hebben op het vloeistoftransport tijdens de core-flow experimenten. (Hoofdstuk 2)

Er zijn twee experimentele opstellingen ontwikkeld (microfluidic en core-flow) om inzicht te krijgen in de dynamiek van mobilisatie van olie en transport in een poreus medium. Het doel was het vergelijken van een grote reeks experimentele resultaten en het vaststellen van enige afwijkingen daarin. Deze aanpak vereiste reproduceerbaarheid van experimentele resultaten en de validatie van variatie in resultaten onder identieke initiële omstandigheden, oftewel temperatuur, druk in het porienetwerk, gebruikte chemicaliën, volume van het porienetwerk etc); in andere gepubliceerde artikelen werden conclusies getrokken uit slechts twee of drie experimenten en was de reproduceerbaarheid van de data niet vastgesteld. Voornaamste onderzoeksvraag was of het fysische proces identiek was of

dat identieke experimenten verschillende resultaten leverden. In de experimenten uit dit onderzoek, door reproduceerbaarheid te garanderen, kon er onderscheid worden gemaakt tussen data die inzicht gaf in de dynamiek van de opbouw van een oliebank en data die statistisch gezien niet relevant is. Aan de hand van herhaling van experimenten kon er worden gegarandeerd dat er geen afwijkingen waren tussen verschillend ontworpen experimenten. (Hoofdstuk 3)

Na het karakteriseren van het poreus medium (de Fontainebleau zandsteen) en het testen van de robuustheid van de experimentele opstelling, werd er onderzoek gedaan naar de verschillende factoren die invloed kunnen hebben op de opbouw van een oliebank. Het effect van het volume van het porienetwerk en de heterogeniteit van het poreuze medium werd geëvalueerd, tegelijk met de invloed van surfactant, viscositeit van de micro-emulsie en vereiste polymeer voor gunstige transport van vloeistoffen. Verder werd de opbouw van de oliebank gevisualiseerd op microscopische schaal, wat enig inzicht gaf in wat er plaatsvindt op die schaal en hoe oliedruppels mobiliseren, samenkomen en verplaats worden vóór de vloed van chemicaliën. (Hoofdstuk 4)

Tenslotte worden er een samenvatting en conclusie van het onderzoek gepresenteerd. De oliebank is gedefinieerd als een continu lichaam van gemobiliseerde olie dat gevormd wordt nadat gemobiliseerde oliedruppels samenkomen. Nadat deze gevormd is zal de oliebank in omvang toenemen terwijl deze getransporteerd wordt door het poreus medium. De opbouw van een stabiele oliebank vergroot de efficiëntie van het EOR-proces, waarin de meeste residuale olie wordt gemobiliseerd, geaccumuleerd en vooruit getransporteerd ten opzichte van de vloed van chemicaliën. Dergelijke olie wordt voornamelijk geproduceerd door water, zo wordt de olie in de micro-emulsie geminimaliseerd. Dit is in de praktijk zeer voordelig voor de faciliteiten in een olieveld, gezien het feit dat olie in de vorm van emulsies het proces verstoord. De mobiliteit van de olie is gunstiger, oftewel olieproductie wordt versneld, als deze geproduceerd wordt in de vorm van een oliebank in plaats van transport in een emulsie. Dit heeft een positieve invloed op de omzet (netto contante waarde) van het EOR-proces. De resultaten tonen een positieve correlatie tussen de grootte van de monsters en de eigenschappen van de oliebank, gebaseerd op porie volume en homogeniteit van de zandsteen. De experimenten tonen dat zelfs onder laboratoriumomstandigheden een variatie bestaat tussen identieke experimenten met dezelfde kern. Zonder herhaalbaarheid zijn alleen de grote verschillen tussen experimenten significant, wat vaak over het hoofd gezien wordt in literatuur omtrent core-flood experimenten.

Chapter 1

Introduction

Global energy demand is expected to grow in the coming 20 years, with the strongest increases in developing countries (BP Review, 2018). Today, fossil fuels supply approximately 80% of the world's energy. With the projected growth in the demand for energy, solutions will be required in the arena of fossil fuels in the form of either new discoveries/fields, which cannot be guaranteed or sustained production from existing fields. Given the success rate, the volumes acquired and the capital investment involved in developing new fields, existing fields will be looked upon when supply begins to fall short of demand. Hence, enhanced oil recovery (EOR) methods for use in existing fields will become more essential.

Enhanced oil recovery is a collection of technologies that involve injection of gases, chemicals and/or thermal energy into a reservoir. It allows operating companies to produce incremental oil from fields that are well into their production life cycle. At this point, the field has most likely undergone secondary oil recovery (water injection for pressure maintenance and oil mobilisation). However, it still contains more than 50% of its initial oil volume (Moreno et al., 2010; Cordiner et al., 1972). The remaining oil is mostly bypassed, including residual oil in the form of ganglia dispersed in the reservoir pores; this remaining oil is the target of EOR.

Chemical EOR consists of recovering the oil remaining after secondary recovery by introducing chemical agents, which work mainly through the following mechanisms (Lake et al., 2014; Larson et al., 1979):

1- Altering fractional flow relations, as by lowering interfacial tension (IFT) (e.g., by adding a surfactant) or by raising viscosity (e.g., using polymers)
2- Changing the phase behavior, as by making oil partially soluble in an aqueous phase (solubilization) or by adding a water-soluble solvent that is miscible with reservoir oil

In this research, surfactant polymer chemical agents are utilized to lower the IFT and improve the sweep efficiency. This application is one of the fundamental mechanisms in chemical EOR. By injecting these compounds into the reservoir, the IFT of the oil/water interface decreases significantly to 10^{-3}–10^{-2} N/m (Shang, 2011). Since the effectiveness of the surfactant is largely salinity-dependent, its formulation must be optimised to ensure that the resulting oil-surfactant micro-emulsions exhibit the ultra-low IFTs required for oil mobilisation. Once injected, the surfactant polymer tends to mobilise dispersed oil droplets,

which begin to propagate ahead of the front (King et al, 1981). As more and more oil is mobilised, the droplets converge to form a coherent oil body, also known as an oil bank. The development of such an oil bank is the most economically advantageous method of producing residual oil from a field, since it requires minimal processing.

To implement the above chemical EOR mechanisms effectively, it is crucial to have a clear understanding of the different parameters and phenomena that influence the mobilization of residual oil and formation of the oil bank. This PhD study is undertaken to investigate the different parameters that influence the mobilization, displacement and transportation of residual oil under chemical EOR mechanisms.

Benefits of Chemical EOR approaches on climate

Fossil fuels are the main energy sources as seen in Figure 1.1 mainly because of their large volumetric energy mass and ease of access and transport (Olah et al., 2009). The current age owes much of its development and prosperity to fossil fuels. Demand for energy is increasing, and this growth is likely to continue due to population increase and higher standards of living.

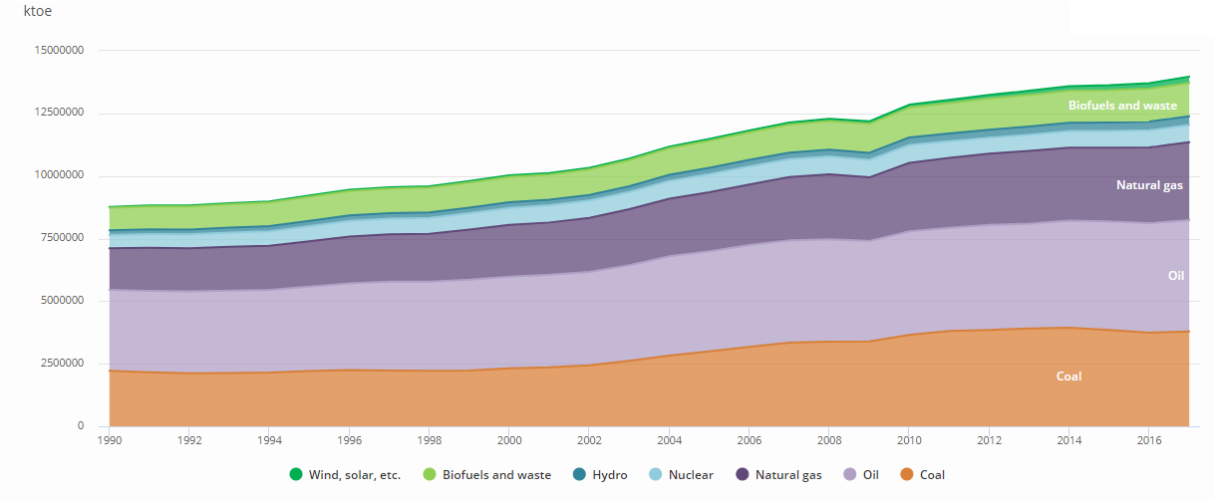

Figure 1.1: Total primary energy supply by source, World 1990 – 2017. Source: World Energy Balance 2019

The combustion of fossil fuels (coal, oil, and natural gas) discharges large quantities of carbon dioxide (and other greenhouse gases) into the atmosphere, which has a wide range of environmental impacts. The full extent of these impacts is not yet known, but they include rising global temperatures, ocean acidification, sea level rise, and a variety of other impacts on weather, natural hazards, agriculture, and more, many of which are likely to increase into the future (EPA, 2019).

The oil industry drives to decrease greenhouse gas (GHG) emission in the next few years by 10%, which includes to compensate for emissions associated with economic growth (Grassian, Bahatem, Scott, Olsen, et al., 2017). The global oil and gas industry has already

made significant improvements in the efficiency of its energy use. One key area for efficiency is reduction in gas flaring. Between 2005 and 2010, flaring of gas associated with oil production has decreased worldwide by 22 percent, according to the Global Gas Flaring Reduction partnership but there is still ways to decrease these values even more.

Our chemical EOR research is going to contribute to the efforts of reducing greenhouse gas emissions by improving the efficiency of the oil and gas processes (i.e. optimizing the energy-intensive components). As an example, It appears that when the fraction of the produced water (water cut) is above 90% the increase in the invested exergy (and consequently the carbon footprint) becomes dramatic. Therefore, reductions in water cut and water management can lead to significant reductions in the invested exergy or emitted CO2 (Farajzadeh, 2019). In our research, we demonstrate that by injecting surfactant-polymer we build an oil bank where the oil production increases and amount of produced water is reduced significantly. Hence, by reducing the produced water at surface thereby minimizing power consumption (i.e. reduce CO2 emissions) to re-process the excess water as well as savings on the actual cost of processing and handling the produced water. Furthermore, water that comes to the surface with the produced hydrocarbons contains many chemical constituents, which are usually not environmentally friendly. Figure 1.2 present field actual data where injection of polymer chemical lead to an evident oil increase and reversal water cut in a giant oil field in south of Oman.

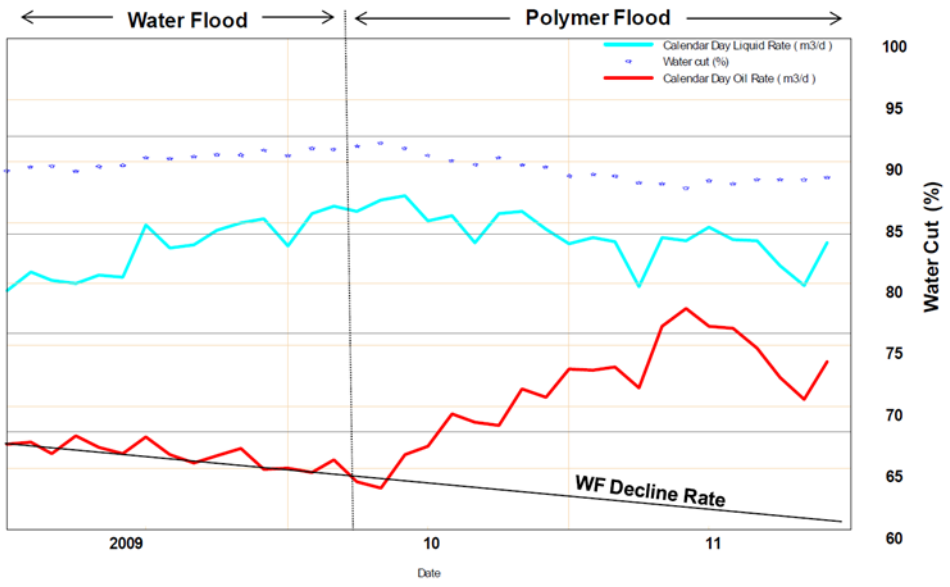

Figure 1.2: Oil gain due to polymer injection (Al-Saadi et al, 2012)

What is an oil bank?

An oil bank is a continuous volume of mobilized oil that forms from the coalescence of mobilized oil ganglia. Once developed, the length of the oil bank extends during its transport through the porous media. The schematic diagrams in Figure 1.3 demonstrate the steps of building an oil bank.

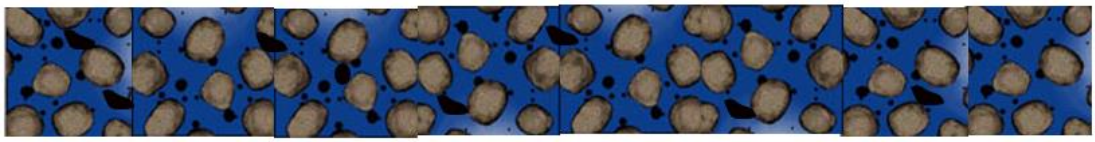

1- After water injection; oil is disconnected and trapped

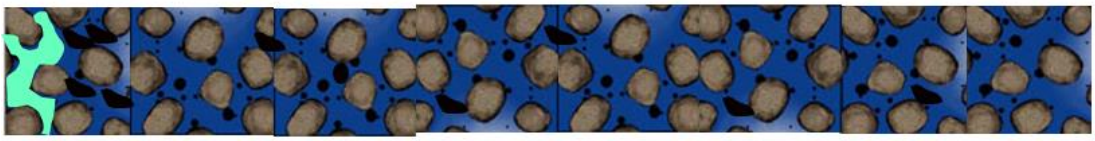

2- SP injection; oil ganglia are mobilized

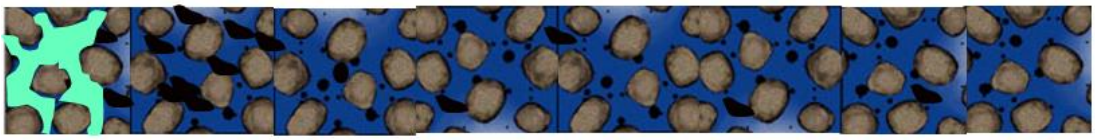

3- Oil ganglia begin to coalescence

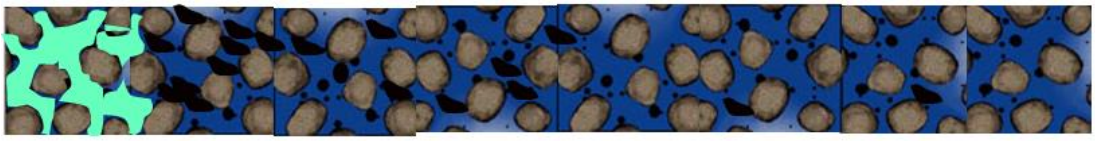

4- Competition between oil coalescence and oil break up, re-trapped oil flowing in dispersed form

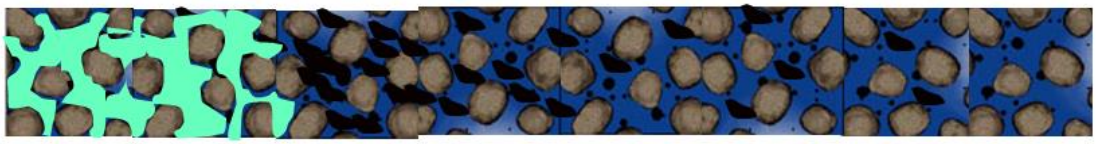

5- Oil ganglia coalesce further and become more stabilized. Water is flowing out of the porous media, influencing/causing some oil movement at the front of the oil bank

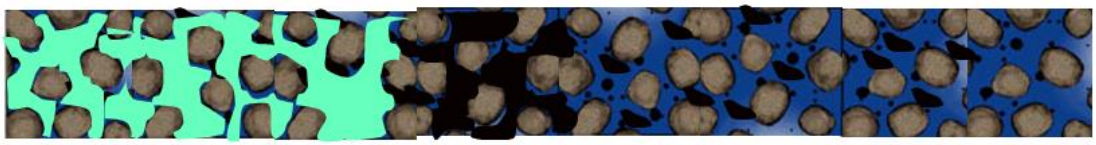

6- Oil bank is formed and stabilized

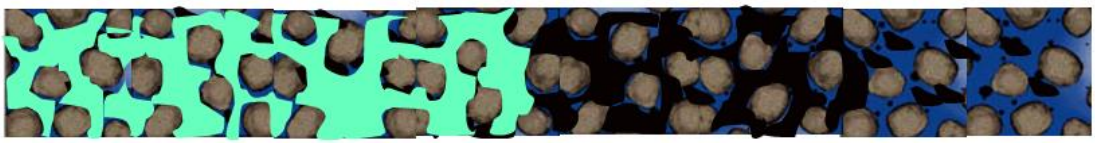

7- Oil bank lengthens and the displacement efficiency improves

Figure 1.3: 2D Schematic of the development of an oil bank. Objective is to demonstrate the conceptual model of the process of building an oil bank. The scaling and dimensions are not representative in this schematic.

Need for the development of an oil bank in a field:

The successful field implementation of a chemical flood process requires mobilization of residual oil where the oil ganglia coalescence at the front of the chemical flood, continually extending its length and developing the oil bank. This mobilization and coalescence increase the sweep efficiency and hence result in high field oil recovery.

If the oil bank does not develop, then the chemical process behaves more like the unstable injection of a surfactant solution alone. As a result, the oil is produced in dispersed form or is emulsified in the flowing surfactant stream, leading to low field oil recovery (Wasan et al., 1979). Building a stable oil bank supports the efficiency of the chemical EOR process, where oil is produced mostly with brine. The amount of oil in micro-emulsion is minimized. This presents a large advantage to the surface facility in the producing field, as emulsified oil usually disrupts the facility's process. Furthermore, the pseudo-mobility of the oil is higher (i.e., oil production is accelerated) when it is produced as a continuous oil bank in comparison with dispersed flow with emulsion. This has a positive impact on the revenue (net present value) of the chemical EOR process.

Laboratory phase behaviour and core-flow tests are usually carried out to characterize physical and chemical processes relevant to the field. These data are used for the design, prediction and analysis of field trials and provide the required input for a field simulator.

Figure 1.4 represents a decision tree for the need to build the oil bank at the core scale. Our focus is on the right branch, where the oil bank is not built up and hence the oil recovery is low. Some researchers/operators might omit the chemical process and conclude that such a reservoir is not favorable for chemical EOR. There are many other reasons that must be investigated prior to excluding chemical EOR. For example, the chemical cocktail might not be effective, requiring more investigation of phase behavior. Another possibility that is also addressed in this thesis is that the cores could be too short to capture the oil bank build up process.

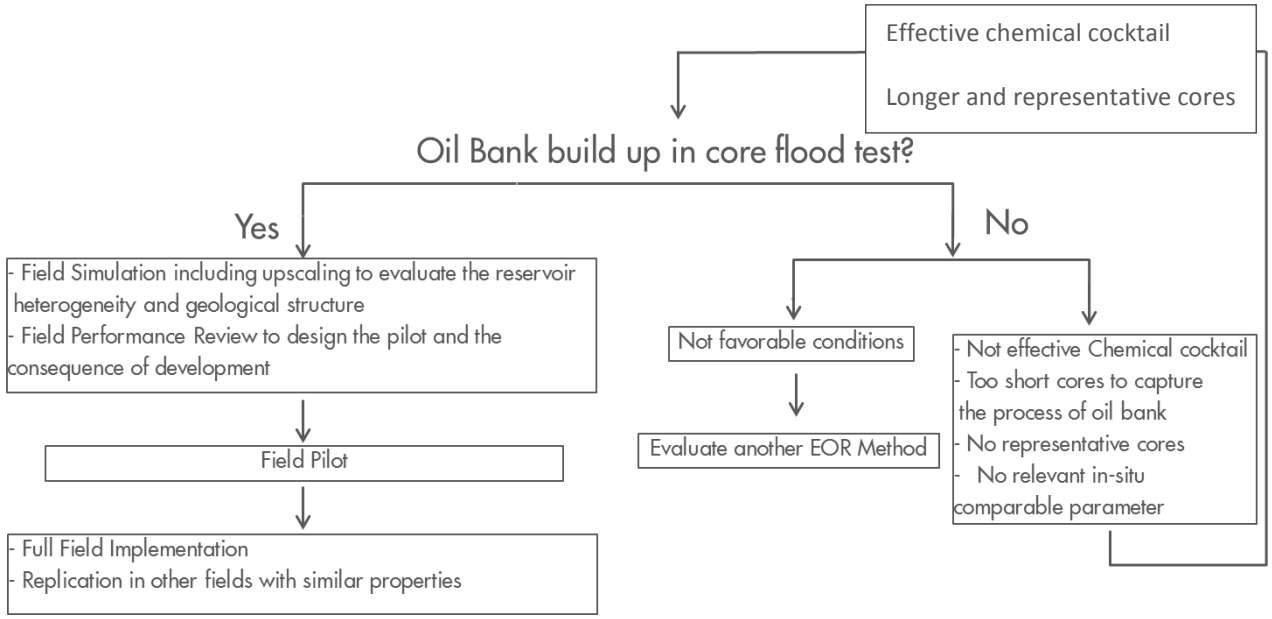

Figure 1.4: A decision tree on building an oil bank in core-flow tests.

Chemical EOR field application is quite expensive due to the cost of the chemicals and the required dedicated chemical plants. Therefore, it is very crucial to have key insights into chemical effectiveness to make the project economically attractive. De-risking of chemical EOR field uncertainties is pursued in a phased approach. Figure 1.5 presents the de-risking process from the laboratory phase, field simulations, and field pilot implementation to full field implementation.

Figure 1.5: Phased approach to de-risking chemical EOR for field application.

Knowing the characteristics of sandstone for a scale-window ranging from micrometre to field scale (Figure 1.6) allows us to assign values to the modelling parameters of bulk reservoir properties, permeability and lateral spatial characteristics.

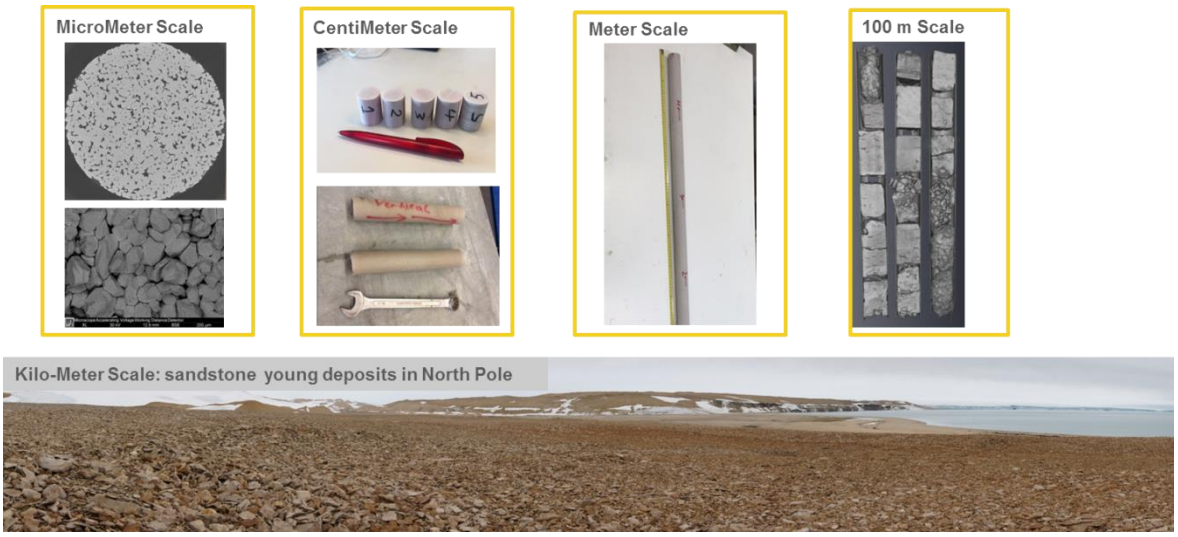

Figure 1.6: Scale-window of sandstone from micrometre scale to kilometre scale. Microeter scale → SEM and micro CTS, CentiMeter Scale → Plugs and cores, Meter Scale → One meter core at 3.9 cm diameter, Kilo-Meter Scale → Artic glacier landscapes with moraines from fines to pebble size compositions, location in Svalbard archipelago, Nordauslandet – Vibebukta.

Research Problem Statements:

The purpose of this research study is to identify and understand the different parameters that influence the mobilization, displacement and transportation of residual oil under surfactant polymer chemical EOR mechanisms. The specific research problems are as follows:

1- Mobilization process:
After water injection, the remaining oil is bypassed or isolated. The mechanism of how residual oil re-coalesces during chemical EOR processes is not well understood. This study is undertaken to understand how residual oil is mobilized by means of chemical EOR and to identify the parameters that influence this process.

2- Displacement/transport process:
No EOR process is free from instability of some sort due to unstable displacement, the formation of emulsions in the reservoir, changes in phase behavior, etc.. Therefore, it is important to understand the fluid-rock interactions, such as ASP, polymers, etc.; fluid-fluid interactions, such as solvent effects; and the impact of residual oil displacement/transportation on fluid/reservoir stability and displacement efficiency, i.e., oil recovery.

Research Questions:

In this research, we investigate the physics and parameters of the chemical surfactant polymer (SP) EOR mechanisms that mobilize, displace and transport residual oil (i.e., build an effective oil bank) after water injection.

The research begins with characterization of the porous media, where we investigate the effectiveness and influence of grain size distribution and clay content on oil bank build up. What are the impacts of micrometre- to metre-scale characteristics of the porous media on the entrapment/mobilization/transport of oil? More specifically, the microstructural properties, grain/pore size distribution and type of quartz overgrowth on the pore framework are evaluated, with their associated heterogeneities and flow behaviour for various sample sizes. Additionally, porosity, permeability, conductivity, zeta potential, and capillary pressure measurements were collected to support the understanding of the geochemical and petrophysical properties of the media.

One important issue that we attempt to address is the reproducibility and repeatability of the core-flow. Our aim is to quantitatively compare a large number of core-flows and their variations. This approach requires experimental reproducibility and a validation of the variance in results under the same input conditions (i.e., temperature, pore pressure, chemicals, PVs, etc.) with the same rock sample. In the literature, scientific conclusions are drawn based on two or three experiments, while reproducibility is not confirmed. The main question is whether the mechanism of a physical process is working properly if the same experiment gives different results when repeated. Irreproducibility may reflect a genuine uncertainty, but it could also be due to error or misinformation.

After understanding the properties of our porous media and the reproducibility of our core-flow experiments, we turn to the process of building an oil bank by SP chemical injection. The current understanding of when, and under what conditions, an oil bank is formed and maintained is very limited. This is relevant when core flow experiments are interpreted and up-scaled from centimetre scale to field scale in various steps. We evaluate various factors that influence the dynamics of building a stable oil bank through an extensive core-flow experimental study with the aid of CT scanning. The following specific questions are evaluated:

- What are the effects of pore volume, heterogeneity of the porous media, surfactant phase behaviour, and microemulsion viscosity?
- What are the polymer requirements for favourable mobility conditions?
- What is the importance of mobility control (i.e., via the injection of polymers in our case)?
- What is the importance of visualizing the process of building the oil bank at the microscopic (pore) and meter scales?
- What is the impact on relative permeability?
- How and when does an oil bank develop during chemical EOR?
- When the oil clusters break up?
- When is a “stable” oil bank formed?

Materials, Fluids and Methods

Materials:

Fontainebleau sandstone cores, consisting almost entirely of pure quartz (99.5%) without any clay, were used in the corefloods. Detailed characterization of the cores can be found elsewhere (Al Saadi et al., 2017) and in chapter 2. These cores were used to conduct highly reproducible corefloods that can be compared quantitatively.

Fluids

- Dodecane and Iodododecane (Saturated alkaline c12, single molecule) were used as the oleic phases. Iodododecane was used in experiments conducted under the CT scanner.
- The aqueous solutions were prepared using laboratory-grade sodium chloride salt.
- Internal olefin sulphonate (IOS) surfactant was used in our experiments. It is an anionic surfactant produced by Shell Chemicals with carbon chain lengths of 20–24 and forms part of ENORDET™. Secondary butanol was used as a co-solvent.
- SNF Polymer Flopaam 3630 was introduced to our surfactant solution to achieve favorable mobility conditions.

Methods

Surfactant phase behavior: The optimal phase behaviour was determined by performing a salinity scan on the chosen surfactant formulation to identify ultralow IFT formulations for dodecane and iodododecane.

IFT measurements: IFT measurements were also performed using a spinning drop tensiometer.

Microemulsion viscosity measurements: Microemulsion rheology measurements were performed using a TA Instruments AR-G2 rheometer for the surfactant formulation that was used in the core-flows.

Coreflood experiments: approximately 80 unsteady state experiments were performed in a coreflow setup with the following specifications:

- Different core lengths of 7, 17, 30, 39, 60 and 100 cm.
- Able to be transported to the CT scanner to monitor oil bank construction and mobilization.

Chemical flood in micro-slim tubes: A microfluidic setup with a micromodel chip with a one-meter pore network path visualizes and monitors the process and dynamics of oil bank formation at the pore scale. Image analysis is used to semi-quantitatively demonstrate the mechanisms underlying the transition from mobilization to oil bank formation.

Thesis Outline

This thesis is based on a number of articles published from this study, describing the outcomes and results of the experimental SP flooding EOR. The dissertation consists of five chapters:

Chapter 1 is the introduction.

Chapter 2 presents an experimental evaluation of the properties of Fontainebleau sandstone to advance the understanding of its quartz overgrowth and petrophysical and electrical transport properties. We measure and quantify the spatial attributes of the grain and pore matrix via Computed Tomography (CT) image analysis, associated with stereological measurements and statistical 2D/3D reconstructions. In addition, traditional petrophysical laboratory methods are applied and linked to the spatial results. Furthermore, our graphical methods are compared to pre-existing literature. Fontainebleau sandstone was selected due to its pure composition (99% Quartz) to ensure maximal reproducibility and comparison of fluid flow experiment results.

Chapter 3 presents the experimental setups and equipment utilized to investigate the dynamics of oil mobilization and transport in a porous medium. We constructed two setups with different volume scales to compare flow results in terms of their reliability and accuracy. Our aim was to quantitatively compare a large number of coreflows and evaluate the variation in results. This approach requires experimental reproducibility and a validation of the variance in results under the same input conditions (i.e., temperature, pore pressure, chemicals, PVs, etc.) with the same rock sample but with varying core lengths. Both set-ups provide us with robust, accurate and repeatable experimental data on oil mobilization at the micrometre/pore scale and the meter scale.

Chapter 4 addresses various factors that influence the dynamics of building a stable oil bank through an extensive core-flow experimental study with the aid of CT scanning. We evaluate the effects of the pore volume and heterogeneity of the porous media, the impacts of surfactant phase behavior and microemulsion viscosity, and the polymer requirement for favorable mobility conditions. Furthermore, we visualize the process of building the oil bank at the microscopic scale (pore scale), which provides insight into what occurs on a microscopic scale and how the oil droplets mobilize, coalesce and advance in front of the chemical flood during the displacement process.

Chapter 5 presents the research discussions and main conclusions of this Ph.D. dissertation.

References:

1- Grassian, D., Bahatem, M., Scott, T., Olsen, D., et al. (2017). Development of an energy efficiency improvement methodology for upstream oil and gas operations. In Abu dhabi international petroleum exhibition & conference.

2- Al-Saadi F, Amri BA, Nofli S, van Wunnik J, Jaspers HF, Harthi S, Shuaili K, Cherukupalli C, Chakravarthi R. 2012 Polymer flooding in a large field in South Oman—initial results and future plans. In Proc. SP EOR Conf. Oil and Gas West Asia, Muscat, Oman, 16–18 April 2012. Tulsa, OK: Society of Petroleum Engineers. (doi:10.2118/154665-MS)

3- The World Bank, Global Gas Flaring Reduction, http://web.worldbank.org/WBSITE/EXTERNAL/NEWS/0,,contentMDK:21032487~menuPK:34480~pagePK:64257043~piPK:437376~theSitePK:4607,00.html.

4- Hassan, A., Ayoub, M., Eissa, M., Musa, T., Bruining, J., Farajzadeh, R., 2019. Exergy return on exergy investment analysis of natural-polymer (Guar-Arabic gum) enhanced oil recovery process. Energy 181, 162–172.

5- IPCC Climate Change, 2007. In: Pachauri, R.K., Reisinger, A. (Eds.), 2007: Synthesis Report. Cambridge Univ. Press.

6- Olah, G.A., Goeppert, A., Prakash, G.K.S., 2009. Beyond Oil and Gas: the Methanol Economy, second ed. Willy-VCH.

7- Sato, N., 2004. Chemical Exergy and Exergy: U.S. Environmental Protection Agency – Global Greenhouse Gas Emissions Data. https://www.epa.gov/ghgemissions/ global-greenhouse-gas-emissions-dat.

8- Farajzadeh, R., Sustainable production of hydrocarbon fields guided by full-cycle exergy analysis, Journal of Petroleum Science and Engineering 181 (2019), https://doi.org/10.1016/j.petrol.2019.106204.

Chapter 2

Characterization of Fontainebleau Sandstone:

Measurements and Literature Review

This chapter is based on the article "Characterization of Fontainebleau Sandstone: Quartz Overgrowth and its Impact on Pore-Throat Framework" which was published in Journal of Petroleum & Environmental Biotechnology, 08(03): 1–12, 2017. D0I: 10.4172/2157-7463.1000328, Saadi, F. A., Wolf, K.-H., and Kruijsdijk, C. v. It describes the presence and petrophysical properties of the Fontainebleau sandstones, especially as used in our experimental work.

1. Introduction

The dynamic of fluid flow in porous media is an area of interest for many researchers in soil, petroleum, hydrology and other sciences. It is well known that the properties of the porous mediums significantly influence the displacement and transport of fluids in those mediums (Stegemeier, 1977; Mohanty, 1987). Therefore, characterization of the porous media is fundamental in understanding the impact of micrometer to meter scale aspects on fluid transport processes.

For our study of the dynamics of oil transport, we chose a porous medium which displays consistent and homogenous properties. This is to ensure repeatability of our flow experiments in porous media and to minimize changes in the properties of the porous media. The aim is to obtain a comparable core flow experimental. Fontainebleau sandstone meets these pre-conditions.

Fontainebleau sandstone is a prime example of a simple natural porous medium (Zinszner, 2007) because of its pure mineral composition (0.995 Quartz) and an almost constant grain size in large sample blocks, however with considerable porosity variations (generally 0.02 to 0.3).

The geology, petrology, petrophysics, and associated reservoir geology are well known (Alimen, 1936; Jacquin, 1964; Thiry et al., 1988). There is a plethora of petrophysical data in scientific literature. This fact and the homogeneous parameters we need for our experiments, led us to further examine the distributions regarding the spatial characteristics, matrix mineralogy and petrophysical parameters such as permeability, porosity, capillarity, pore framework, pore-network, coordination distribution, etc. Hence our findings are

compared with results from literature (Doyen et al., 1988; Fredrich et al., 1993; Coker et al., 1996; Lindquist et al, 2000).

A site visit to Fontainebleau provided us with five large blocks weighing about 1 ton in total. The depositional environments and burial history of the sandstone are known.

In order to acquire the pore and grain frameworks, we measure and quantify spatial attributes of the grain and pore matrix by Computed Tomography (CT) image analysis, associated to stereological measurements and statistical 2D/3D reconstructions. In addition, the regular petrophysical laboratory methods are applied and connected to the spatial results. Furthermore, our graphical methods are compared to pre-existing literature.

The petrophysical results are needed for volumes ranging in scale from micrometer to meter. It provides essential information on the microstructural properties of the pore framework with associated heterogeneities and its flow behavior for various sample sizes. Knowing the results for this scale-window of Fontainebleau sandstone allows us to assign bulk electrical properties, permeability and spatial characteristics to modelling parameters. X-Ray devices (like Micro-CT, XRF/XRD, SEM) determine mineral phases, and grain/pore surface attributes. They support the geochemical processes associated to the burial stage. We think of shifts in grain/pore size distribution, type of quartz overgrowth, and leaching effects. Additionally, porosity, permeability, conductivity, zeta potential, and capillary pressure measurements have been included to support the understanding of the geochemical and petrophysical properties.

Our laboratory experiments provide spreads in petrophysical and petrological data. They are used for frequency distributions as an input for modelling. In return, the modelling results are used for the pre-definition of set-up and sample parameters for laboratory experiments.

This article provides a comprehensive review of the properties of Fontainebleau sandstone on a scale ranging from micrometer to meter scale for our porosity range of 0.05 – 0.15 and our permeability range of 10 – 400 mD. The combined measurements, and petrophysical and spatial properties, are used for the prediction, modelling and interpretation of comparative core-flow experiments. Similarly, mapping the pore framework allows us to model the mobilization and transport of oil on the entire micrometer to meter scale.

2. Literature review

2.1 Regional Geology

Fontainebleau sandstone occurs south of Paris and covers the central part of the Paris Basin (Figure 2.1). It is of Rupelian age (24-34 Ma) and usually 50-60 m in thickness. It is a fine-grained, well-sorted sandstone. Its base consists of a marine beach and its top contains

aeolian dune sands (Alimen, 1936; Thiry et al., 1988). The sandstone is used as building material and overlies the Mesozoic in the center of the Basin.

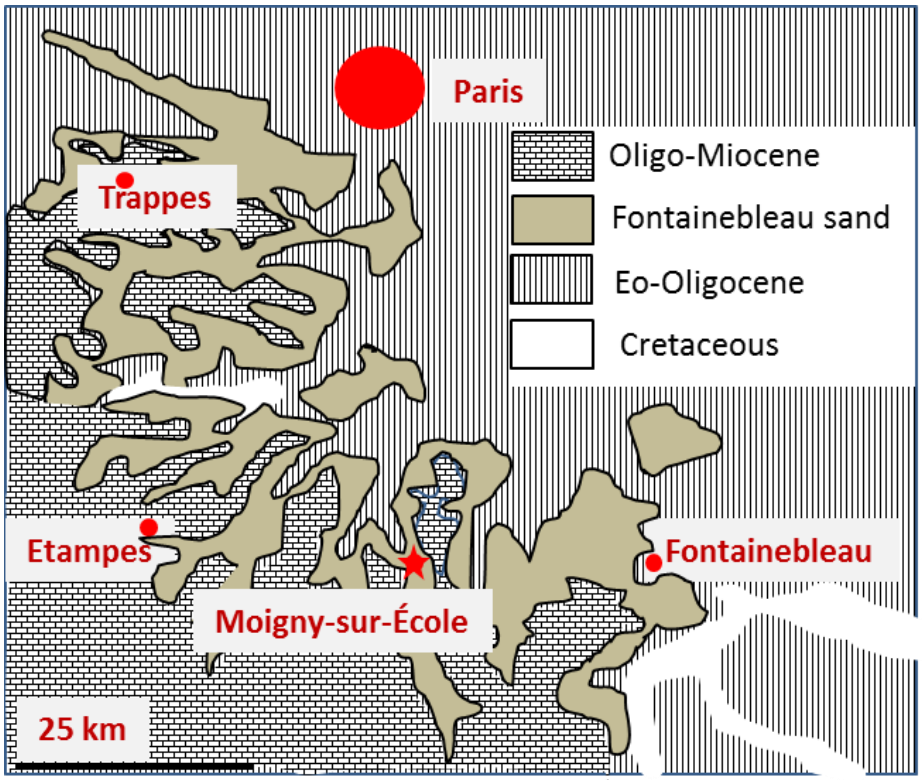

Figure 2.1: The layout of Fontainebleau sandstone. ★ The Grès de Fontainebleau & Cie quarry in Moigny-sur-École for rock sampling (Quarry coordinates: 48.434237,2.433944). Modified after: Thiry et al., 1988.

2.2 Stratigraphy

The upper part of the Fontainebleau sandstone extends laterally for tens of kilometers in the Paris Basin and it is approximately 10 meters high. It is white in color due to water leaching over the past 30,000 years and it is considered to have originated from aeolian dunes. The base of the Fontainebleau sandstone (Figure 2.2) is marine and contains “detrital quartz and clays” (Thiry, 1988). According to Dollfus (1911) and Thiry (1999), “dark glauconite, organic- and pyrite-rich” sands were formed when the unit was below the water table. The block that we are characterizing originates from the white upper part, from an outcrop in the Grès de Fontainebleau & Cie quarry in Moigny-sur-École, Essonne, 90 km south of Paris (Figure 2.1). These aeolian sandstone blocks have been leached.

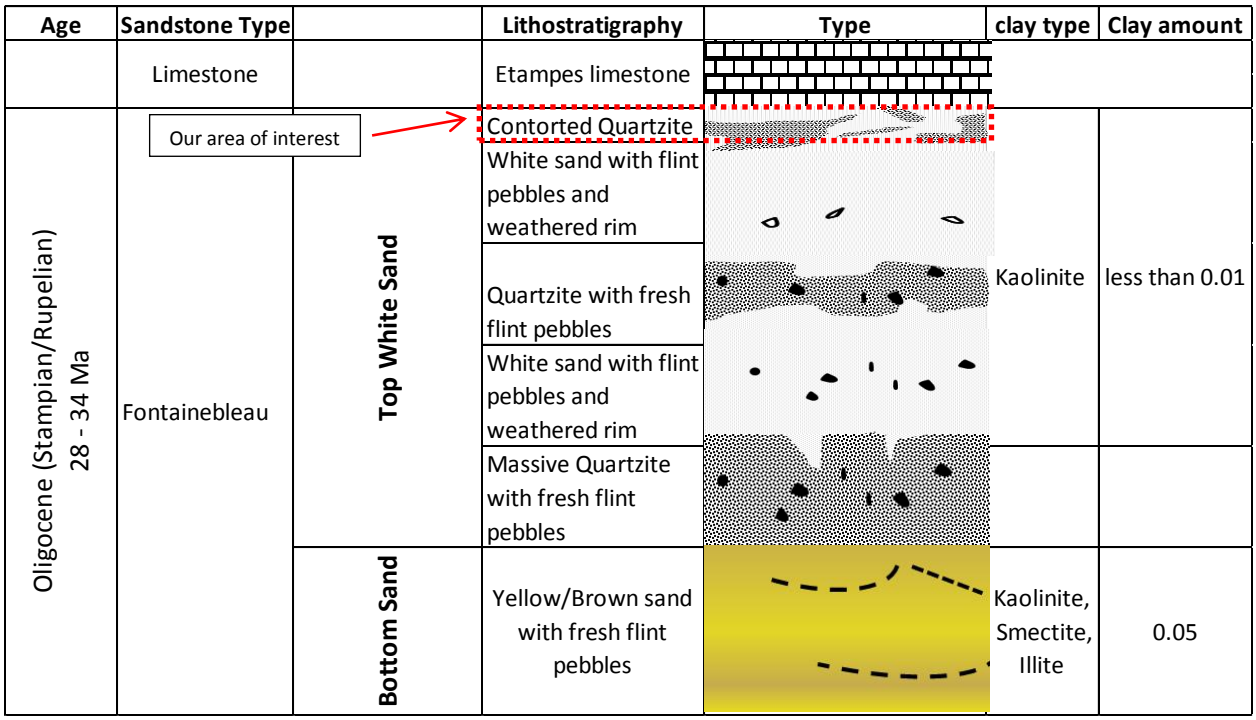

Figure 2.2: Fontainebleau cross section (Modified after: Thiry et al., 1988.)

2.3 Petrography

Bottom sand section

The sand at the bottom of the formation's base is "a yellow and brown coloured" section, containing approximately 5% clay which is a combination of "kaolinite, illite, and smectite". As we move up the formation's base the amount of clay decreases, and illite and smectite disappear leaving only kaolinite (Thiry, 1988, 1999, 2001). Due to its heterogeneity, the base is exempt from our experiments and is not considered to be relevant for this article.

Top white sand section

The sand at the top of the formation, the white sand section, is very clean and at first sight does not contain any clay minerals. It consists of more than 99.5% SiO2 (Thiry et al., 1988, 1999, 2001) in the form of quartz minerals.

Quartzite lenses in the white sand section

Silification in Fontainebleau sandstone produced "flat-lying, very tightly cemented sandstones or sedimentary quartzite lenses" (Thiry et al., 1988) at a former water table. They consist of partly dissolved quartz grains with secondary quartz overgrowth. In addition, microcrystalline quartz (chalcedony) is the subordinate silica phase. The overgrowth may reach as much as 0.35 in volume, and has average values from 0.15 to 0.20 (Thiry et al., 1988; Haddad et al., 2006; French et al., 2013). The toughness of the rock correlates positively with decrease in porosity and increase in quartz overgrowth.

2.4 Petrophysics

Zinszner et al (1985) presented two groups with different permeability-porosity relations that are recognized in Fontainebleau sandstone. In cases of high porosities ($\varphi > 0.08 - 0.09$), for a given porosity the average grain sizes are constant and the specific surface area and tortuosity are independent of porosity. As a result, according to Zinszner (1985), "the Carman-Kozeny model leads to a permeability proportional to φ^3". In cases of low porosity ($\varphi < 0.08 - 0.09$), some of the pores remain relatively large, while the pore throats are cemented gradually by quartz overgrowth and may disappear (Zinszner et al., 1985 and Doyen et al., 1985). Fredrich et al (1993) states that "porosity reduction in Fontainebleau sandstone was accomplished over geologic times by dissolution and precipitation of silica from mobile pore fluids. The silica may have originated from outside the formation". Cooper et al. (2000) suggest that "the porosity reduction is related to mechanical compaction, which acted homogeneously. It is likely that cementation occurred prior to completion of mechanical compaction".

2.5 Pore Framework and Connection

Pore framework plays a major role in controlling porosity (table 2.1). Fontainebleau sandstone is well sorted with grain size distributions in the range of 150 – 300 µm, and with a wide range of porosities between 0.02 - 0.3 (Jacquin, 1964; Bourbie and Zinszner, 1985; Doyen, 1988; Cooper, 2000). In the literature, pore space diameter appears to range from 16 to 30 µm. When reduction in porosity occurs, it is caused by shrinkage of the pore throat diameter due to quartz overgrowth. For porosities between 0.1 – 0.2, the specific surface areas remain constant despite "the decrease in the solid-pore interface area" (Fredrich, 1993). This reduction in porosity creates angular mineral phase type pore shapes (Fredrich, 1993; Lindquist, 2000). Permeability is dominated by tortuosity and coordination number of the pore bodies and is directly related to the previously mentioned quartz overgrowth in the pore framework. Hence, the pore size distribution and connections are more significant than pore throat size distributions (Lindquist, 2000).

Reference	Porosity	Permeability mD	Coordination Number	Throat Size µm	Pore size Mm	Channel Length µm	Grain Density cc/g	Specific Area
Doyen 1988	5.2 7.5 9.7 15.2 18 19.5 22.1	4 33 54 569 593 1123 784	2.3 3 4.4 5.6 5.9 5.7 6	5.8 5.8 10.4 13.7 11.7 16 18.7	16.1 13.2 18.9 27.3 21.8 26.8 30.2			
Fredrich 1993	F1 4.1 F4 10.3 F7 15.5 F8 20.3	0.42 199 586 4139			13 13 17.6 19		2.648 2.646 2.648 2.642	0.9×10^{-4} m^{-1} 2.03×10^{-4} m^{-1} 2.24×10^{-4} m^{-1} 1.97×10^{-4} m^{-1}
Cocker 1996	14.8	1317			10			1.54×10^{-4} m^{-1}
Lindquist 2000	7.5 13 15 22		3.37 3.49 3.66 3.75	18.4 21.3 24.7 22.6		198 159 154 131		
This Study 2016	6 10	18 240	3 3.5	5 - 20 10 - 30	20 - 80 20 - 80		2.64 2.64	0.0968 m^2/g 0.1066 m^2/g

Table 2.1: Spatial characteristics and permeability from literature (Doyen et al., 1988; Fredrich et al., 1993; Coker et al., 1996; Lindquist et al, 2000)

2.6 Electrical Conductivity

The brine saturated porous media in the sandstone are by far the main contributor to conduction through fluids, i.e. high amounts of charged cations and anions (Schon, 1996; Tiab et al., 1996). However, additional contributions are made by the pore framework such as effective porosity and tortuosity (David and Darot, 1989) and mineral heterogeneity by the most probable presence of accessory oxides. Contributions are also made by the degree of brine saturation, i.e. the percentage of pore occupation by conductive fluids (Pirson, 1963).

Archie (1942) defined the correlation between the conductivity of the pore fluid and the bulk conductivity of fully-saturated mono-mineral clean sandstones by introducing formation factor F, which is related to porosity through eq.1:

$$F = \frac{\alpha}{\emptyset^m} \qquad \text{Equation 1}$$

The *m* and α coefficients, known as the cementation exponent and α texture factor, are usually determined empirically. Schon (1996) reports that both parameters are controlled by pore channel geometry, including pore shape and connectivity. Worthington (1993) provides a range of α and m values based on Timur et al. (1972): degree of cementation, shape, sorting and packing of grains, type of porosity, tortuosity, pressure, wettability of rock surface, pore geometry, and clay content.

The conductivity of a brine saturated rock is proportional to brine conductivity (Gomez, 2010) for clean sand (silica with no clays) like the Fontainebleau sandstone. Gomez (2010) reports a cementation exponent in the range of 1.8 – 2.1. Similarly, Revil (2014) presented a

cementation exponent between 1.4 – 2, while Borner (1992) reports 2 samples of Fontainebleau with a cementation factor of 1.6 – 1.7.

2.7 Zeta Potential

Zeta potential describes the surface charge of the particle, and the nature and composition of the surrounding suspension which, in turn, depends on the surface chemistry and the ionic concentration of the bulk solution (Shehata and Nas-El-Din, 2015).

Zeta potential gives a good indication of the magnitude of the electrostatic repulsive interaction between particles (Weiner, 1993). Lorey (2013) presents it as a physiochemical parameter, which describes the ion adsorption and double layer interactions between charged particles and provides important details on the electrochemical properties of the electrical double layer (EDL) (Leory, 2013).

The electrical double layer of a charged surface is formed by the redistribution of ions in the surrounding medium (electrolyte). The origin of surface charge may be caused by:

- Ionization of the surface
- Differential dissolution of ions from insoluble crystals
- Isomorphic substitution of ions
- Changes in crystal surface
- Specific adsorption of species

Sandstones (including Fontainebleau sandstone) are negatively charged and their zeta potential is a negative value.

2.8 Capillary pressure

Capillary pressure is considered to be the elementary parameter to describe the behavior of two or more immiscible fluid phases in the porous media. The capillary pressure presents the static force between the non-wetting phase and wetting phase in the porous media and it is an increasing function of the non-wetting phase saturation. (Lake, 2014; Dullien, 2012).

Pickell (1966) highlighted that for water-wet rocks (i.e. like Fontainebleau), capillary forces predominate in the distribution of fluids and that viscous forces in the range normally of interest in the reservoir have a minimum influence on residual oil saturation (Pickell, 1966).

3. Samples and Methods

3.1 Samples

For this study, outcrop blocks of Fontainebleau sandstone of different sizes (0.008 m^3 to 0.04 m^3) were collected from the Grès de Fontainebleau & Cie quarry near Fontainebleau. One of the blocks (0.018 m^3) has been characterized regarding its porosity, permeability, spatial characteristics, electrical properties, and capillarity by analyzing 70 samples. Those samples are cylindrical with a diameter of 3 cm and a length of 3.4 cm. They have been used to quantify the lateral and vertical variation within the block.

3.2 Methods of Analysis

Several techniques and methods are used to characterize the petrography and petrophysical parameters of the chosen block. Those methods are categorized under image analysis procedures to process 2D/3D images & laboratory procedures.

3.3 Petrography

Thin sections

Polished thin sections with blue dye impregnation and covered with glass (Figure 2.3) were prepared for petrographical characterization and quantification. Two-dimensional mineral composition, pore and grain size distribution, and mineral growth phases were studied. For the image acquisition and quantification we used a Leica Camera, Polarization/fluorescence microscope and Qwin image analysis software.

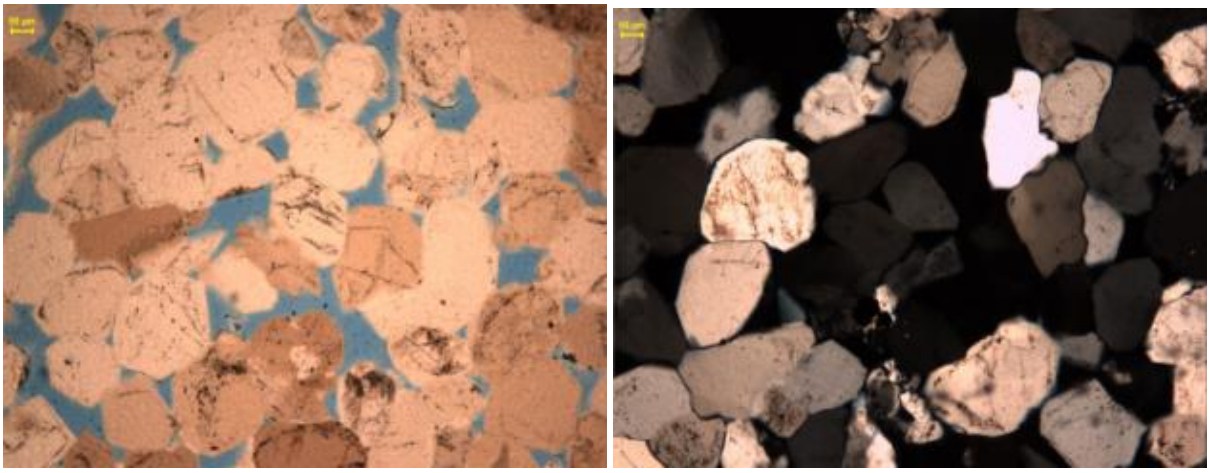

A **B**

Figure 2.3: A: Fontainebleau thin section image. B: Image with polarized light

Micro-CTS and Scanning Electron Microscopy (SEM)

A Phoenix Nanotom™ Micro-CT scanner (mCT) of 180 kV/15 W, with a nanofocus computed tomography system, was used to create 2D stacks of Fontainebleau sandstone (Figure 2.4 A). It is equipped with a 5 megapixel detector and a maximum voxel resolution of <5 µm. A pencil type sample, 120 mm in length and with a diameter of 6.7 mm (or ca. 30

grains width) provides a representative number of grains and associated pore framework. The stacked 3D volumes were reconstructed with AVIZO™ software. Also, several photos at different magnification/scale were taken using scanning electron microscopy (Philips FEG XL40, equipped with Apollo EDX detector) (Figure 2.4 B).

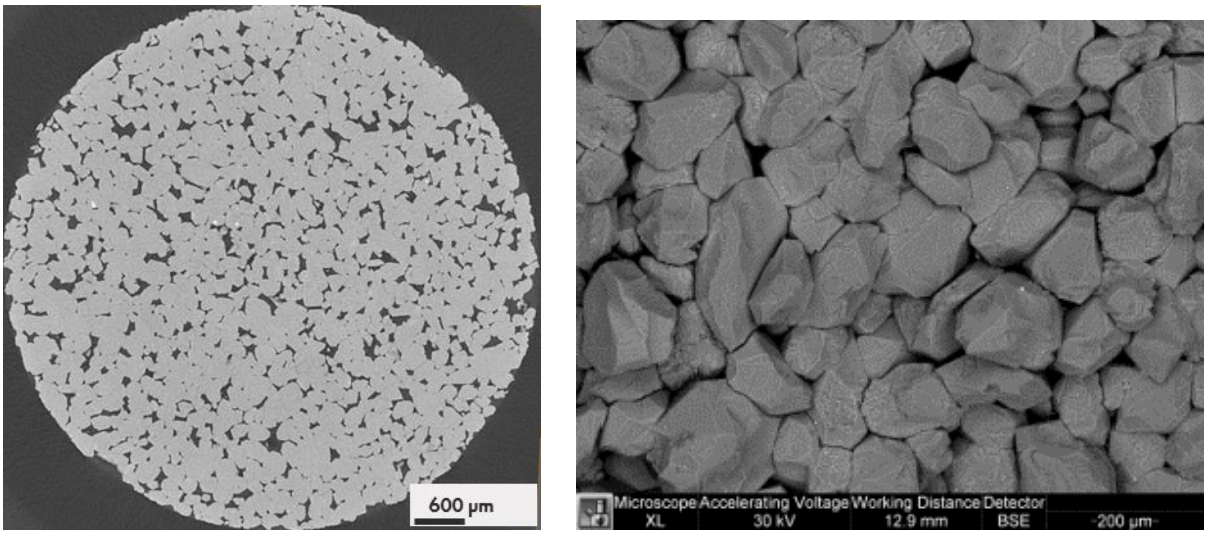

Figure 2.4: Fontainebleau images, A: Micro-CT, B: SEM

XRD

X-Ray diffraction is used to identify the crystallographic nature of minerals, irrespective of their chemical composition. The set-up consisted of a Bruker D8 advance diffractometer and a Lynxeye position sensitive detector, with Cu Ka radiation. Moreover, it indicates the presence of amorphous phases and indicates the approximate abundance of different mineral phases.

XRF

The X-ray fluorescence measurements were performed with a Panalytical Axios Max WD-XRF spectrometer and data evaluation was done with SuperQ5.0i/Omnian software. Powder was pressed into a tablet with binder and measured in vacuum. The X-ray fluorescence analysis provides the chemical composition of the oxidized elements in weight %.

XRD/XRF combination

By combining XRD mineral content and XRF element distribution, synthetic mineral composition can be reconstructed in weight %, volume % and mole %. The method is explained by Wolf (2006).

Image analysis

Analysis of the 2D and 3D discrete images from the thin sections, SEMs and micro CT were performed to determine the grain and pore size distributions, specific surface area, pore throat size distribution and channel lengths. Furthermore, 2D thin section image analysis was performed using polarization microscopy. This method is used to identify mineral grain perimeters by their polarization color and extinction angle. In addition, simple

pore/grain distribution is possible with point counting of about 100 – 120 random points in each thin section. The proportion of each mineral in the rock and, consequently, the quantitative mineralogical composition are obtained by mineralogical determination at each randomly selected point.

3.4 Petrophysics

Di-electrical measurements

Conductivity measurements were done on 9 different Fontainebleau samples for 5 different brine salinities. The porosity of the samples was between 0.07 to 0.1 with NaCl brine salinities varying from 30 ppm to 60,000 ppm. Figure 2.5 shows a comparison between the conductivity measurements and literature. The set-up has a range of 1000 µS/cm with a precision of 0.01 µS/cm.

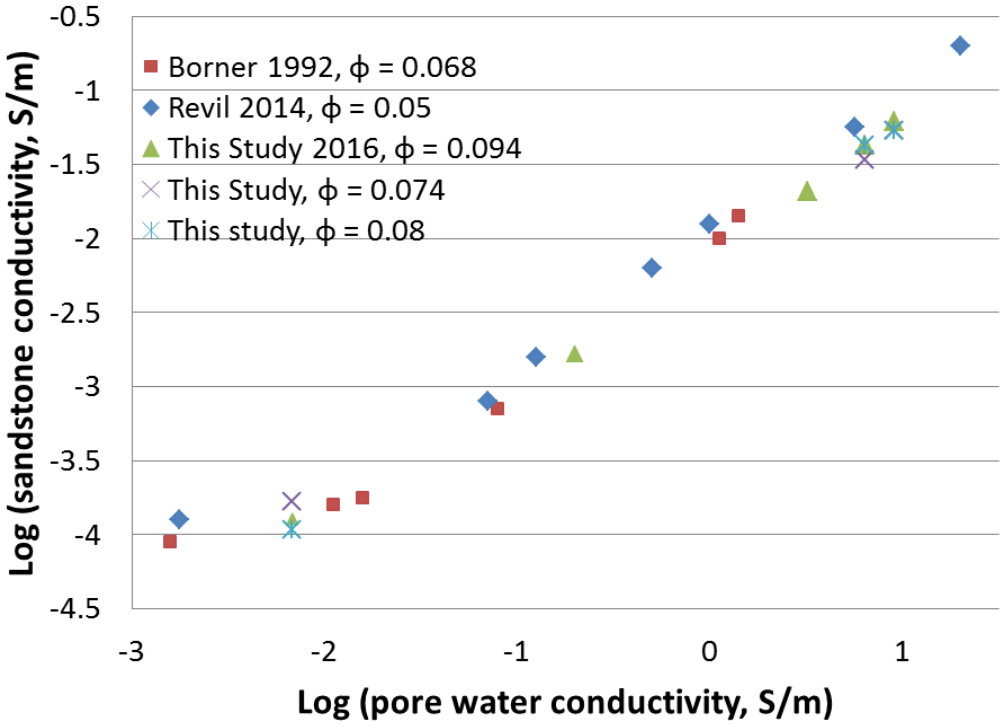

Figure 2.5: Saturated Fontainebleau sample conductivity vs brine conductivity

Experimental Procedure

Conductivities were measured at 23 °C on fully saturated samples with different, known conductivities. All samples were fully evacuated before saturation. The sample was then placed into an insulator and the conductivity of the saturated core samples was measured, in order to determine the formation and cementation factors.

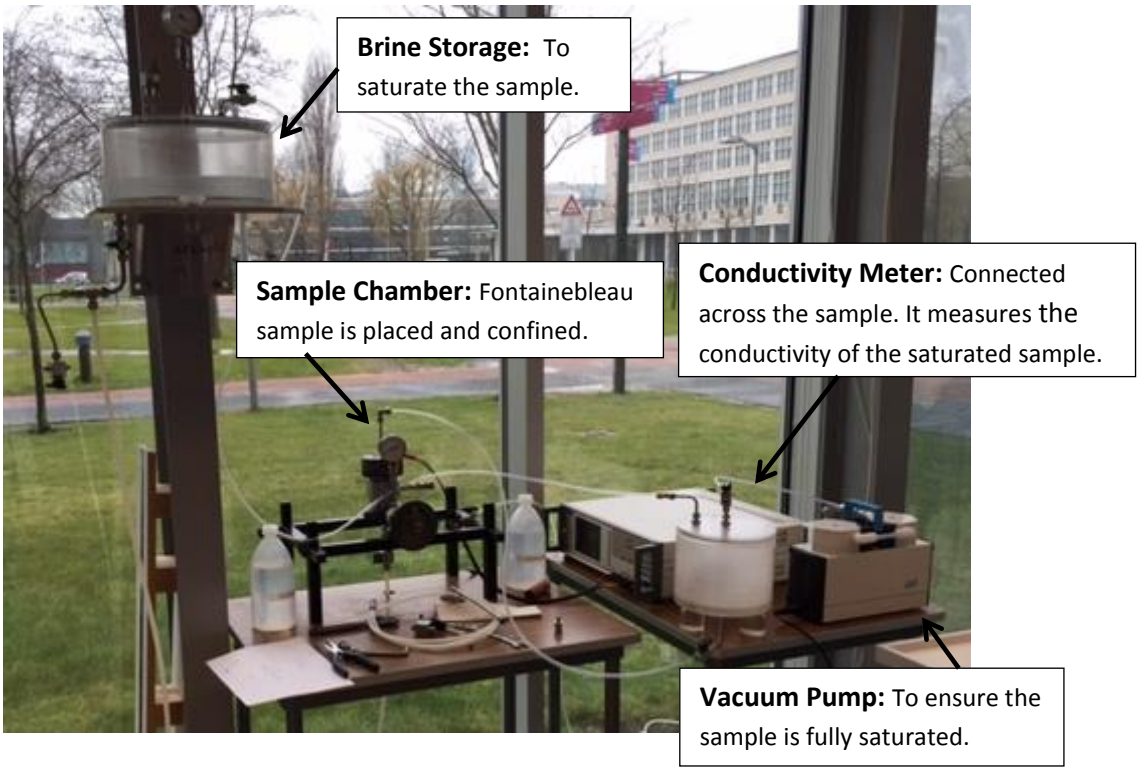

Figure 2.6: Set-up for measuring conductivity.

Zeta potential

The zeta potential measurements are carried out in a Malvern Zetasizer-nano ZS90. Zeta potential is measured using a combination of electrophoresis and laser doppler velocimetry. To increase sensitivity, the instrument uses both the Mixed Mode Measurement (M3) and the Phase Analysis Light Scattering (PALS) techniques.

The essence of a classical micro-electrophoresis system is a cell with electrodes at either end, filled with brine and crushed sandstone sample material, to which a potential is applied. Particles move towards the electrode of opposite charge, and their velocity and size are measured and expressed in unit field strength as being their mobility by using laser-Doppler techniques.

Capillary pressure:

Capillary pressure curves have been measured by centrifuge (CM) (Figure 2.7 A), and mercury intrusion porosimetry (MICP) (Figure 2.7 B). Porous plate technique is the most accurate, however, it was not used since it was too time consuming as it could take more than 20 weeks to acquire an oil–water drainage curve (Wilson et al, 2001).

1- Multi-speed centrifuge experiments:

Hassler and Brunner (1945) proposed a fast method to set up the saturations in a high speed centrifuging. The core sample is placed into a centrifuge tube and rotated at a number of different speeds selected to cover pressure differences between phases required for the particular cores. At each step, the rate of rotation is maintained constant until phase stabilization.

2- Mercury Injection Capillary Pressure (MICP) analysis:

MICP directly measures pore volume distribution by forcing Hg (mercury) into pore space. The injection determines the sample's interconnected pore system and the size distribution of pore apertures (capillaries) that strongly influence the non-wetting phase (e.g. hydrocarbon) saturations and fluid flow (e.g. permeability).

MICP measures pore-throat size distribution, total pore volume, total pore surface area, sample density and imbibition/drainage capillary pressure data.

A B

Figure 2.7: A: Centrifuge experiment, B: Micromeritics autopore IV

4. Data, Results and Discussion

Our experimental results, presented here below, are when possible explained and discussed in relation to the data available from literature. Most conclusions will also be stated as a comparison between our work and other academic literature.

4.1 Petrography, Mineralogy and Texture

XRD-XRF results: The detected XRD mineral is only quartz (Figure 8). XRF shows trace amounts of other oxides (Table 2.2). After processing the XRD and XRF data by using MINCOMP software (Wolf, 2006), the synthetically reconstructed clays are illites (0.0015) and kaolinite (0.0039).

Compound	Concentration Weight (%)	Absolute Error (%)
Silica (SiO_2)	99.451	
Aluminum Oxide(AL_2O_3)	0.246	0.010
Iron III Oxide (Fe_2O_3)	0.056	0.007
Calcium Oxide (CaO)	0.052	0.007
Sodium Oxide (Na_2O)	0.035	0.006
Sulfur Trioxide (SO_3)	0.033	0.005
Titanium Dioxide (TiO_2)	0.031	0.005
Chloride (Cl)	0.023	0.005
Magnesium Oxide (MgO)	0.023	0.005
Phosphorus Pentoxide (P_2O_5)	0.019	0.004
Potassium Oxide (K_2O)	0.014	0.004

Reconstructed Minerals	Mole	Weight	Volume
Quartz	0.9972	0.9903	0.9906
Kaolinite	0.0009	0.0038	0.0039
Illite	0.0002	0.0015	0.0015
Pure Albite	0.0003	0.0013	0.0013
Chloride	0.0001	0.0008	0.0008
Calcite	0.0003	0.0005	0.0005
Siderite	0.0002	0.0004	0.0003

Table 2.2: XRF Data and Reconstructed Minerals

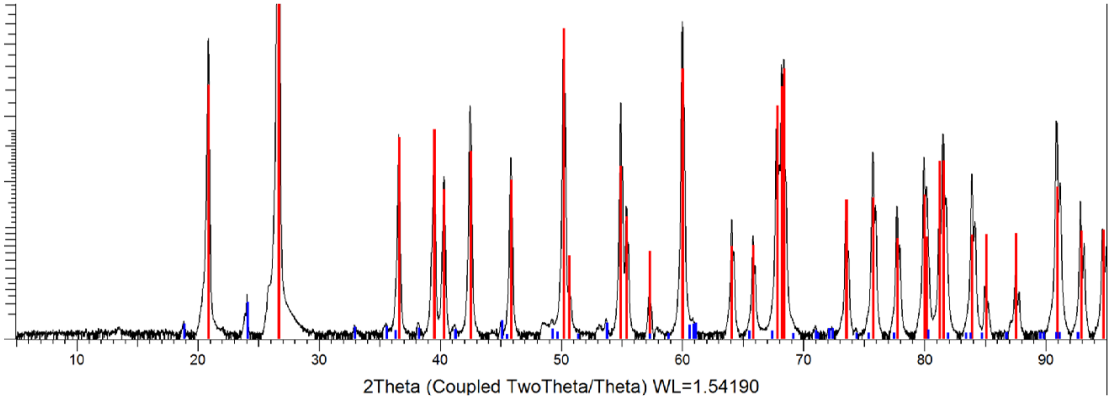

Figure 2.8: The measured XRD pattern in black, after background subtraction. The red lines are peak positions and intensities of known mineral phases. Only quartz was found; the extra peaks, indicated with the blue stick pattern, are due to the Kb contribution in the incident X-ray beam.

Thin section results:

Scanning the images with polarized light showed that visually only quartz is present and no clays are found in the pores (Figure 2.9). Moreover, as inclusions in the overgrowth quartz, some dirt oxides and clays may be available. They are, however, not connected to any of the pores.

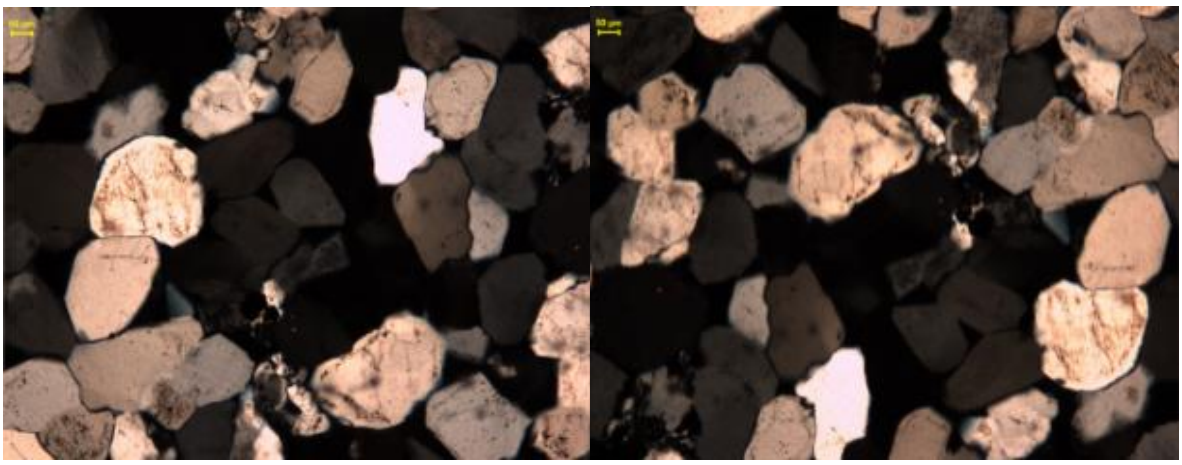

Figure 2.9: Images with polarized light: crossed Nicolls; the view field length is 1 mm.

SEM results.

Using spot analysis, accessory clay was examined in several areas (Figure 2.10). All results indicate that the minerals are mostly quartz with minor traces of clay at fractured interfaces and NOT on the pore-walls. (See 1 and 2 of the polished sample where the small amount of aluminum is indicated).

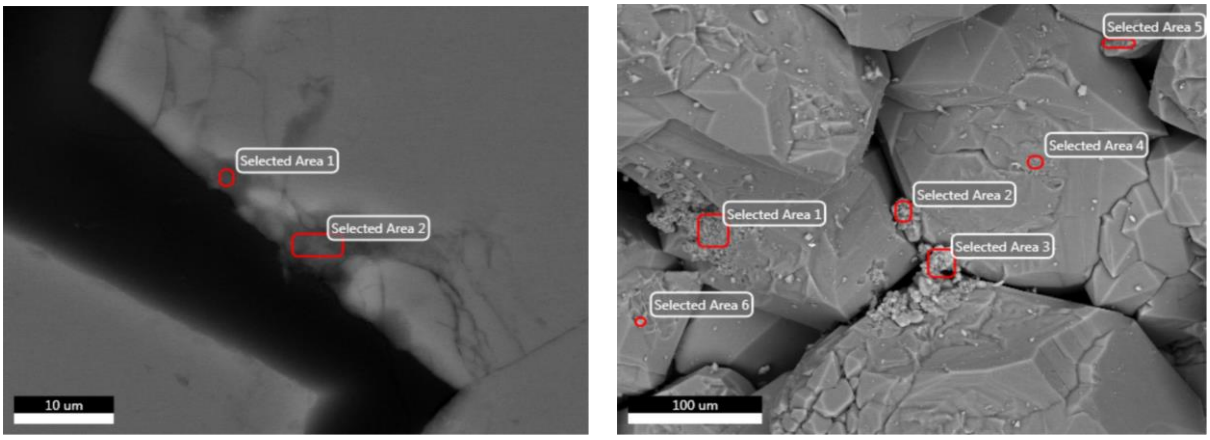

Figure 2.10: Selected Areas via SEM to examine the presence of clay.

Quartz Overgrowth

Quartz-overgrowth clearly dominates the cementation around the original detrital quartz grains (Figure 2.11 A). Based on image quantification, the measured overgrowth is estimated to be around 0.15 for high porous sandstones, increasing to 0.20 for lower porosities. The overgrowth in these lenses may reach as much as 0.35 BV.

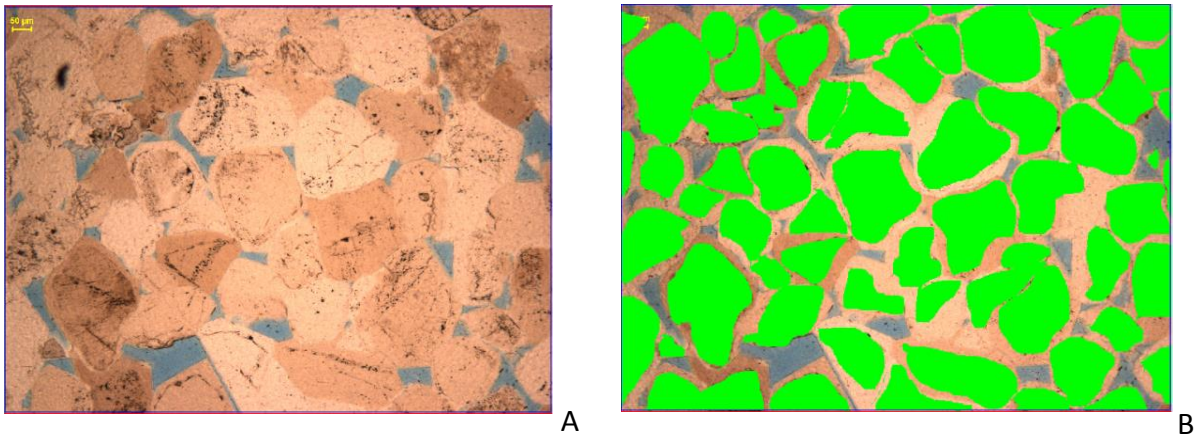

A B

Figure 2.11: A. Quartz overgrowth around original “dirty” grains, In thin sections, the fines can be recognized as dark brown patches. These circular dust lines represent an earlier grain shape, which has overgrown at a later stage. The fines in the overgrowth part represent the rims of the grain shape before quartz overgrowth started. B. Definition of the original grain core (green) in the right image; the beige color shows the overgrowth, blue represents the pore space.

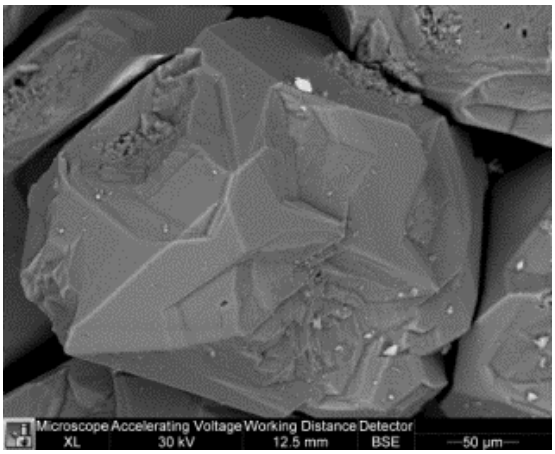

A

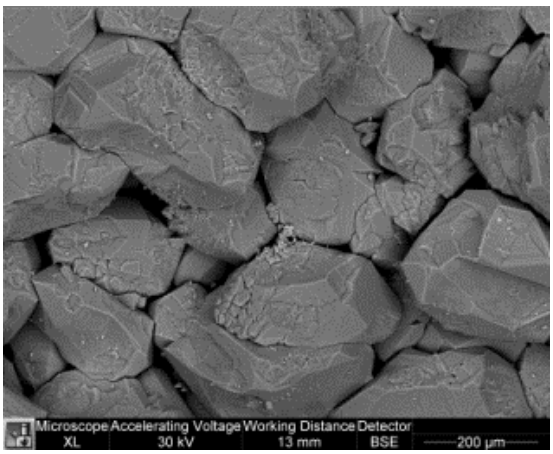

B

Figure 2.12: SEM images, angular surface and sharp edges due to the quartz overgrowths

It can be concluded that XRF/XRD, polarization microscopy & SEM confirm that Fontainebleau sandstone consists of almost pure quartz (over 0.995% SiO_2) with very clear quartz overgrowth starting from a smaller grain that is represented by the inclusions. The amount of clay is less than 0.005 and has not been observed in thin sections or SEM at a pore face. This result is in line with the literature (Thiry et al., 1988; Haddad et al., 2006; French et al., 2013). Quartz overgrowth is evident and causes the reduction in porosity by reducing the pore throat size.

4.2 Pore and Grain Framework:

For the two clusters of porosities in our sandstone sample (0.06 and 0.10), micro-images from thin sections, micro-CT and SEM, (Figure 2.13) were prepared and analyzed on their spatial characteristics.

Comparison of the two different thin sections (Figure 13, Table 3), shows that the pore area hardly changes but the pores' throats reduce in area. It results in a slight reduction in porosity and a more significant reduction in permeability. The CT-scan pore area distribution (Figures 13C, 13D) and the SEM surface images (Figures 13E, 13F) confirm this statement.

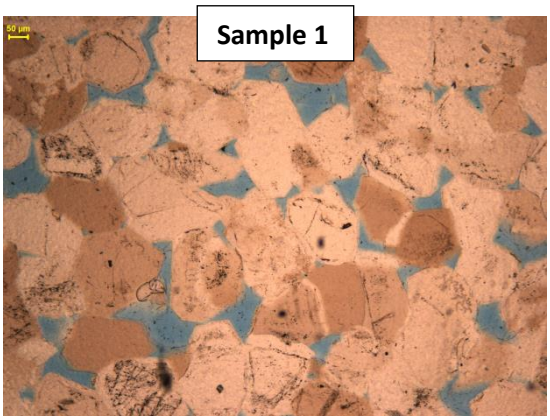

A

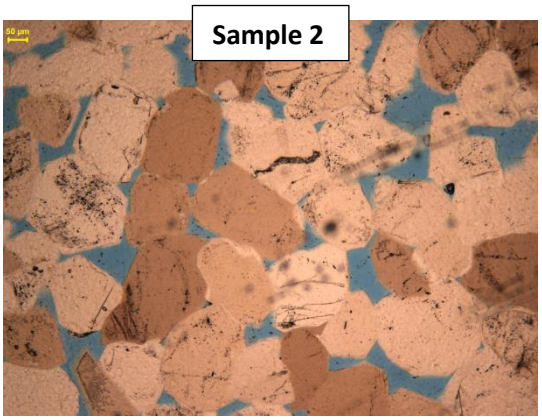

B

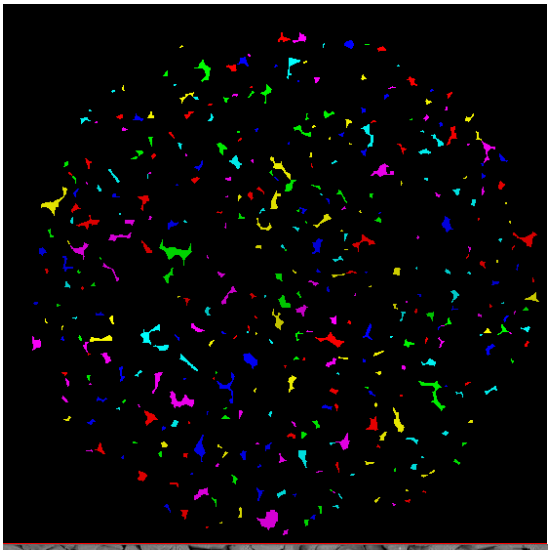
C

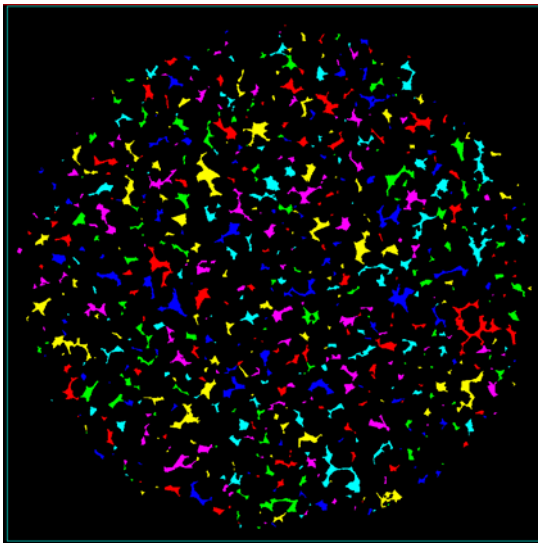
D

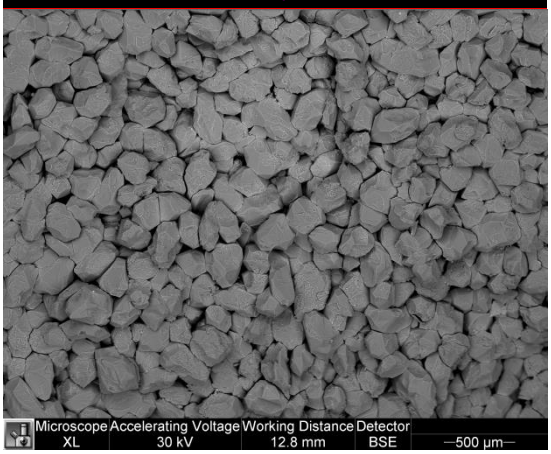

E

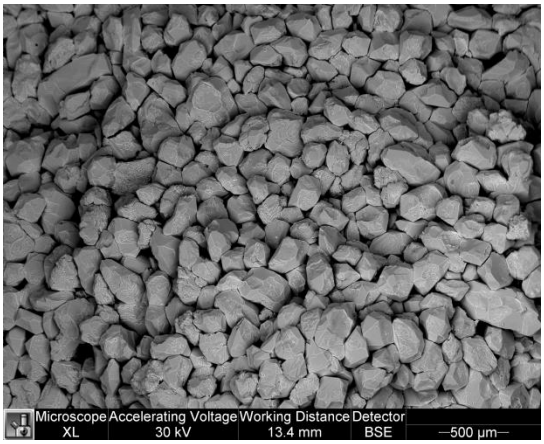

F

Figure 2.13: Thin sections (matrix grains and overgrowth and pores), Micro-CT images (pore space detection) and SEM (grain framework surface characterization)

	Measured porosity	Image porosity	Grain size distribution, µm	Pore size distribution, µm	Permeability mD
Sample 1	0.06	0.063	100 – 300	20 – 100	18
Sample 2	0.101	0.104	100 – 300	20 – 100	250

Table 2.3: Fontainebleau sample comparisons

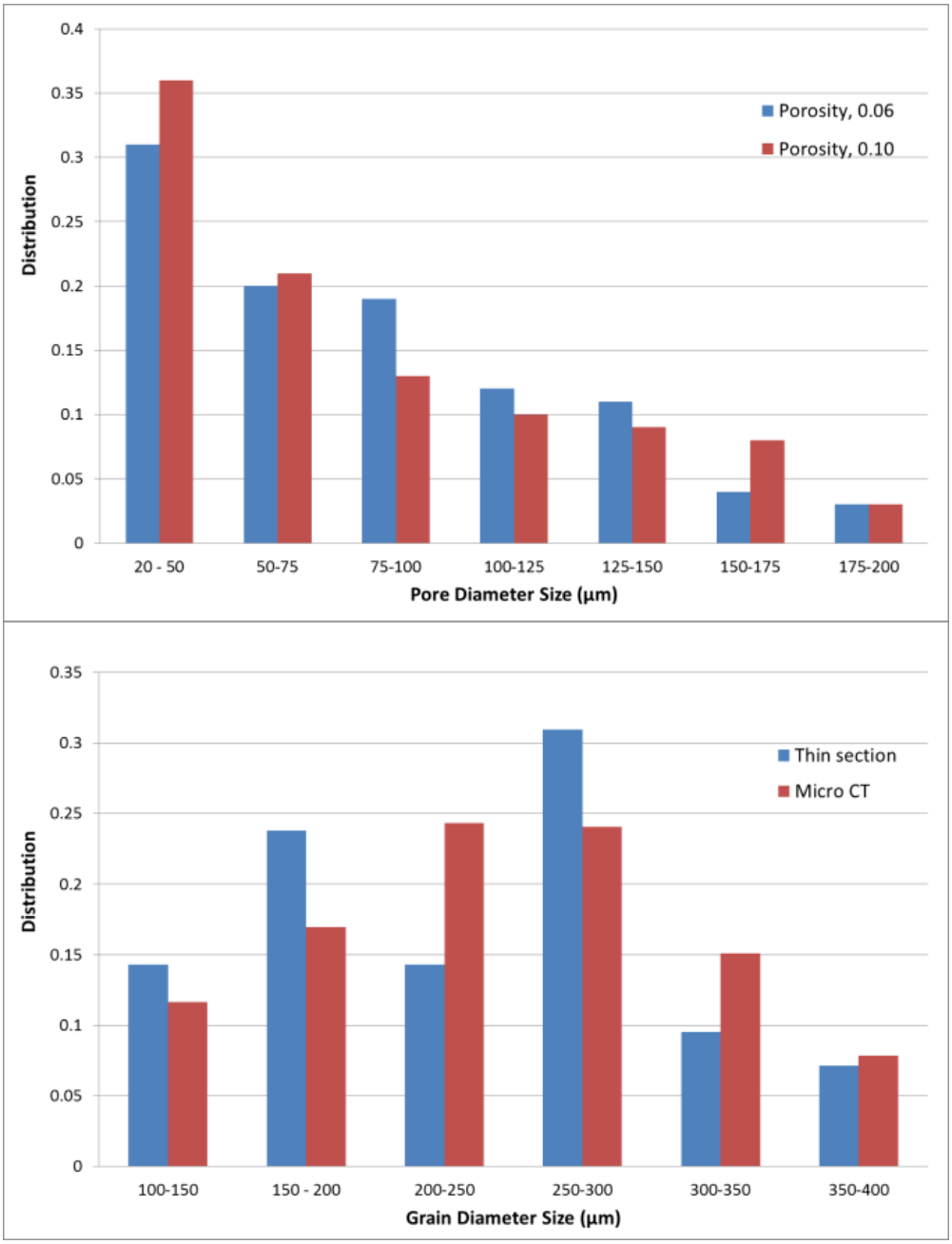

Figure 2.14: Pore and grain size distribution.

In summary, results and comparisons between micro CT, SEM and thin sections indicate almost constant pore size and grain size distributions. The grain diameters are in the 100 – 300 µm range; the pore sizes are in the 20 – 100 µm range; the throat diametres vary between 10 – 30 µm. These results are comparable with the literature (Table 2.1).

4.3 Petrophysics

Permeability-Porosity relation:

Within the sample block, 70 plugs were measured on their porosity and permeability, showing the variation sub-parallel to the stratification (Figure 2.15). In general, the permeability was between 10 mD to 400 mD and the porosity ranged from 0.05 to 0.15.

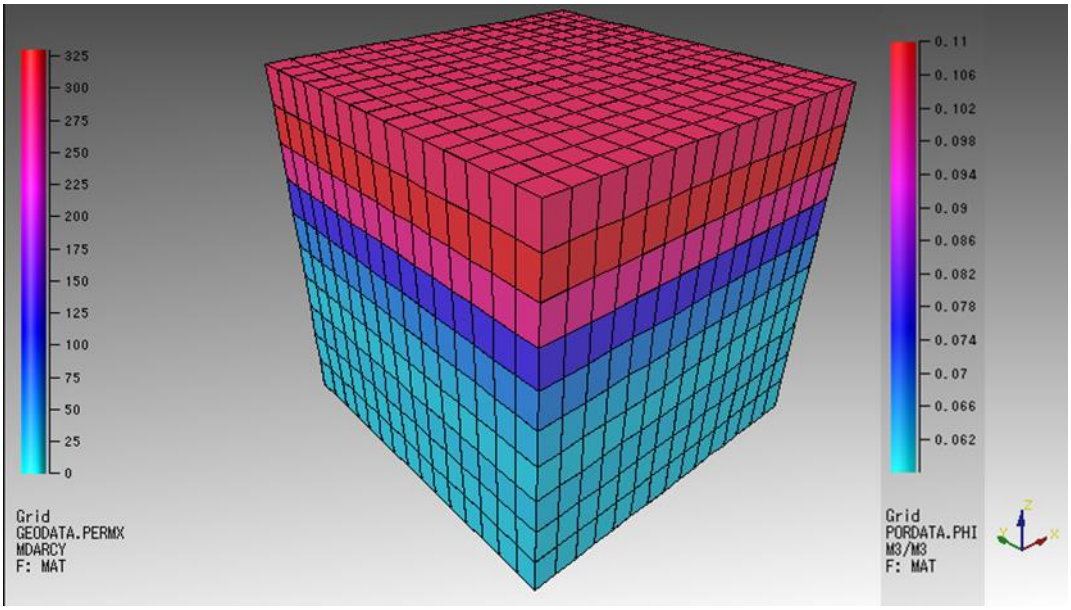

Figure 2.15: Permeability and Porosity variation within the block.

The measured permeability and porosity of the samples are consistent with Zinszer's data set (Zinszer et al, 1985). Combining the experimental results of Bourby (1985), Doyen (1988), Fredrich (1993), Gomez (2010), Reveil (2014), and this study (2016), an improved phi/k-relation was developed; $k = 10^{6.5 + 4.6 \log(\phi)}$; $R^2 = 0.95$. Note that the grain size distribution, degree of leaching and cementation were not considered for this relation.

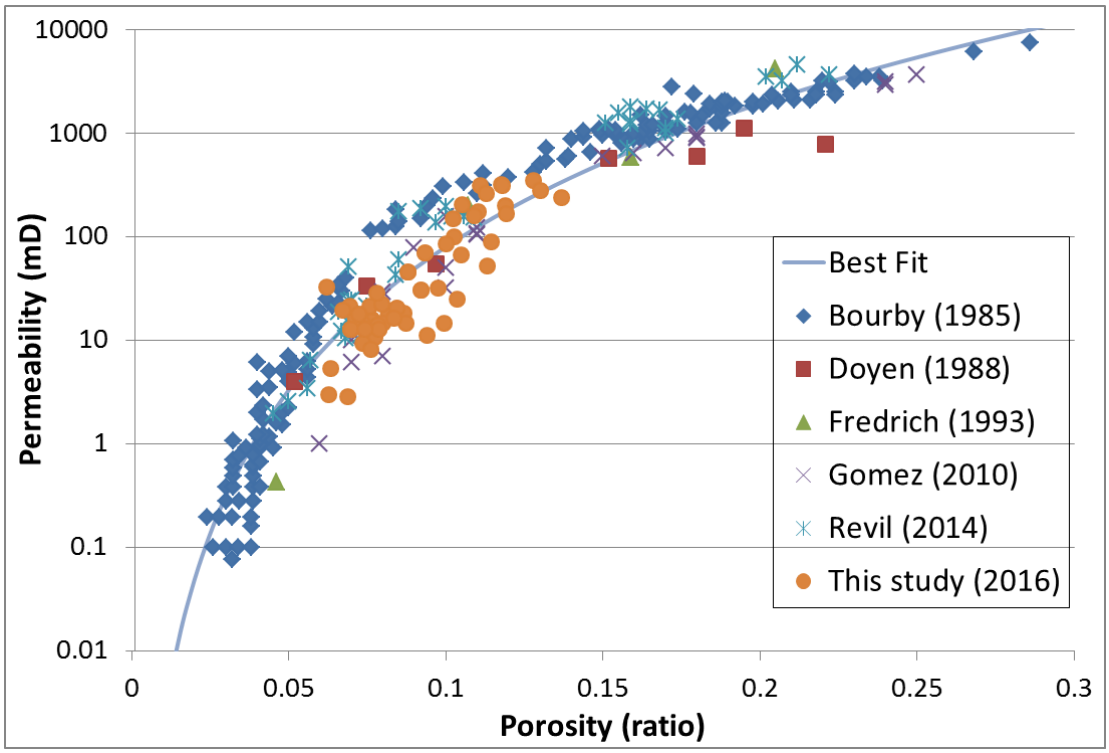

Figure 2.16: Porosity vs Permeability of Fontainebleau sandstone

Prediction of Fontainebleau Permeability with cementation following the Panda and Lake Model

Panda and Lake (Panda and Lake, 1994 and 1995) proposed a modified Carmen-Kozeny (CK) model, which analytically relates the contribution of the particle size distribution statistics (i.e. mean, standard deviation and skewness) and the contribution of the types and amounts of various cementing clays present, to the permeability. We applied the model to calculate a theoretical permeability and compare it with the measured permeability.

$$k = \left[\bar{D}_P^2\,\theta^3\,(\gamma C_{D_P}^3 + 3C_{D_P}^2 + 1)^2\right] \div \{2\tau_e(1-\theta)^2[6(1+C_{D_P}^2)\frac{1-\theta_o}{1-\theta} + (a_{vb}P_b + a_{vl}P_l + a_{vf}P_f)\bar{D}_P(\gamma C_{D_P}^3 + 3C_{D_P}^2 + 1)]^2\}) \qquad \text{Equation 2}$$

The symbols are explained in the symbols list.

In essence the values for spatial characteristics and their statistical values have been obtained through image analysis on the thin sections, CTs and SEM:

- Particle size distribution statistics through the spatial analysis of SEM and thin sections and Micro CT
- Mineral composition through XRD/XRF; it confirmed that accessory minerals and oxides are present.
- SEM and thin sections confirmed that the accessory phases are inclusions in the quartz overgrowth
- The amount of cementation (i.e. quartz overgrowth) was directly estimated from thin sections through image analysis

Following the steps of Panda and Lake (Panda and Lake, 1995), we first estimated the permeability using the original equation neglecting the effect of cements (Figure 2.17A). Thereafter the cement component was included (Figure 2.17B). It can be seen that the Panda and Lake Model estimate gives a good match with the experimental data. For our porous medium, it confirms that permeability is more influenced by the volume of cements than the parameters of particle size distribution. When implementing the modified equation, the contribution of the “cementation-relation” gives a good match.

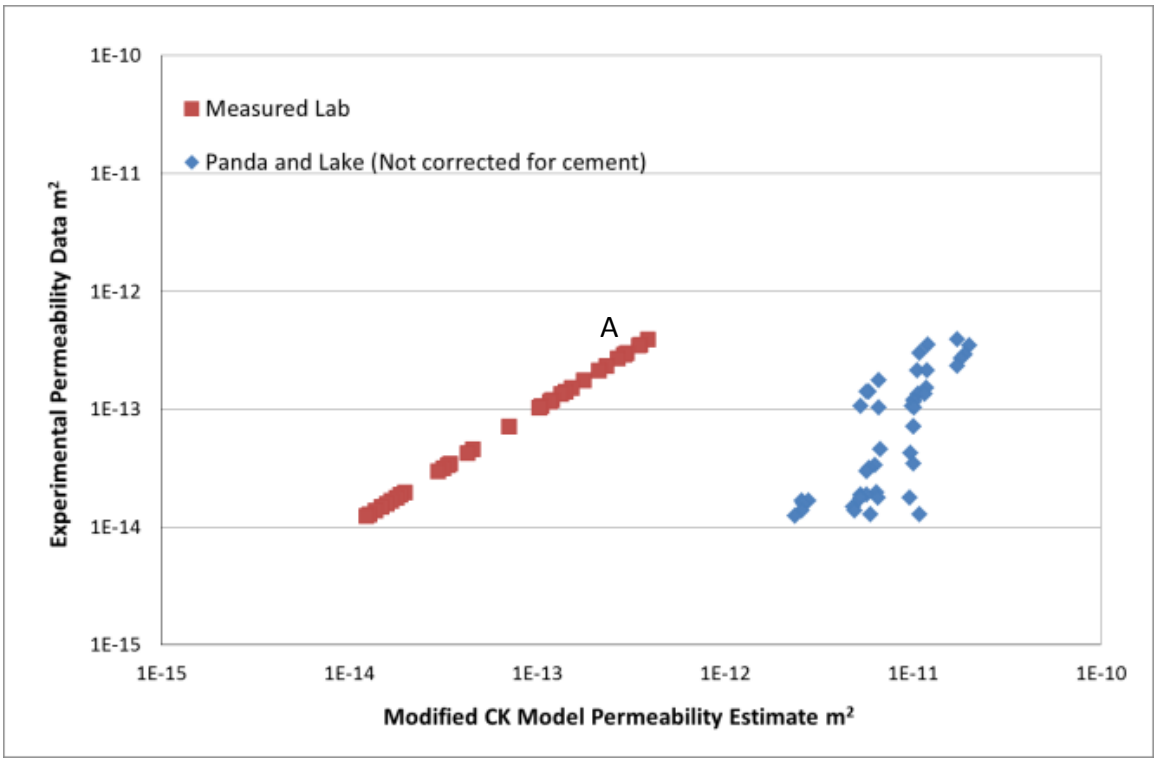

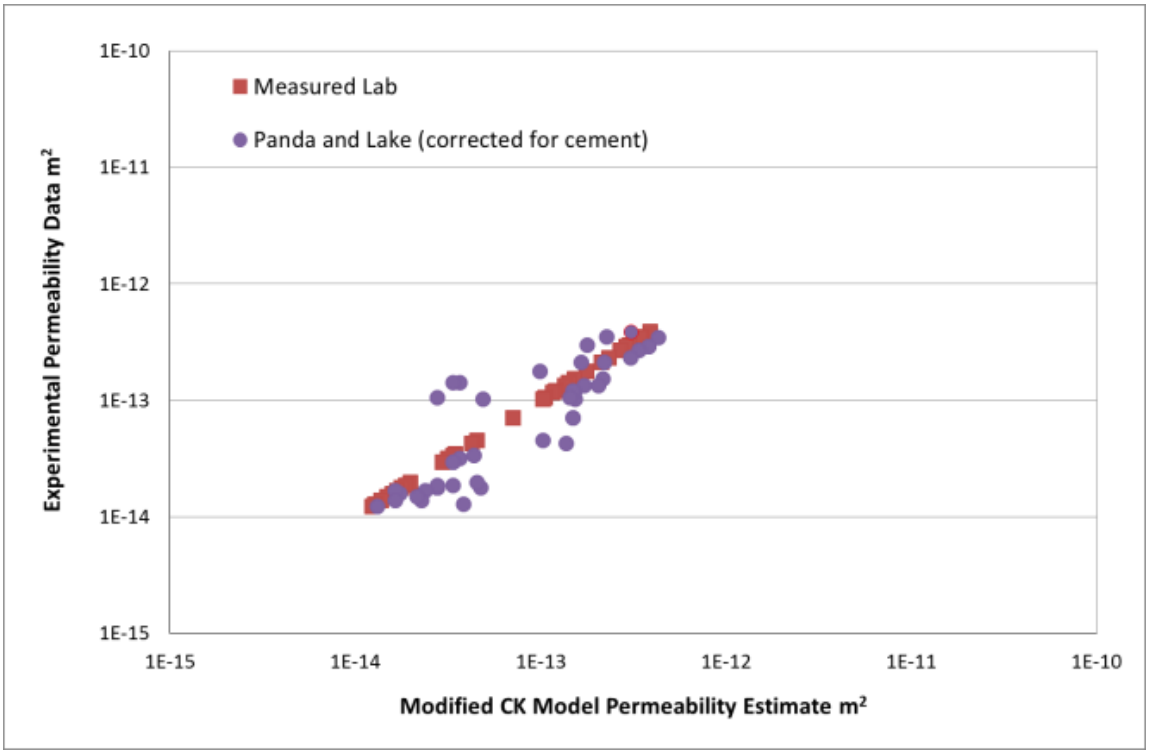

Figure 2.17. A. Variance between the permeability model estimation (not corrected for cement) versus the experimental data. B. Comparison but using the modified CK Model as proposed by Panda and Lake, which includes the effects of cements.

MICP and centrifuge: Fontainebleau pore throat size distribution and capillary pressure

The results in the previous sections already demonstrated that the permeability depends on the reduction of pore throat diameter through quartz overgrowth. To verify this pore throat size distribution, mercury injection measurements of six samples used for poro/perm measurements were taken. The capillary pressure curve was caclulated through oil-brine drainage. The results show pore throat size distribution from 10 to 30 µm (Figure 18) and shows the impact of the permeability reduction on the pore throat sizes. Permeability decreases with decreasing pore throat size and it explains the permeability reduction with a limited decrease in porosity (Figure 16).

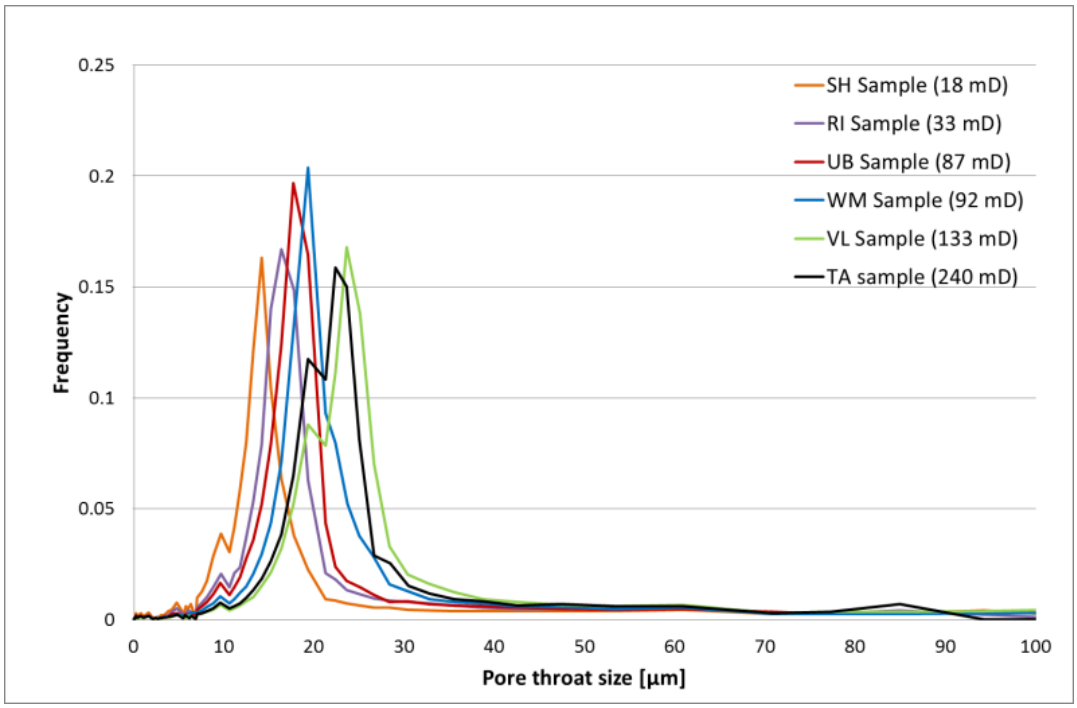

Figure 2.18: Fontainebleau Pore throat size distribution from MICP

The measurements also provide the relation between pressure and water saturation (Figure 2.19). The results show for samples one pressure step, which means that a narrow range of capillary curves in the porous medium are present. In other words, a narrow band homogeneous throat size distribution.

Centrifuge experiments were performed as a verification of the MICP data (Figure 2.19). They indicate that the centrifuge results agree with those of the MICP. This is another indication that the Fontainebleau is a homogeneous system with limited band widths in porosity, pore throat diameter and associated permeability.

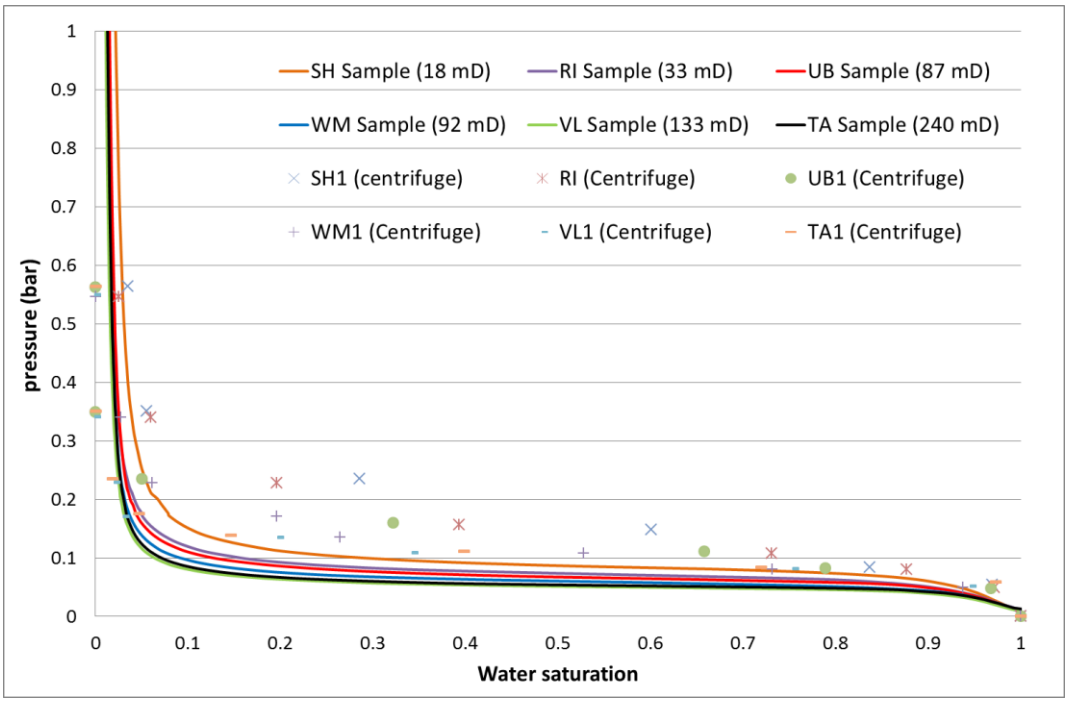

Figure 2.19: Fontainebleau centrifuge experiments (crosses, dots and lines) compared to the MICP data

Both measurements show that the Fontainebleau is strongly water wet. A characteristic feature of the drainage capillary pressure curve for two nearly incompressible fluids (like oil and water) is the minimum value of the wetting-phase saturation; the residual saturation (Swi), is reached asymptotically as the capillary pressure increases toward extreme values. Specifically, when considering an oil-water reservoir, the wetting phase (i.e. water) occupies the small spaces and oil droplets tend to sit in the center of the pores (Figure 2.20). During waterflooding, both phases flow and the oil relative permeability (kro) will be high, since oil flows through the largest pores, and decreases as oil saturation decreases. Eventually, all continuous flow paths are water-filled, and oil stops flowing.

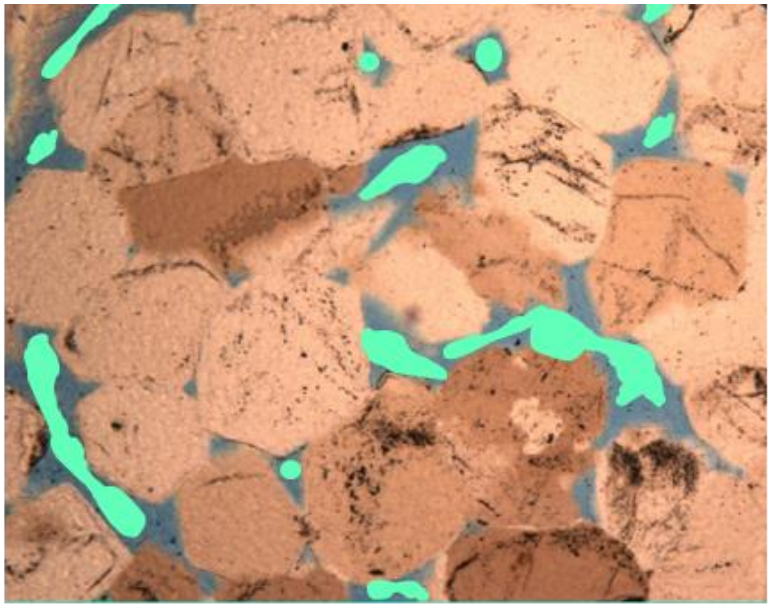

Figure 2.20: Thin section of Fontainebleau Sandstone. Green colour represents oil phase; blue colur represent water phase; rest is grains.

Di-electric properties

The conductivity of the saturated brine samples increases in proportion with the salinity (Figure 2.21). Note that the brine only involved Na and Cl-ions. In addition, the brine sample conductivity shows a positive correlation with porosity. This is due to the increase of pore throat area size and the creation of more flow area for the electrical current.

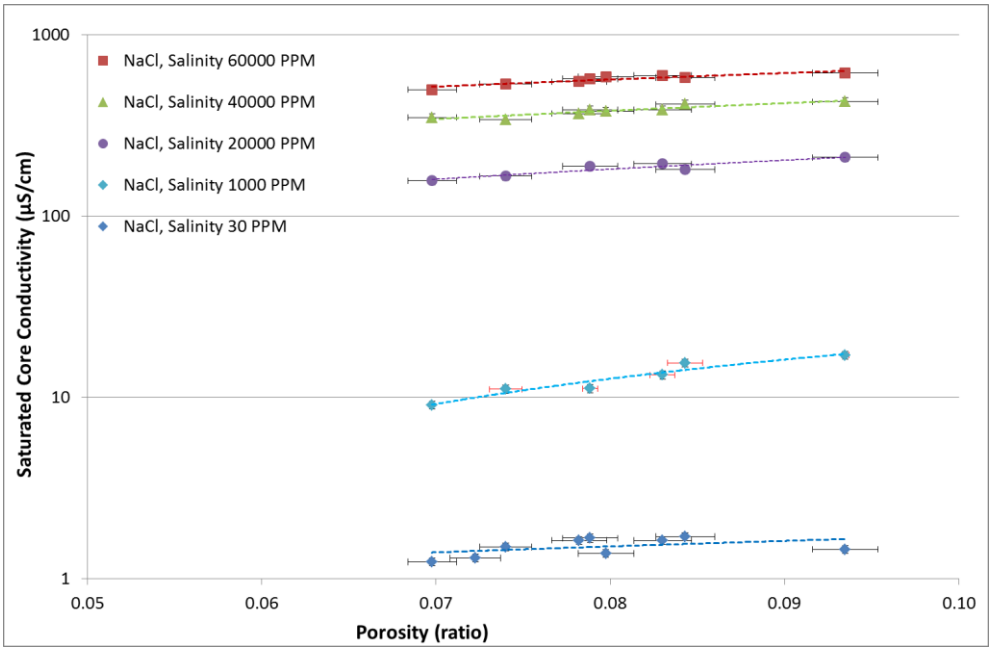

Figure 2.21: Saturated sandstone brine conductivity versus porosity: both, the x- and y-error bars are present; however, for y-error is in log scale.

The formation factor was calculated from the measured conductivities of the brine and saturated brine in the plugs. Figure 2.22 shows that, for the low salinity results (30 ppm), the formation factor is not in agreement with the higher brine salinities. This is attributed to the influence of the grain surface conduction (Revil, 2014) and an uncertainty effect caused by the resolution of our set-up which was too low. Therefore, the 30 ppm results have been excluded from analysis.

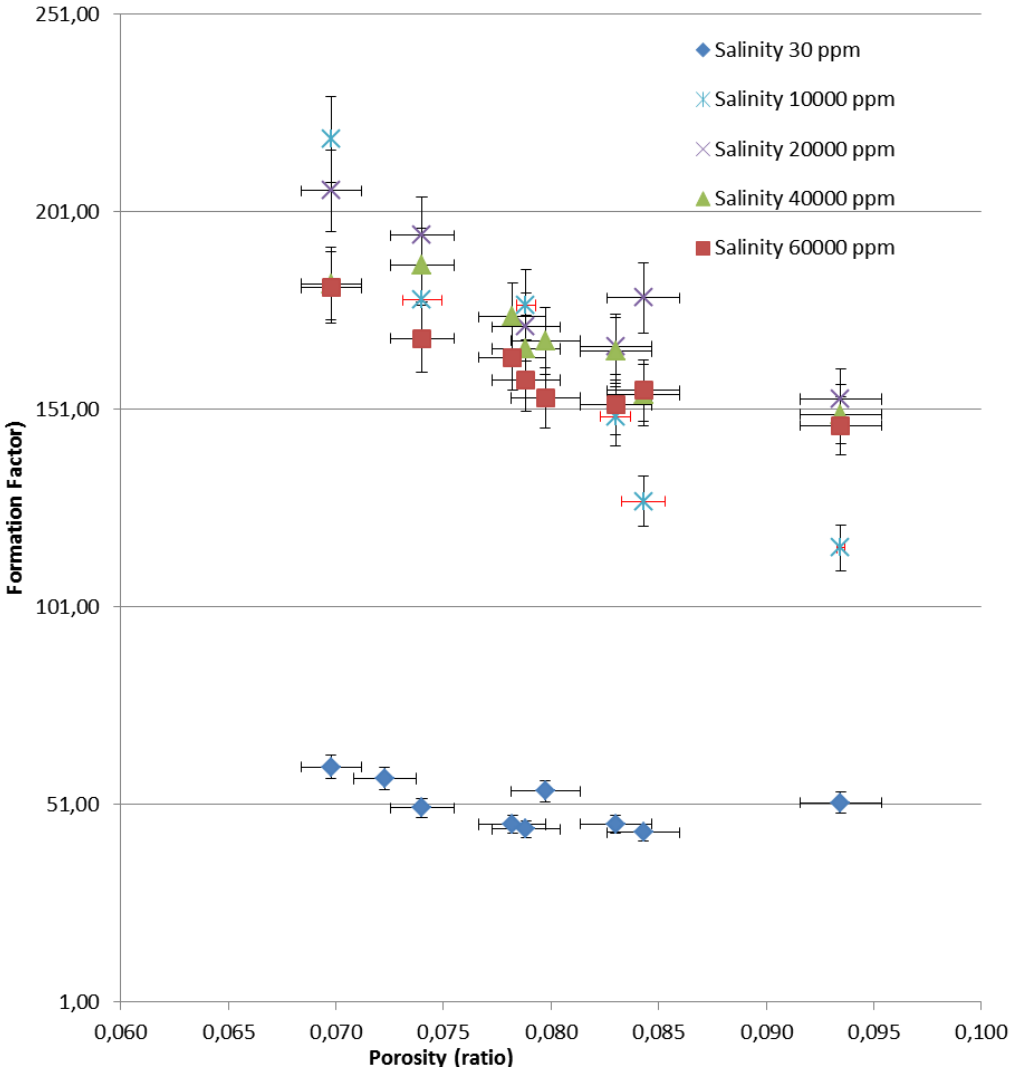

Figure 2.22: Formation Factor vs Porosity

Comparison with the Literature

Figure 2.23 compares the literature data from Doyen (1988), Borner (1993), Gomez (2010), Revil (2014) and this research. The cementation factor (1.95 – 2.05) from our samples is slightly higher than the literature (1.8 – 1.9). This could be attributed to two reasons:

- Our samples are from the top white clean sandstone and from the same spot. The quartz overgrowth and cementation are more evident and dominating. This is also in line with

the CEC which shows zero value. The findings in the literature refer to samples from different locations and different horizons in the top layer.

- Our conductivity results cover a small range of porosities (0.07 – 0.1), which influence the slope (i.e. cementation exponent calculations).

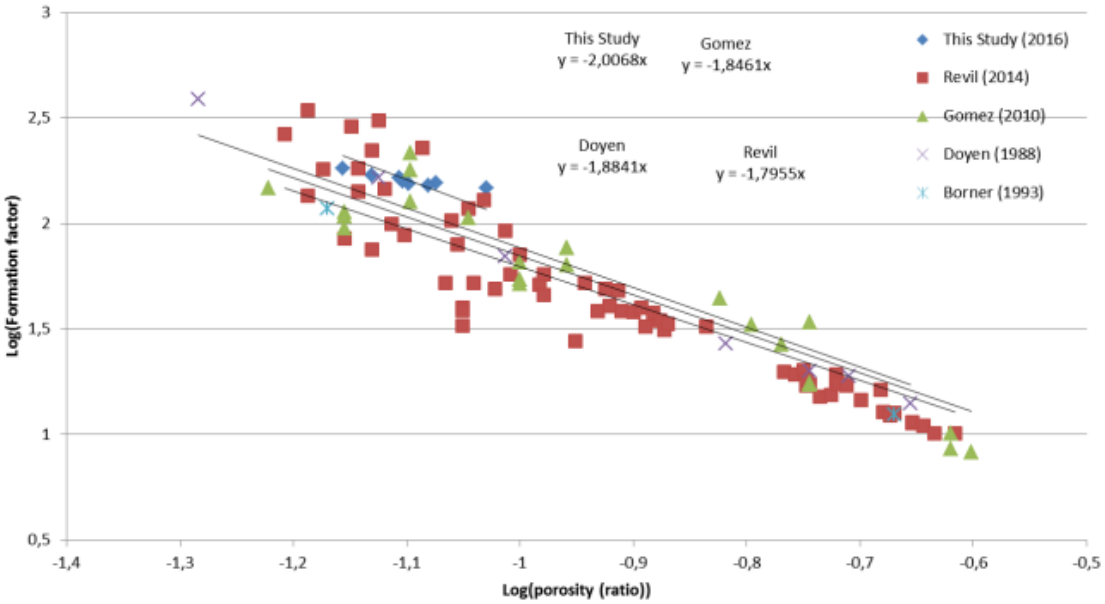

Figure 2.23: Log (formation factor) vs log (porosity).

Fontainebleau sandstone exhibits clean sandstone behavior and the measured formation factor follows Archie 1, i.e. a very insignificant clay content. This is in line with the other measurements from XRD/XRF.

Zeta Potential Results:

1- Zeta Sizer:

For one sample, charged with different brine concentrations, it is clear that the measured zeta potential for Fontainebleau becomes more negative as the salinity decreases (Figure 24).

2- Empirical relationship between the pore fluid concentration and zeta potential:

Pride and Morgan (1991) created a relationship to estimate the zeta potential from pore fluid concentration:

$\zeta = a + b \log (NaCl)$,

where ζ is the zeta potential (mV) and (NaCl) is the brine fluid concentration (mol/l).

Revil et al. (1999) and Jaafar et al (2009) studied this relation over a wide range of fluid concentration in different porous rock types. They concluded that the parameters a and b are -6.43 and 20.85 respectively. This empirical equation is shown in Figure 25.

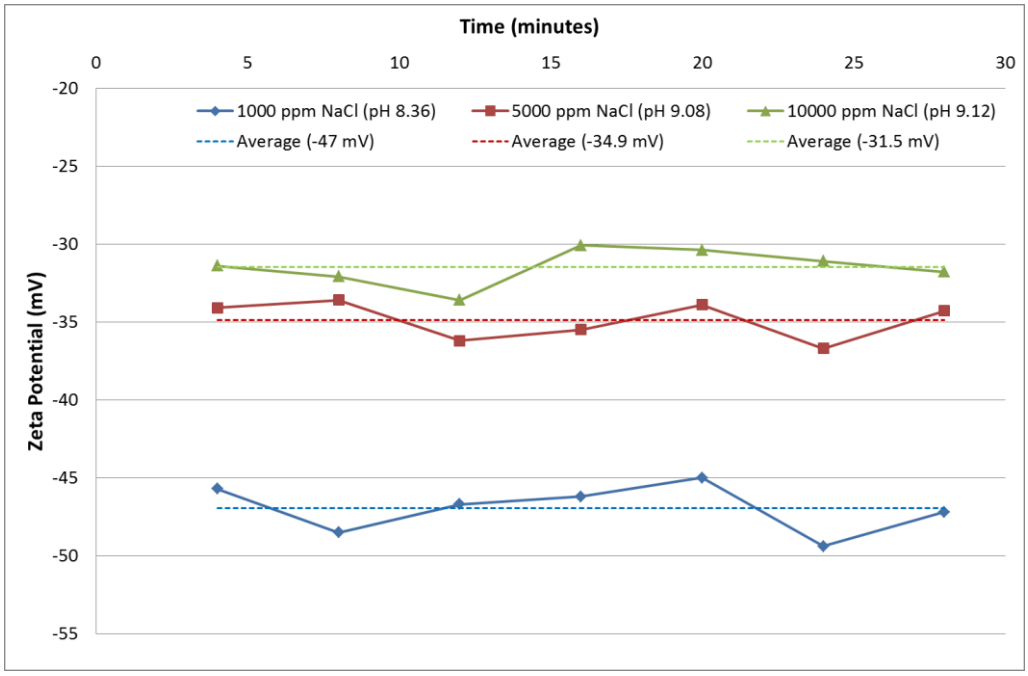

Figure 2.24: Fontainebleau Zeta Potential and pH at different brine salinities.

3- *Streaming-potential coefficent to zeta potential: literature and experimental data of Fontainebleau sandstone.*

The streaming potential is the electric potential that is generated when electrolyte fluid flows through a stationary charged solid, such as porous media, by an applied pressure gradient. Helmholtz and Smoluchowski (1997) quantified streaming potential (CS) in capillary tubes and they developed an equation knows as HS equation given as:

$$C_s = \frac{\Delta V}{\Delta P} = \frac{\varepsilon_r \varepsilon_o \zeta}{\eta_f \sigma_f} \qquad \text{Equation 3}$$

Here, C_s (V/m) stands for streaming potential coupling co-efficient and is the ratio of ΔV (V) the measured streaming potential to ΔP (Pa) the applied fluid pressure difference that drives the fluid through the capillary tube; ε_r is the relative permittivity of the pore fluid; ε_o is the electric permittivity of free space (≈8.854 10 – 12 F/m); η_f is the dynamic viscosity of the pore fluid (Pa.s); ζ refers to zeta potential and σ_f represents the pore fluid electrical conductivity.

Further modifications in streaming potential formula, mentioned above, have been published by Glover et al. in 2010. They develop formula that links the streaming potential coefficient (Cs) to the zeta potential (ζ) with respect to the mean pore radius and the mean grain diameter respectively, which yield:

$$C_s = \frac{\Delta V}{\Delta P} = \frac{\varepsilon_r \varepsilon_o \zeta}{\eta_f (d\sigma_f + 6\Sigma_s(F-1))} \qquad \text{Equation 4}$$

where, Σ_s refers to the specific surface conductance, d is the mean grain diameter and F is the formation factor,

The streaming potential coupling coefficient in the NaCl saturated core of Fontaineblau sandstone measured and from the results, the zeta potential was calculated using Eq 3 and imperical Eq 4 (Figure 2.25)

The calculated zeta potential from the streaming potential experimental data is slightly higher. The Zetasizer measurement is a quick and easy method to determine the small amounts of dispersed particles. However, it requires fine-grained crushed rock (300 µm). Crushing creates new surface areas and a higher specific area per unit volume, which is considered to be representative for the original larger grains with exponentially less specific pore area. Therefore, the definition of a representative surface sample is important. Figure 25 shows that the measured zeta potential from the Zetasizer is in line with literature data and the empirical equation.

As an alternative, the streaming potential can be measured in exactly the same conditions as the coreflow experiments. However, the methodology of conversion of streaming potentials into zeta potentials needs further investigation because the zeta potential relates directly to a surface of a few grains while the streaming potential is an up-scaled measurement of a core with many more grains and with heterogeneities in pore size and surface composition. The measurements could give an average of the zeta potential of the rock.

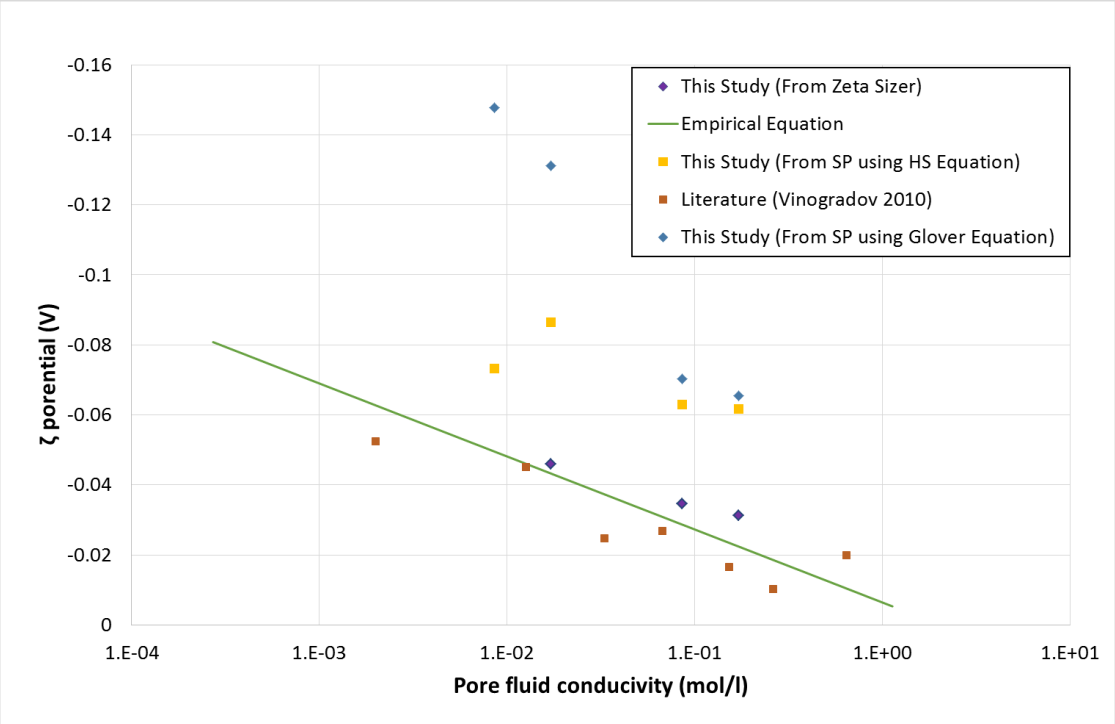

Figure 2.25: Fontainebleau Zeta potentials

Zeta Potential and clay

For a salinity of 5000 ppm of NaCl, the zeta potential decreases with clay content from pure quartz (-65 mV) to (-15 mV) in illite (Figure 2.26). The surface charge of clay minerals differs from quartz because of its layered crystalline sheet structure with inter and intra-mineral porosity. For sandstones with an increased clay content, the Zetasizer results are within the measurement error and therefore we are not able to observe clay effects in our Fontainebleau sample. The zeta potentials are very pH sensitive, with less negative zeta potentials at lower pH values and more negative zeta potentials at higher pH values. Vinagradov (2010) recorded similar results, within experimental error, in samples which do not contain clay.

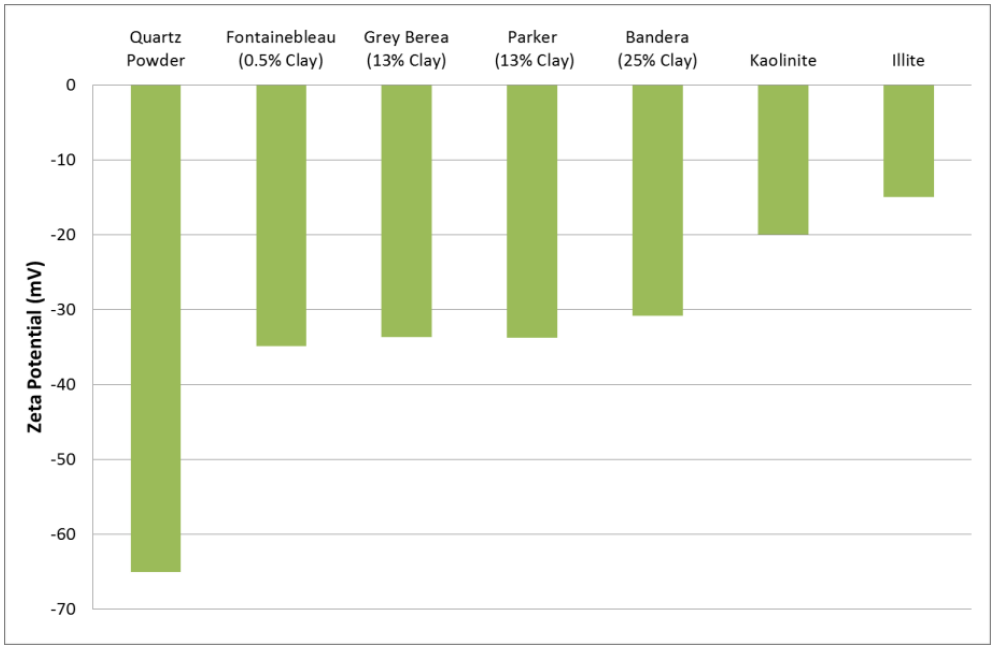

Figure 2.26: Zeta potential from Zetasizer for different type of minerals and rocks.

Summary of results

In this article we summarize the petrophysical characteristics of Fontainebleau sandstone based on the literature to date and our experimental work. Our experimental results are from one sample block of about 0.018 m^3, from one specific site and one specific layer; they are compared with results from the entire outcrop area in the vicinity of Paris (France).

The following laboratory experimental methods and image analysis techniques were conducted to characterize the porous media. The techniques used and results are summarized as follow:

- Mineralogy:

XRD/XRF data shows that our samples consist of only quartz mineral (0.995). There are traces of other oxides. Synthetically reconstructed clays are illite (0.0015) and kaolinite (0.0039). Polarized light of the thin section images shows that visually only quartz is present; no clays were found in the pores.

- Quartz overgrowth:

The quartz overgrowth dictates the cementation around the original grains. It is estimated to be in the range of 0.15 to 0.2 BV.

- Porosity and Permeability:

The porosity and permeability of Fontainebleau sandstone have a constant bandwidth and do not vary laterally in our sample blocks. Our data set covers a range of porosity of 0.05 to 0.15 which was not properly covered in the literature. By combining literature data, an improved phi/k-relation is developed; $k = 10^{6.5 + 4.6 \log(\phi)}$; $R^2 = 0.95$.

- Pore and grain framework:

The pore, grain and pore-throat size distribution of our Fontainebleau sandstone appears to be constant and well sorted. Our samples indicate constant pore size (20 – 100 µm), pore-throat size diameter (10 – 30 µm) and grain diameter distributions (100 – 300 µm). Concerning capillarity, quartz is the only mineral, making the Fontainebleau system strongly water-wet.

- Dielectric properties:

The dielectric measurements exhibit clean sandstone behavior and the measured formation factor follows Archie 1, i.e. very insignificant clay content. This is in line with the other measurements from XRD/XRF. Zeta potential measurements show that the Fontainebleau surface charge is negative. This is due to the fact its grain surface is composed purely of quartz. So, the dielectric behaviour of the pore wall can be considered uniform homogeneous.

5. Conclusions

In conclusion, the porous media of Fontainebleau sandstone meets the required conditions for our core-flow experiments. It reveals homogeneity in its texture and mineralogy due to its pure composition. Clay minerals are almost non-existent and only accessories of clay have been recognized in the inclusion areas around the original grain perimeters. It has no impact on the fluid flow behavior during core-flow experiments. This will ensure maximal reproducibility and comparison of fluid flow experimental results.

Furthermore, we demonstrated that the quartz overgrowth (i.e. cementation) is playing a central role in the pore-throat geometry and impacts both permeability and porosity by

reducing the pore-throats (i.e. coordination number) and not so much the pore volumes. By applying the Panda and Lake approach (Panda and Lake, 1995) we demonstrated that the permeability of Fontainebleau is impacted more by the quartz overgrowth (i.e. cementation) than the grain size distribution. Moreover, we defined a pore-throat diameter distribution based on the degree of authigenic cementation and porosity. In other words, this microstructure property (i.e. quartz overgrowth) has a significant impact on fluid flow. The tortuosity is higher and by that influences the path of the fluid during the transport. Note that mapping the pore framework allows us to model the mobilization and transport of the oil on the entire micrometer to meter scale.

Regarding dielectric behavior, the high negative surface charges of the Fontainebleau grains influence the geochemical process (for example adsorption of injected chemicals) when it is used in enhancing the oil mobilization and transport. This will help in pre-defining the experimental protocol for the core-flow experiment.

As a final conclusion we state that all spatial characteristics do have a direct correlation with porosity, permeability and capillarity. In other words, these cross-textural and physical relations may be used as input parameters for the porosity, permeability and pore throat area distribution outside our experimental scope of research and for modeling purposes.

Acknowledgement:

The authors want to thank the TU Delft technical team (Michiel Slob, Karel Heller, Joost van Meel, Jens van den Berg) for their contributions to the sample preparation, experimental work and image analysis discussions. Special thanks to Fons Marcelis from Shell for SEM, thin sections and BET measurements. Furthermore we would like to thank staff of the Grès de Fontainebleau & Cie quarry in Moigny-sur-École for their assistance in the quarry.

References:

1- Alimen, H., 1936. Étude sur le Stampien du Bassin de Paris. Mémoire, *v.31. Société Géologique de France, pp. 1–304.
2- Archie, G.E., 1942. Electrical Resistivity Log as an Aid in Determining Some Reservoir Characteristics, Trans., AIME, 146, 54-61.
3- Börner, F., 1992. Complex conductivity measurements of reservoir properties", Proc Third Europ. Core Analysis Symp. Paris, 359-386.
4- Bourbie T., and B. Zinszner (1985), Hydraulic and acoustic properties as a function of porosity in Fontainebleau sandstone. Journal of Geophysical Research: Solid Earth, 90(B13), 11524–11532.
5- Coker D., Torquato S. and Dunsmuir J., (1996), Morphology and physical properties of Fontainebleau sandstone via a tomographic analysis. Journal of Geophysical Research: VOL. 101, NO. B8, P 17,497 – 17,506, August 10, 1996
6- David, C., and Darot, M., (1989). Permeability and conductivity of sandstones Rock at GreatDepth, Maury & Fourmaintraux (eds), Rotterdam.

7- Dollfus G.-F., 1911, Feuilles de Fontainebleau et de Châteaudun au 80 000. Bull. Serv. Carte Géol. Fr., XXI, 128, p. 8-30.
8- Doyen, P., 1988, Permeability, Conductivity, and Pore Geometry of Sandstone, Journal of Geophysical Research, 93(B7), 7729-7740.
9- Dullien, F., (2012) Porous Media: Fluid Transport and Pore Structure, 2nd ed, Howard Brenner.
10- Fredrich, J. T., Greaves, K. H., and Martin, J. W., (1993), Pore geometry and transport properties of Fontainebleau sandstone, Int. J. Mech. Min. Sci. Geomech. Abstr., 30, 691– 697
11- French, M., Worden, R., 2013, Orientation of microcrystalline quartz in the Fontainebleau Formation, Paris Basin and why it preserves porosity. Journal of Sedimentary Geology 284–285 (2013) 149–158
12- Glover, P. W. J., Walker, E., and Matthew D. Jackson, M. D., (2012). Streaming-potential coefficient of reservoir rock: A theoretical model. Geophysics, 77(2):D17–D43.
13- Gomez C. T., Dvorkin, J., and Vanorio T., 2010, Laboratory measurements of porosity, permeability, resistivity, and velocity on Fontainebleau sandstones. Geophysics,Vol. 75, No. 6 P. E191–E204,
14- Haddad, S., Worden, R., D.J., P., and Smalley, P. (2006). Quartz Cement in the Fontainebleau sandstone, Paris Basin, France; Crystallography and implications for mechanisms of cement growth. Journal of Sedimentary Research, 244-256.
15- Jacquin, C., 1964 Corrélations entre la perméabilité et les caractéristiques geométriques du gres de Fontainebleau, Rev. Inst. Fr. Pet. 19, 921- 937.
16- Jaafar, M. Z., Vinogradov, J., and Jackson., M. D. (2009). Measurement of streaming potential coupling coefficient in sandstones saturated with high salinity NaCl brine. Geophysical Research Letters 36.21.
17- Lake, L. W., Johns, R. T., Rossen, B., and Pope, G., (2014) Fundamentals of Enhanced Oil Recovery, Society of Petroleum Engineers.
18- Leroy, P., Devau, N., Revil, A., and Bizi, M., 2013, Influence of surface conductivity on the apparent zeta potential of amorphous silica nanoparticles: Journal of Colloid and Interface Science, 410, 81–93
19- Lindquist, W. B., Venkatarangan A, Dunsmuir, J., Wong, T., 2000. Pore and throat size distributions measured from synchrotron X-ray tomographic images of Fontainebleau sandstones, Journal of Geophysical Research, 105(B9), 21509-21527.
20- Mohanty, K. K., Davis, H.T., Scriven, L.E (1987) Physics of Oil Entrapment in Water-Wet Rock". SPE Reservoir Engineering, SPE-9406.
21- Panda, M. N., and Larry, W. L., (1994) Estimation of Single-Phase Permeability from Parameters of Particle-Size Distribution, AAPG Bulletin, V. 78, No. 7, P. 1028–1039.
22- Panda, M. N., and Larry, W. L., (1995) A Physical Model of Cementation and Its Effects on Single-Phase Permeability, AAPG Bulletin, V. 79, No. 3, P. 431–443.
23- Pickell. J.1., Swanson. B.F .. and Hickman. W.B., (1966). "\Applications of Air-Mercury and Oil-Air Capillary Pressure Data in the Study of Pore Structure and Fluid Distribution, SPEJ 55-61; Trans .. AIME, 237, SPE1227.
24- Pirson S. J., (1963). Handbook of well log analysis. Prentice-Hall Inc., New York
25- Pride, S., and F. D. Morgan, F. D., (1991) Electrokinetic dissipation induced by seismic waves, Geophysics, 56, 914-925.

26- Revil, A., Kessouri, P., and Torres-Verdín, C., (2014) Electrical conductivity, induced polarization, and permeability of the Fontainebleau sandstone, Geophysics, Vol. 79, No. 5 ; P. D301–D318
27- Revil, A., Pezard, P. A., and Glover P. W. J., (1999) Streaming potential in porous media: theory of the zeta potential. Journal of Geophysical Research: Solid Earth, 104(B9):20021– 20031.
28- Schon, J., 2015. Physical properties of rocks, second edition, developments in petroleum science, volume 65, Elsevier
29- Shehata, A., Nasr-El-Din, H., (2015). Zeta Potential Measurements: Impact of Salinity on Sandstone Minerals., SPE International Symposium on Oilfield Chemistry, Texas, USA. SPE-173763
30- Song, I. (2008). Hydromechanical properties of Fontainebleau sandstone: Experimental determination and micromechanical modeling. Journal of Geophysical research: solid earth , 113(B9).
31- Stegemeier, G. L. (1977). Mechanisms of Entrapment and Mobilization of Oil in Porous Media", in Improved oil Recovery by Surfactant and Polymer Flooding, Shah, D. O. and Schechter, R. S. ed., Academic Press, New York.
32- Szymczyk, A., Pierre, A., Reggiani, J. C., and Pagetti, J., 1997. Characterisation of the electrokinetic properties of plane inorganic membranes using streaming potential measurements. Journal of membrane science, 134(1):59–66.
33- Tiab, D., and Donaldson, E., 2015. Petrophysics: Theory and Practice of Measuring Reservoir Rock and Fluid Transport Properties, fourth edition, Elsevier
34- Thiry, M., Bertrand-Ayrault, M., Grisoni, J.C., 1988. Ground water silicification and leaching in sands: Example of the Fontainebleau Sand (Oligiocene) in the Paris Basin: Geological Society of America. Bulletin 100, 1283–1290.
35- Thiry, M., 1999. Diversity of continental silicification features: examples from the Cenozoic deposits in the Paris Basin and neighbouring basement; Palaeoweathering, Palaeosurfaces and Related Continental Deposits, special publication Number 27, 87-127.
36- Thiry M., & Marechal B. (2001). Development of tightly cemented sandstone lenses in uncemented sands: Example of the Fontainebleau Sand(Oligocene) in the Paris Basin. Journal of Sedimentary Research, 71(3), 473-483.
37- Tiab, D., and Donaldson, E., 2015. Petrophysics: Theory and Practice of Measuring Reservoir Rock and Fluid Transport Properties, fourth edition, Elsevier
38- Timur, A., Hempkins, W.B., and Worthington, A.E., 1972. Porosity and Pressure Dependence of Formation Resistivity Factor for Sandstones, Formation Evaluation Symposium, Canadian Well Logging Soc., Calgary
39- Vinogradov, J., M. Z. Jaafar, and Jackson, M. D., (2010). Measurement of streaming potential coupling coefficient in sandstones saturated with natural and artificial brines at high salinity. Journal of Geophysical Research: Solid Earth 115.B12.
40- Weiner, B. B., Tscharnuter, W. W., Fairhurst, D., (1993) Zeta Potential: A New Approach, the Canadian Mineral Analysts Meeting, Manitoba, Canada.
41- Wilson, O. B., Tjetland, B. T., Skauge, A., (2001) Drainage rates in capillary pressure experiments. In: 15th International Symposium of the Society of Core Analysts, No. SCA2001-30, pp. 1–12. Society of Core Analysts, Edinburgh
42- Wolf, KH., (2006), the interaction between underground coal fires and their roof rocks, Phd dissertation/Thesis, TU Delft.

43- Worthington, P. F., (1993), The uses and abuses of the Archie equations. 1. The formation factor–porosity relationship. J Appl Geophys 30:215–228
44- Zinszner, B. T., 1985. Hydraulic and Acoustic properties as a function of porosity in Fontainebleau Sandstone. Journal of Geophysical Research: Solid Earth, 90(B13), 11524–11532.
45- Zinszner, B. T. (2007). A Geoscientist's Guide To Petrophysics. IPF Publications : Publisher: Editions Technips.

Chapter 3

Developments in Coreflow and Microfluidic Experimental Setups for Oil Mobilization in Porous Media.

This chapter is based on the article that has been submitted to the journal "Review of scientific instruments". It is currently under review . The article describes the developments of coreflow and microfluidic setups that we built for this research. It also demonstrates the importance of reproducibility of the experimental data.

F. AL Saadi,[1] M. Slob,[1] KH. Wolf,[1] and C. Van Kruijsdijk[2]

[1] Faculty of Civil Engineering and Geosciences, Delft University of Technology,2600 GA Delft, The Netherlands.

[2] Shell Global Solutions International B.V, Grasweg 31, 1031 HW Amsterdam, The Netherlands.

Abstract:

We present the development of experimental setups and equipment to investigate the dynamics of oil mobilization and transport in a porous medium. Our aim is to quantitatively compare a large number of core-flows and differentiation in results. This approach requires experimental reproducibility and a validation of the variance in results under the same input conditions (i.e. temperature, pore pressure, chemicals, PV's, etc.) with the same rock sample. In many articles, the scientific conclusions are drawn based on two or three experiments, while the reproducibility is not confirmed. The main question is whether the mechanism of a physical process is working properly, when the same experiment gives different results when repeated. In our multiple experiments, by ensuring the reproducibility, we distinguish the data that provide true insight into the dynamics of oil bank build up and the results that are mere statistical anomalies or flaws in the design of the experiments.

Key words: Microfluidic, Core-flow, Oil Mobilization, Micromodel, Experimental Data, Pressure, Rate, Enhanced Oil Recovery, Sandstone, integrity precision and accuracy

1. Introduction: Objectives and Motivation

The dynamics and physics of multi-phase fluid flow in bulk porous medium are complex and by that challenging to predict, simulate and model. It becomes more complicated when the researchers start to deal with chemical Enhanced Oil Recovery (EOR) processes. Additional fluids (i.e. the chemicals) are introduced causing more physical and chemical rock-fluid-fluid interactions (Interfacial tension, micro-emulsions, etc.). It is therefore essential to produce in-situ representative, high resolution, accurate and

repeatable experimental data to evaluate the behaviour of multiphase fluids in porous media for the design of oil field applications.

Literature shows a wide range of laboratory experimental setups (De Groot 1929, Leverett and Lewis, 1941; Chatenever and Calhoun, 1952, Saraf and Fatt 1967; Leonmard and Zarcone 1985, Vinegar and Wellington 1987, Blunt et al 2002; Brown et al 2014; Wegner et al 2015; Unsal et al 2016) , which have been used to provide cheap, representative and quick platforms replicating the dynamic process of fluid flow in porous media for field application. The most frequently used methods are associated to core flooding experiments. The majority of these core flooding setups have been developed to address areas, such as, efficiency of EOR processes or the characteristics of these processes.

In this study we describe the development of two different laboratory facilities (i.e. microfluidic setup and a core-flow setup), which provide a more detailed and comprehensive sets of experimental data at different length scales and thickness. They address the research questions for the investigation of the dynamics and mechanisms of oil bank buildup during chemical flooding. The microfluidic setup enables the visualization of an oil bank at a one pore thick, ten pores width and one meter long porous glass chip. This glass chip has been designed and manufactured according to a pore-grain framework analogue to Fontainebleau sandstone. The second set-up, the core-flow facility, has been upgraded with peripheral equipment, such as multiphase meters, conductivity meters, pressure sensors across, and for varying core lengths. The experiments are carried out under a CT scanner where the mobilization process of the oil is monitored and characterized.

In this research we describe and calculate repeated experimental results at various scales, we assess the reproducibility and consider the effect of sample length. In many articles, as described in the next paragraph, the scientific conclusions are drawn based on two or three experiments, while the reproducibility is not confirmed. The main question is whether the mechanism of a physical process is working properly, when the same experiment gives different results when repeated. Irreproducibility may reflect a genuine uncertainty but also could be due to misinformation (i.e. mistakes, flukes, falsifications, etc.). We consider the reproducibility of experimental data essential to provide more reliable outcomes and ensure data integrity. Then, results in variations confirm that the errors are statistically insignificant. So, in our multiple experiments, by ensuring the reproducibility, we distinguish the data that provide true insight into the dynamics of oil bank build up and the results that are mere statistical anomalies or flaws in the design of the experiments.

2. Design and Development of the laboratory setups

2.1 Microfluidic Setup:

The use of micromodels to visualize and investigate pore-scale physical and chemical process started in the early 1950s (Chatenever and Calhoun, 1952). Since the 1980s, the micromodels are more and more used to study the transport properties through porous

media (Chen and Wilkinson 1985, Leonmard and Zarcone 1985, Corapcioglu et al 1997, Blunt et al 2002). In recent years, they are used for detail microscale studies for EOR studies (Unsal et al 2016; Wegner et al 2015).

Consideration and Design of the Micromodel

The pore size distribution and pore configurations are governing the fluid distribution and entrapment in a porous medium (Dullien et 1972; Stegemeier 1977; Wardlaw 1982), and are the spatial input parameters for the texture of the design of the micromodel. In this research, we image the rock texture and structure of a Fontainebleau Sandstone to quantify the grain-framework and pore-framework by using Micro-CTs, MICP, SEM, and thin sections (figure 3.1). We measure and calculate the grain, pore and throat size distributions (Al Saadi et al, 2017).

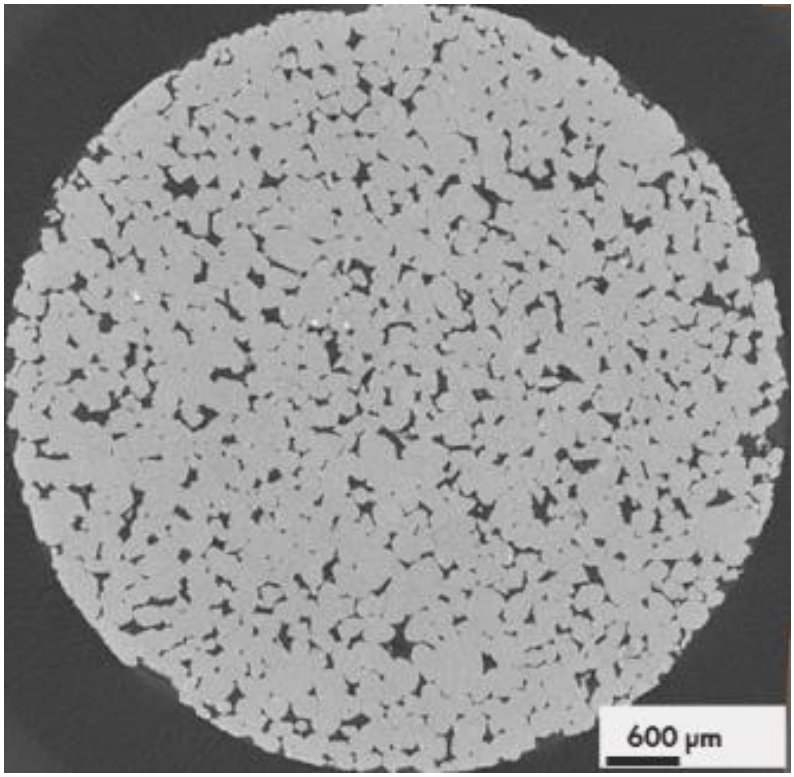

Figure 3.1A: Images of Fontainebleau sample, Micro-CT slice, representing the grain aggregate (light) and pore space (black).

Figure 3.1B: Images of Fontainebleau sample, SEM where the grain aggregate representation shows the angular particles due to quartz overgrowth.

Then, we construct a 2D porous media microfluidic chip (Figure 3.2), which mimics 3D Fontainebleau porous media by using geometry features (pores, grains, tubes and throats) of the porous media. For this chip, the same wettability (i.e. water wet) is maintained. The path length of the fluid flow in our Microfluidic chip is 1 meter. To fit this one meter structure on the chips, the overall chips size is 30*90mm in size and the flowpath is designed in a serpentine fashion, 0.3 mm wide. The process and the dynamic of mobilization, forming of clusters to an oil bank as well as cluster break-up can be monitored along flow path.

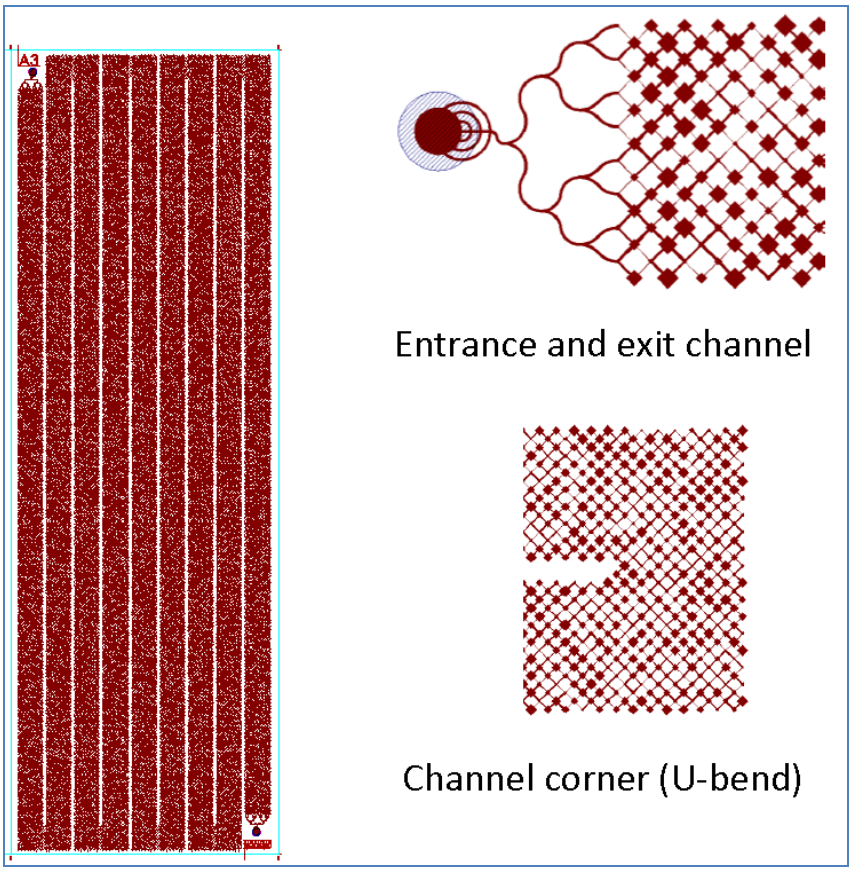

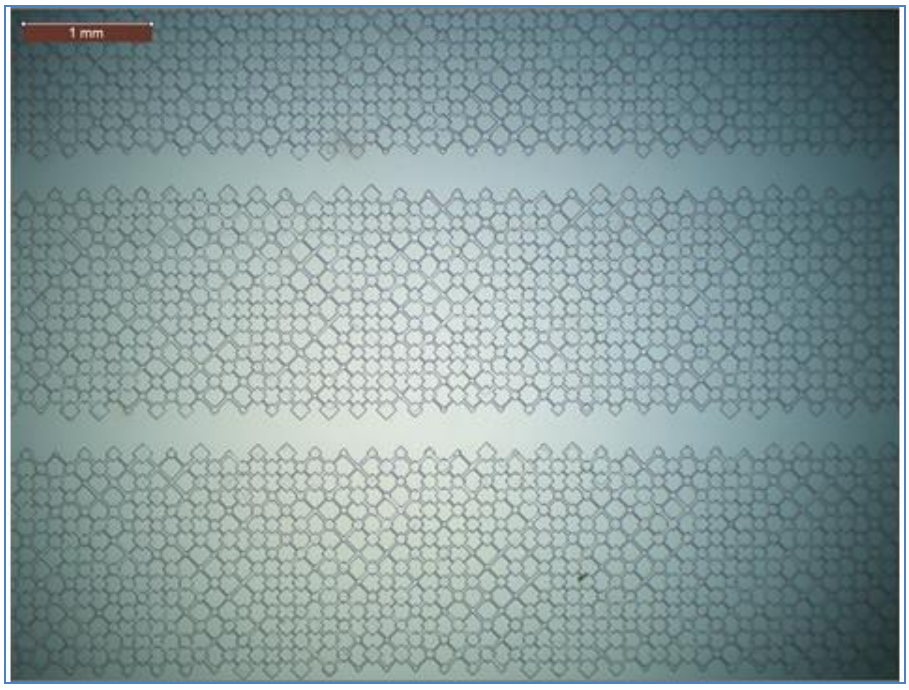

Figure 3.2: Design of the micromodel chip (top) , Fontainebleau Micromodel Chip (bottom)

2.1.1. The setup and the experimental Protocol of the microfluidic device

The set-up as shown in figure 3.3, consists of 2 Harvard Apparatus syringe pumps (Infuse/Withdraw PHD Ultra™ 4400 programmable Syringe Pump), with custom-made

stainless steel syringes , with a volume of 2.5 ml to 8 ml. In order to measure the pressure within the system a pressure sensor was installed (General Electric™), with a maximum pressure of 120 bar. The pumps were connected through Peek (PolyEtherEtherKerone) lines with an inner diameter of 250 µm. For optimum flow, a T-joint has been installed between the two syringes pumps. Further two one-way valves avoid back flow. To achieve a full saturation and to mimic fluid pressurized core flow experiments, a precise back pressure regulator was installed, maintaining a constant outflow pressure of 100 psi.

For image capturing of the microfluidic chip, a Leica DMi8 DFC7000 inverted, transmitted light microscope was employed. Two magnifications were used, (1.25 X, 10 X). However, usually 1.25 X objective was used so that a larger field of view was realized. The images were recorded with a Leica DFC7000T camera. The whole set-up was positioned within a black box to avoid outside light interference.

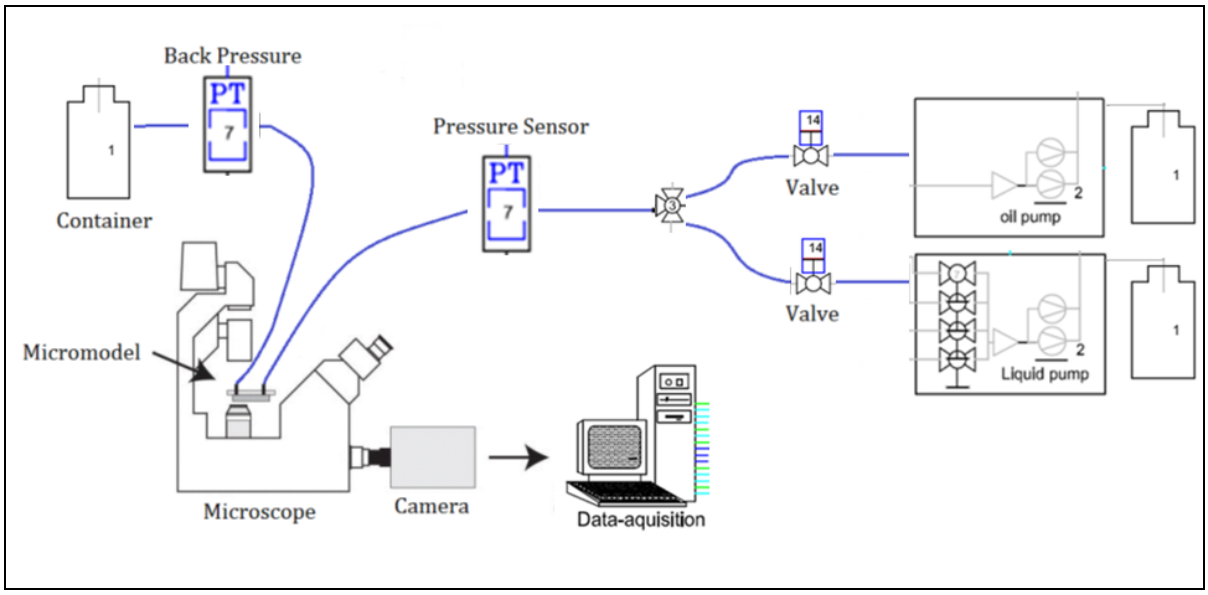

Figure 3.3: Schematic design of the Microfluidic setup

For our microfluidic experiments, we follow as much as possible, the same experimental protocol as for the sandstone coreflows:

1. Saturate the chip with Brine (5,000 ppm NaCl)
2. Displace the brine with Oil (n-dodecane)
3. Waterflood (3500 ppm NaCl) the oil by Brine (remaining oil is the residual)
4. Inject Surfactant-polymer (3500 ppm NaCl salinity) to sweep the remaining oil.

The Microfluidic chip under the microscope visualizes the flow regimes and monitor coalescence rate of the residual oil droplet, provides information on the mechanisms and dynamic to during an oil bank formation. The micromodel was operated at room temperature and horizontally. Therefore gravity forces can be neglected.

2.1.2. Visualization of Oil bank build up and monitoring Oil Ganglion Velocity in the Microfluidic

Fluid flow through porous rocks depends on pore geometry properties at the scale of 10^{-6} m. However, our cores are of the magnitude of 10^{-1} m to 1 m, at what is called the Darcy scale. Therefore, we designed the microfluidic chip which allows us to visualize the movement of oil ganglions at pore scale level from the qualitative best areas of the channel-images. Usually the issue with the microfluidic chips is the size of pore framework where a measured property, e.g. porosity and permeability, gives a suitable representation of the whole systems; it is also defined as representative elementary volume (REV) (Bear 1972). In our chip, we ensured that the size of the representative elementary volume (REV) (Bachmat and Bear 1987) covers the distribution of the pores (i.e. void) and grains (i.e. solid) within our microfluidic chip and sufficiently large so that the macroscopic changes do not affect the result and are statistically meaningful. Furthermore, we ensured similar size pores and throats in the micromodels compared to the core to avoid any difference in the ratio of the time for a fluid to diffuse over a distance compared to the flow time. One fact that could not be eliminated is our 2D micromodels do not have the same level of continuity as 3D models due to absence of sufficient thickness in these models.

At a certain point during the experiments 3 fluids were in the micromodel. As they were all transparent fluids, they could only be distinguished from each other at the interface of the fluids. In order to distinguish the fluids better from each other and to obtain more valuable quantitative results a dye was added to the oil. This is Nile Red, a fluorescent solvachromatic dye, which is most commonly used to dye lipid molecules due to its hydrophobicity (Brujic et al. 2007). Fluorescence is the emission of light by a material when it is excited by a wavelength within a specific range (the excitation spectrum). The Nile Red gives a fluorescence red glow at a wavelength between 559 - 637nm (Greenspan et al. 1985 and Datta et al. 1997).

Figure 3.4 represents the process of oil bank build up as we capture it in our microfluidic channel.

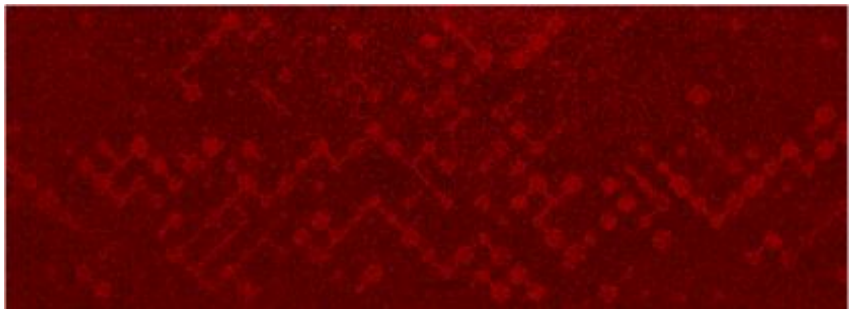

A: After Waterflooding, Oil is disconnected and at residual condition, the lighter red parts represent the accumulated oil phase, the dark parts are the brine phase and pore space.

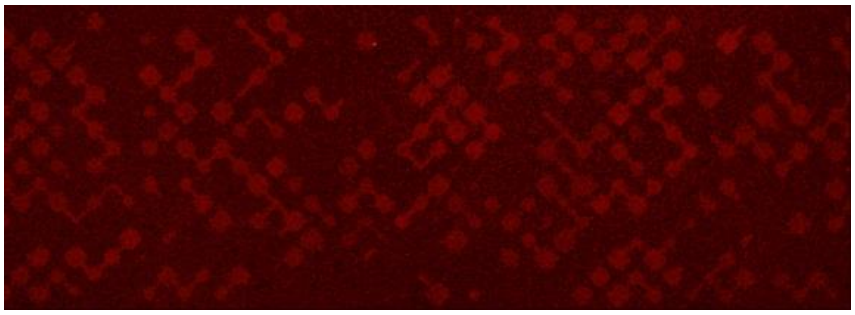

B: During SP, Oil gets connected and starts build oil bank

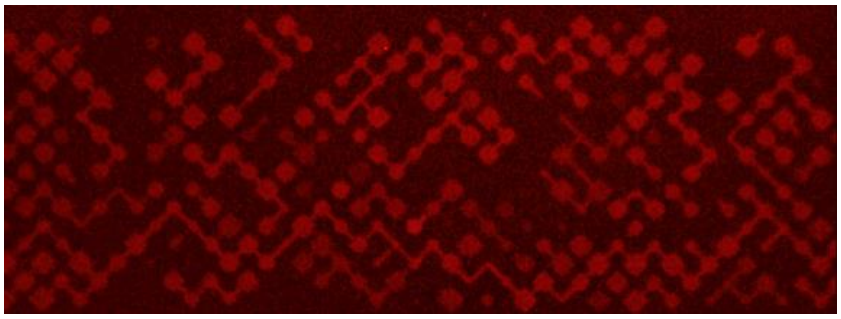

C: More oil gets together and oil bank is continuous

Figure 3.4: Visualization of oil bank build up at Microfluidic, each image is 8mm X 3mm, red colur indicates oil, black is the pore space and grains. Figure 3.4.A shows the distribution of residual oil after waterflood where we could see some oil ganglion isolated in single pore and trapped by mechanism of snap-off (Roof, 1970) and others as clusters of oil (i.e bypassed oil). Figure 3.4.B represents the start of the surfactant-polymer flood where the interfacial tension reduced and residual oil is mobilized and started to coalescence. As we continue the surfactant polymer injection and mobilized more oil; the oil bank is formed and stabilized as we could see it in Figure 3.4.C.

From images collected during SP injection, we could see that oil ganglia with the smaller size goes at higher velocity through the micromodel compared to the oil ganglia with the larger size, (see table 1). Furthermore, we could also observe that the oil ganglia are moving faster than the flood front.

Table 3.1: velocity of flood front and oil ganglia

Phase Type	**Velocity [µm/s]**	**Ganglia size [mm^2]**
Floodfront	270	-
Oil Ganglia 1	298	0.187
Oil Ganglia 2	288	0.235
Oil Ganglia 3	280	0.240
Oil Ganglia 4	275	0.242
Oil Ganglia 5	275	0.241

The mobilized oil moves with a velocity larger than the velocity of the chemical front. It will tend to accumulate in the front of the flood. As result of collisions and coalescence between the mobilized oil a denser zone of mostly connected oil (i.e. oil bank) is formed. Consequently, it supports an efficient sweep of other mobilized oil seen downstream. This process is influenced by many factors like the capillary number and the size of the ganglia. As the oil ganglia coalescence with other ganglia, they merge and size increase, velocity reduces and starts to form a stable displacement. Without coalescence, the mobilized oil droplet starts to break up to small sizes, increases its velocity and move as a disperse flood.

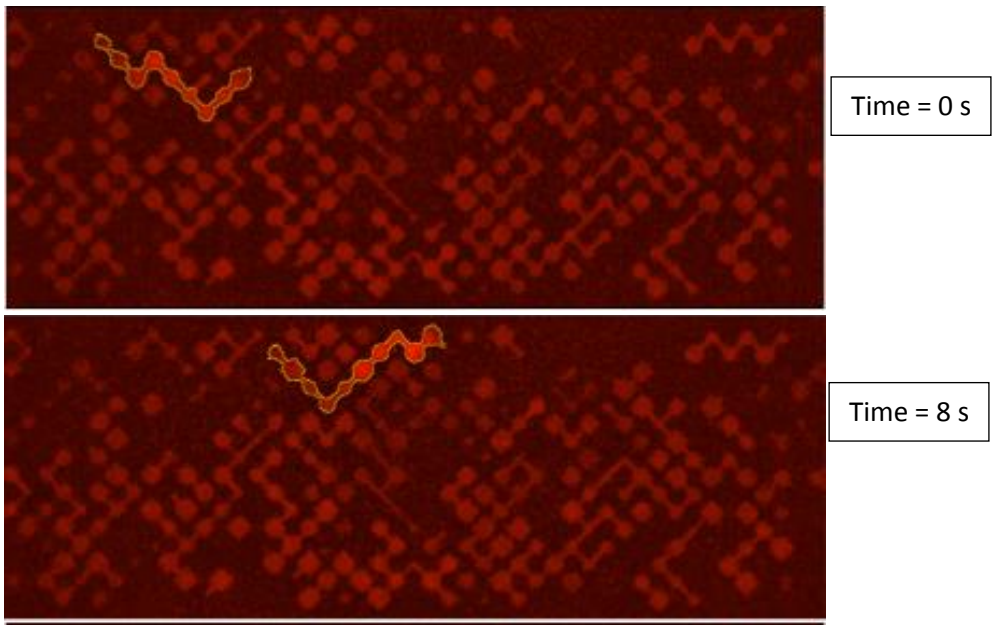

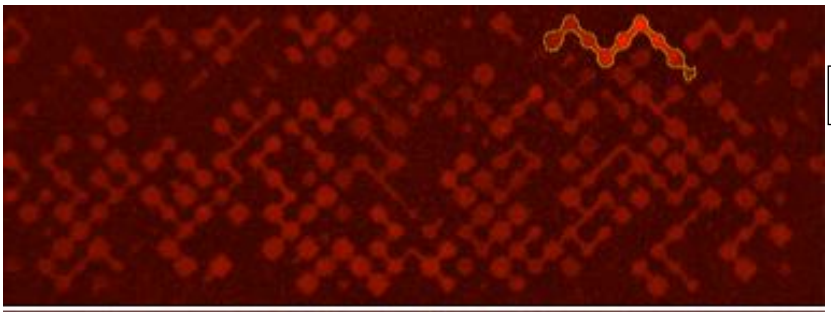

Figure 3.5: The propagation of an oil ganglion, size 0:187 mm^2 at different time steps.

2.2 . The Core-flow set-up

The first multiphase flow laboratory experimental work was reported in the late 1920's to measure the oil recovery factor for a sand reservoir (Mills et al 1928, De Groot 1929, Chalmerst et al 1930). Subsequently, the experimental two-phase water-oil relative permeability data set from displacement experiments (Wyckoff and Botsol, 1936) in an unconsolidated sandpack was followed by the measurement of the three-phase relative permeabilities in a similar medium (Leverett and Lewis, 1941). In the 1950s, coreflood experiments proved the efficiency of tertiary recovery methods, eg CO2 flooding, solvent, surfactant, … etc (Eugene et al 1952, Teter and Friedman 1954, Binder 1954, Binder and Edward 1956, Holbrook 1958, Helm and Bernard 1959, Csaszar 1961). Saraf and Fatt estimated the fluid saturations to visualize the displacement processes with Nuclear Magnetic Resonance (NMR) techniques (Saraf and Fatt 1967). However, with the X-ray CT by Hounsfield (Hounsfield 1973) the image quantitatively became satisfactory for petroleum engineering application. Since the 1980s (Wang et al 1984; Wellington and Vinegar 1985; Vinegar and Wellington 1987), CT scans provide 3D images of multiphase saturations during the coreflood experiments. It contributes high-resolution, three-dimensional and even pore-scale (micro-CT) observations to investigations of multiphase fluid transport in porous media (Brown et al 2014).

Consideration and design of the core-flow setup

The main considerations for developing this core flow facility are; continuous quality data (data-acquisition), measurement precision and repeatability of experiments. Therefore, high precision mass flow meters (MFM) were installed at the inlet and outlet of the setup to ensure accurate reconstruction of the mass flow leading to a closed material balance. The Mass Flow Meters (mini CORI-FLOW™) are based on the Coriolis principle, measuring both the mass flow and density of fluids. Next to the mass balance, the density date provides the fluid types. The mass flow ranges from 5 g/h to 200 g/h, at an accuracy of $\pm$ 0.2% of rate and a density accuracy of less than 5 g/liter. As with the mass flow meters, conductivity monitors (AZURA CM 2.1S) were used to measure the electrical resistance of the solution ion concentrations. The flow cell in the monitors can handle flow rates up to 10 ml/min. The precision in the measured range (0.1-300 mS/cm) is < 2 %. The conductivity measurements

confirm the change in fluid phase composition and breakthrough as parallel values to the density measurement results. Moreover, it picks up any salinity change in the single phase parts of the experiment.

Another consideration is monitoring the fluid movement through the core pore system. This subject has been addressed in two ways: first, the installation of pressure transducers across the length of the tube, into the porous medium, and second, running core flow experiments in a dual beam medical CT scanner. Pressure transducers provide absolute pressure data at ca. each 5 cm interval along the core with a confirmation through a delta pressure transducer across the entire core. For imaging saturation monitoring in the core we use a Siemens™ medical CT scanner with dual source technology of 80 kV to 140 kV. It delivers a highest voxel resolution of 250µm x 250µm x 250µm and smoothed calibrated, result over the entire view field. Rather than the often used aluminum core holder, we preferred a peek (Polyetheretherketone) coreholder. PEEK has a lower density, absorbs less X-rays and has a comparable strength to aluminum.

A constant and continuous injection rate is ensured by a BlueShadow 40P™ pump. Two exchangeable pump heads allow a wide range of flow rates, of 0.001 – 10 mL/min (per pump) at pressures up to 100 bar. The flow rate accuracy is giving ± 1%, using a flow rate range from 5 - 80% of the total flow range.

Porous plate:

The porous plate is a ceramic disc that has been manufactured from aluminium oxide (Al2O3). It is available at different sizes (diameter, thickness) and different characteristics (pore size, water wet, oil wet). Figure 6 represent an example of a porous plate. We installed a water-wet porous plate at the end of the core. During oil filling and due to its wetting conditions, the porous plate does not allow the oil to flow out of the core and as a result we could achieve high initial oil saturation. The porous plate is permanent and it does not need to be removed during water or chemical injection as we inject from the other side and oil could flow outside the core from the other end.

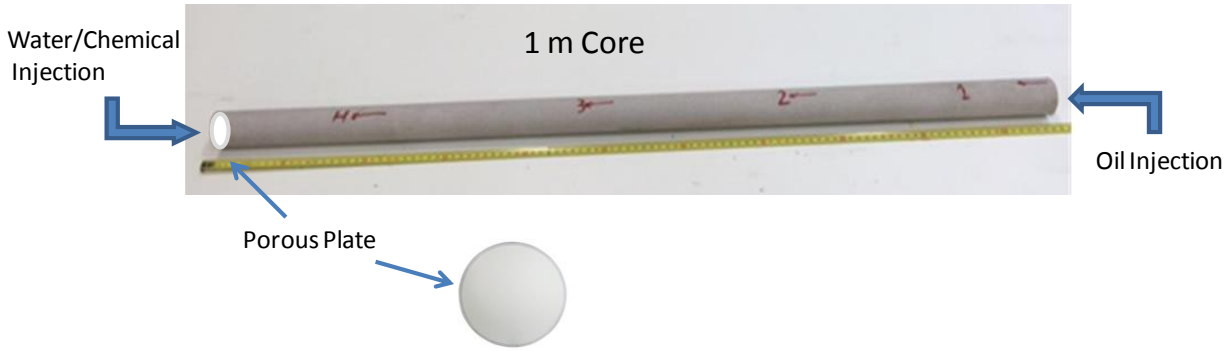

Figure 3.6: The flow configuration of the 1 m sample with the porous plate at the water/chemical injection side.

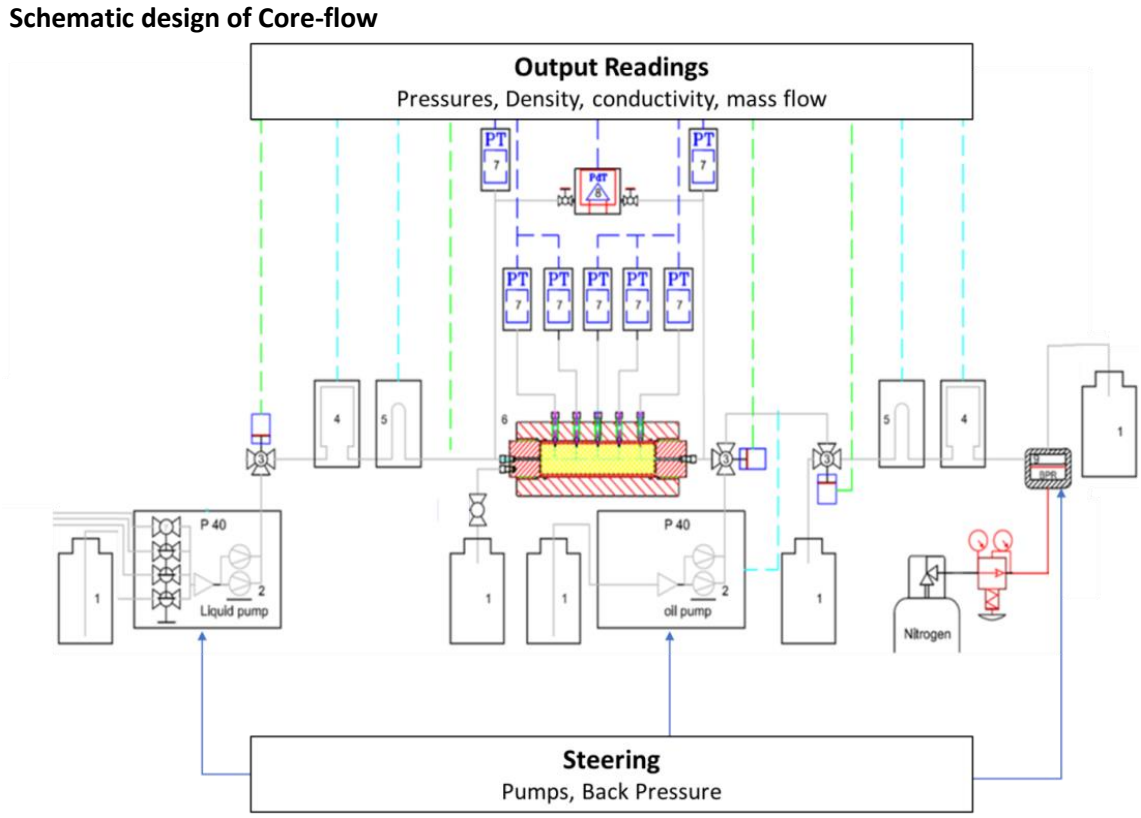

Figure3. 7: Schematic design of the core flow setup. The numbers correspond with the set-up description here below.

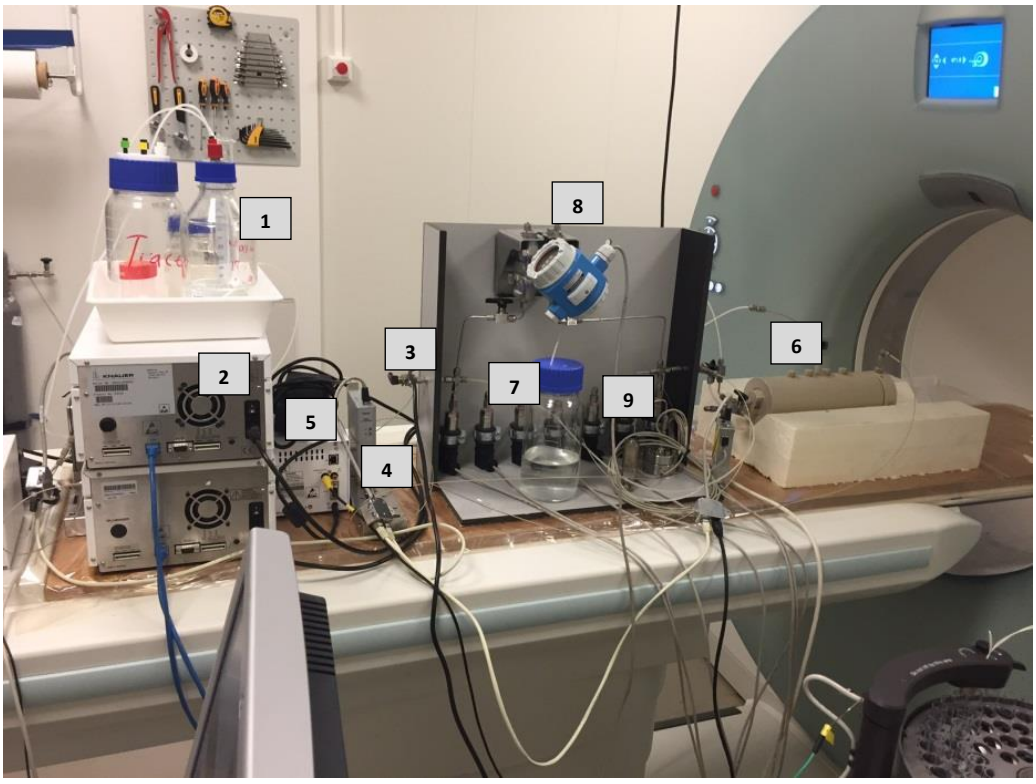

Figure 3.8: the coreflow setup under the CT scanner

Legend of the set-up parts and DAS lines and tubing

1	**Bottles**:	with the fluids to be injected, i.e. brine, oil and chemical solutions.
2	**Pump, BlueShadow 40P™**:	for oil, brine and chemical solutions.
3	**Electrical 3 way Valves**:	for fluid direction control across the fluid transport system.
4	**Mini CORI-FLOW™ :**	Flow rate control with the Mass Flow Meters (MFMs).
5	**Conductivity monitors:**	effluent Bulk conductivity meausurements.
6	**Coreholder:**	various sizes. Length 0.07 to 1.00 m, diameter constant at 0.039 m. Core position is horizontal in the CT scanner and vertical outside the CT scanner
7	**Pressure transducers:**	Pressure variation 0 – 100 bar.
8	**Pressure difference transducers:**	Pressure difference variation 0 – 100 bar.
9	**Dome-loaded back pressure regulator**:	Up to 50 bar maximum.

2.1.3. The core-flow experimental protocol

For the comparison of all core flooding experiments using the different core lengths, a general experimental procedure has been developed. The experimental steps are, as followed in the columns here below.

Procedure step:	**Description:**	**Objective:**
1. Bring the setup to vacuum and clean the core.	• The outlet of the set-up is connected to a vacuum pump. • Connecting the inlet line with a CO_2 source while the vacuum pump is connected.	• Removing any gas from the set-up while replacing with CO_2. S_g=1 • Note that the CO_2 will dissolve in the brine.

2. Saturating the core with brine.	• While the outlet of the set-up is connected to the vacuum pump, we inject 1 PV of brine into the core at a flow rate of 2.5 cc/min.	• Filling the tubes of the set-up, other dead volumes and saturate of porous medium with brine. $S_g \rightarrow S_w$
3. Heating up the core.	• Brine was injected for 10 PV; • During brine injection an increase of core's temperature was done up to 30 °C.	• Equilibrium of rock-fluid interaction is supposed to be reached after 10 PV of brine injection. $S_w = 1$ • Temperature during the experiment will reach 30°C, where it stays during the experiment.
4. Permeability test	• Differential pressure tests at various flow rates: 0.4, 1, 1.6, 2.2, 3 cc/min.	• Definition of the permeability of the core.
5. Tracer Injection.	• Injection of brine together with potassium iodide (KI=20 ppm) into the core at 0.12 cc/min (1 ft/day) for 2PV. Concentration of KI in the effluent was detected by a spectrophotometer.	• Estimation of the porous volume of the core.
6. Brine Injection.	• The injection of brine without the tracer was done for 5 PV.	• It helps to wash out the KI-tracer from the core. •
7. Saturating the core with oil.	• Injection of oil at low rate while monitoring the pressure. Porous plate allows only brine to flow out of the core.	• The goal is to achieve good saturation and distribution of the oil into the core. So= 0.7 to 0.8.
8. Injection of brine (waterflooding).	• Injection of brine at the desired salinity for several pores.	• To produce the mobilized oil and keep the porous media at residual oil saturation. So is going down to Sor.
9. Tracer Injection.	• Injection of brine together with KI (20 ppm) into the core at 0.12 cc/min (1 ft/day) for 2PV. Concentration of KI in the effluent was detected by a spectrophotometer.	• Estimation of the accessible porous volume of the core after waterflooding.

10. Chemical Injection.	• Injection of 0.5 PV of Surfactant Polymer and chase it with 1 PV of polymer slug.	• To build the oil bank and connect the residual oil.
11. Brine Injection.	• Inject several pore volumes of brine	• To produce the chemical mixture of oil, brine, surfactant and polymer, from the core.
12. Tracer Injection.	• Injection of brine together with KI (20 ppm) into the core at 0.12 cc/min (1 ft/day) for 2PV. The concentration of KI in the effluent was detected by a spectrophotometer.	• Estimation of accessible porous volume of the core after chemical flooding.
13. Clean the core	• Inject several pore volume of Isopro- Propanol Alcohol (IPA)	• To clean the core, S_{or}, $S_w \rightarrow 0$ and $S_{ipa}=1$
14. Repeat the experiment	• Repeat from step 2 onwards	• To ensure reproducibility and repeatability of the coreflow experiment

3. Error Analysis of Experimental Tracer Profile in a Porous Media

In most sciences, experimental data provide reliable source of information. It is widely carried out to verify theories and develop new technologies. It is always safer, less time-consuming and much cheaper to do experiments in the laboratory than implementing the theory or the concept immediately in the application.

One of the main concerns on the experimental data is the measurement errors. The measurements errors could lead to wrong data and accordingly wrong conclusions. Therefore, it is crucial to understand the set of experimental data and capture the measurements error.

There are a lot of techniques to analysis the measurement errors. One of these techniques is the variance which is the average squared deviation of all possible observations from the population mean. Another technique is the standard deviation which is the square root of the variance. Over two – third of observations will fall within one standard deviation on either side of the mean value while for two standard deviation it is going to be 96% (Fig. 3.9). Therefore, an error below 5% considered as an acceptable based on the sum of the precision characteristics of all included transducer results.

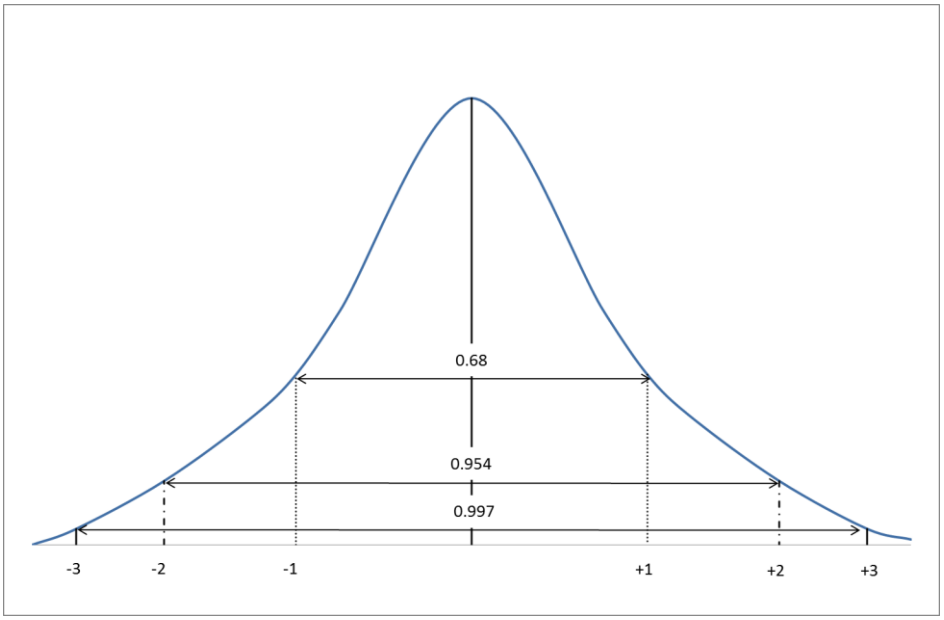

Figure 3.9: Areas enclosed by standard deviations of the standard normal distribution.

4. Experimental Results and Discussions

4.1. Determination of Brine Permeability in the core:

In order to investigate the flow processes in our Fontainebleau samples, we measure the average brine permeability by using a constant flow rate and differential pressure over the sample at high precision. Therefore, we apply Darcy's equation for a linear incompressible fluid;

$$q = \frac{kA}{\mu L}(\Delta p) \qquad \text{Equation 5}$$

Where;
q is the volumetric rate of flow in m^3/s
K is the brine permeability in m^2
μ is the brine viscosity (Pa s) measured
Δp is the differential pressure across the core in Pa
A is the core cross section in m^2
L is the core length in m^2

To determine the reproducibility/accuracy of the core permeability measurements we varied the flow rate and through that the differential pressure over the sample. The permeability is $9.29*10^{-15}m^2 \pm 0.15*10^{-15}m^2$.

Table 3.2: Calculations of Brine permeability

Parameters	**Scenario 1**	**Scenario 2**	**Scenario 3**	**Scenario 4**
All back to SI system				
Core Diameter and Length in m	D=0.039;L=0.38	D=0.039;L=0.38	D=0.039;L=0.38	D=0.039;L=0.38
Flow Rate 10^{-9} m^3/s	0.869	8.836	17.643	26.495
Brine viscosity 10^{-4} Pa.s	8	8	8	8
Pressure difference 10^5 Pa	0.237	2.45	4.896	7.324
Brine Permeability $10^{-15}m^2$	**9.34**	**9.14**	**9.29**	**9.33**

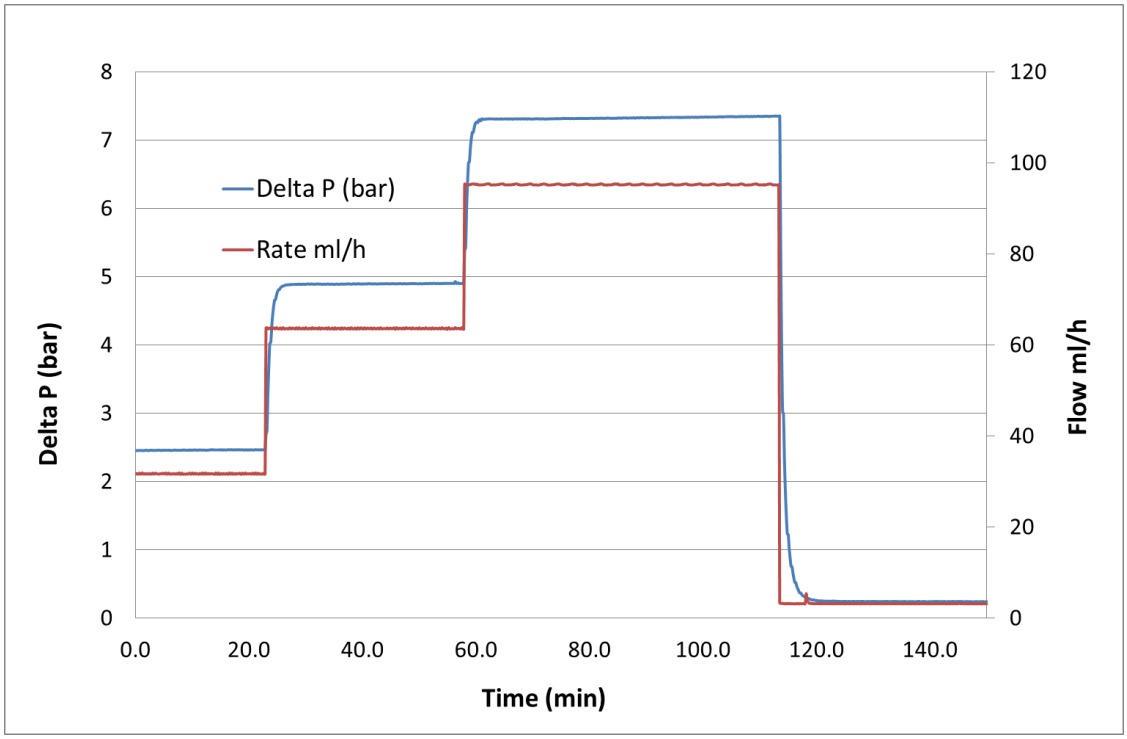

Figure 3.10: Differential pressure and flow rates vs time.

4.2. Determination of the effective porosity

Understanding the effective pore volume in the various phases of multi-phase flow is required to design the chemical slug sizes. We measure the accessible pore system to water by injection of a Potassium Iodide brine tracer. The effluent of the injected brine is

collected at the outlet in 3 cc tubes. The concentration of the tracer is measured through spectrometry, providing a tracer profile per stage and stage transition against pore volumes (PV) (Fig. 3.10).

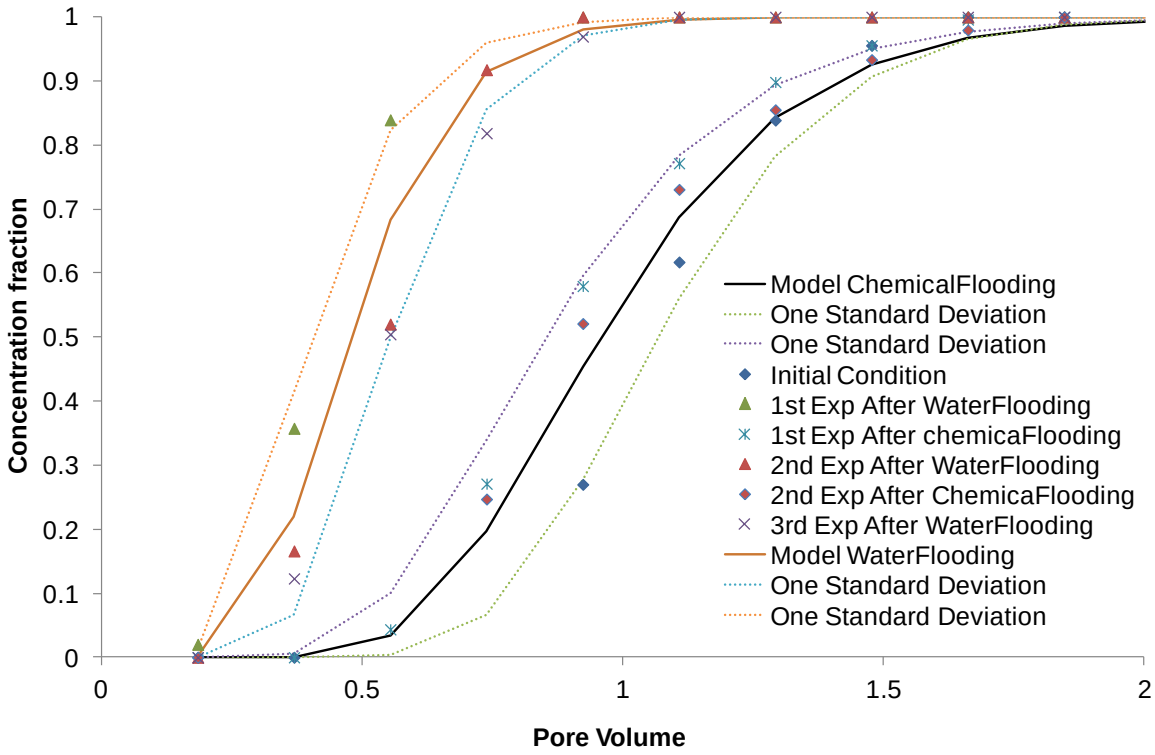

Figure 3.11: Tracer experimental data in effluent and model data.

The homogeneity of the porous media is defined by the error functions of the tracer profile. In addition, the reproducibility of the profile, for both the water flooding and chemical flooding process, is shown in figure 3.11, i.e. we used (Pancharoen et al, 2010).

Matching the experimental with the modelling results, we obtained the effective porosity and the bulk volume. On data certainty and dependency, Figure 3.12 shows that the objective function of the accessible pore volume is more certain than the dispersion coefficient. Figure 3.13 shows the dependency between the effective porosity and the dispersion coefficient.

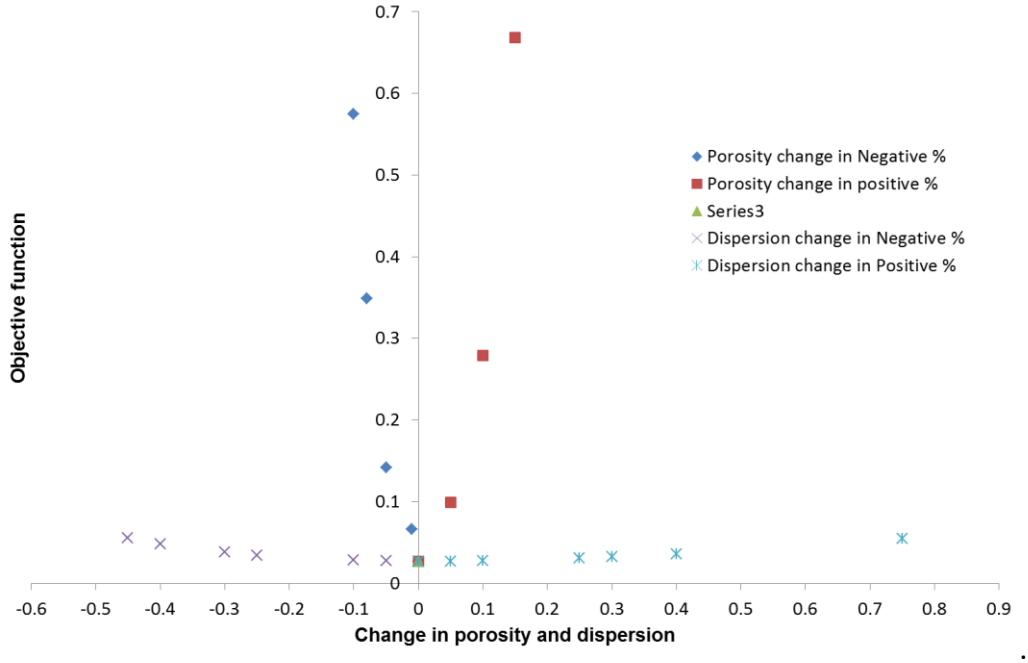

Figure 3.12: Change in porosity and dispersion.

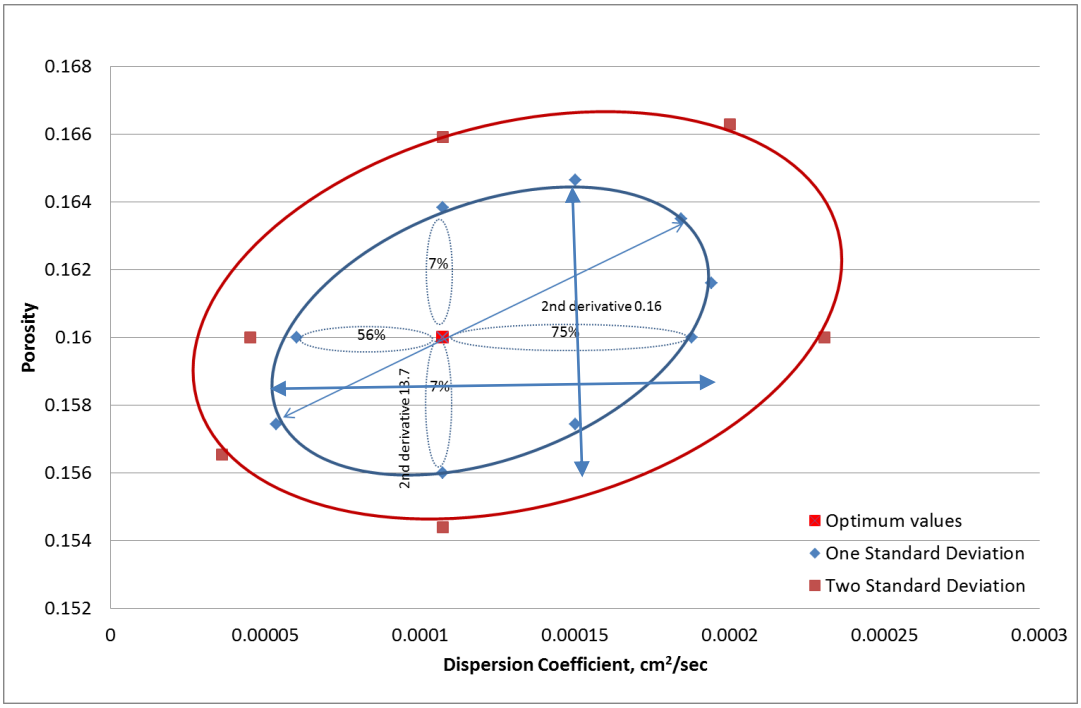

Figure 3.13: Statistics of the effective porosity against dispersion based on Gaussian LSQ analysis

3.3 Visualization of Oil Bank build up Process:

For coreflow experiments at scales ranging from 0.07 m to 1 m, we monitor slug movements across the core and study fluid flow and distributions during the chemical coreflood experiments via X-ray computerized tomography. The X-ray tubes rotate around the horizontal situated core in the center of the target ring. At the same time, the sample

moves on the couch, this creates a helical scan path out of which tomographic 2-D density images are created based on the X-ray attenuation. They are rendered to 3-D saturation profiles, where the X-Y resolution in the plane is 250 µm x 250 µm. The image analysis was done using standard AVIZO™ workflows as well as in-house Avizo codes developed by the authors.

Following our experimental protocol after step 8 (i.e. waterflooding), a fraction of the oil originally in the core or micromodel is displaced. This leaves the residual oil in the form of discontinuous oil blobs in the pore framework, named ganglia (Constantinides , Payatakes 1991).

We inject a surfactant-polymer brine mixture to reduce the interfacial tension and mobilize these ganglia. They tend to move faster than the chemical flood, i.e. at the beginning, as disperse and discontinuous ganglia, and later they start to collide with other ganglia and coalesce. Consequently, a zone of dense concentration of moving ganglia is expected to form near the advancing flood front of mostly connected oil. The oil bank in turn, supports to increase the displacement efficiency on other ganglia encountered downstream.

Degree of repeatability and reproducibility of the coreflow experimental data by the set-up

One of the main concerns on the experimental data is the summed measurement errors caused by the operator, the dead volume sensitivity, the calibration of the transducers, thermos couples, pumps, the external environment (temperature, humidity, air pollution, etc.), the time elapsed between measurements, etc.. We reduce operator errors/variability by automating our setups through labview™. We define the reproducibility as repeatability of the experimental results under the same conditions, using the same core. As a consequence, in the experimental protocol, we repeat each experiment (including the cleaning and initialization/charging) more than once.

Figure 3.14 shows two experiments in the CT scanner on a 0.17 m core. Here, the objective is to compare the movement and shape of a chemical slug across the core. Figure 3.14 A shows the distribution of residual oil after waterflood. The oil ganglia are disconnected and trapped due to capillary forces. After 0.14 and 0.26 PV of chemical injection, the residual oil starts to merge, forming an oil bank moving through the porous media. Chemical breakthrough is observed after 0.68 PV, while oil has been displaced after 1.5 PV of chemical injection.

We clearly observe reproducibility of chemical movement and oil bank formation when we compare the first experiment and repeat the experiment. In addition, we observe the effect of core heterogeneity when the chemical slug starts to take preferential flow paths and re-traps ganglion oil. With continuous chemical injection and distribution through the pore framework improves conformance and increases sweep efficiency. Figure 3.15

demonstrated the reproducibility of the experimental data from the effluent productions of the two experiments.

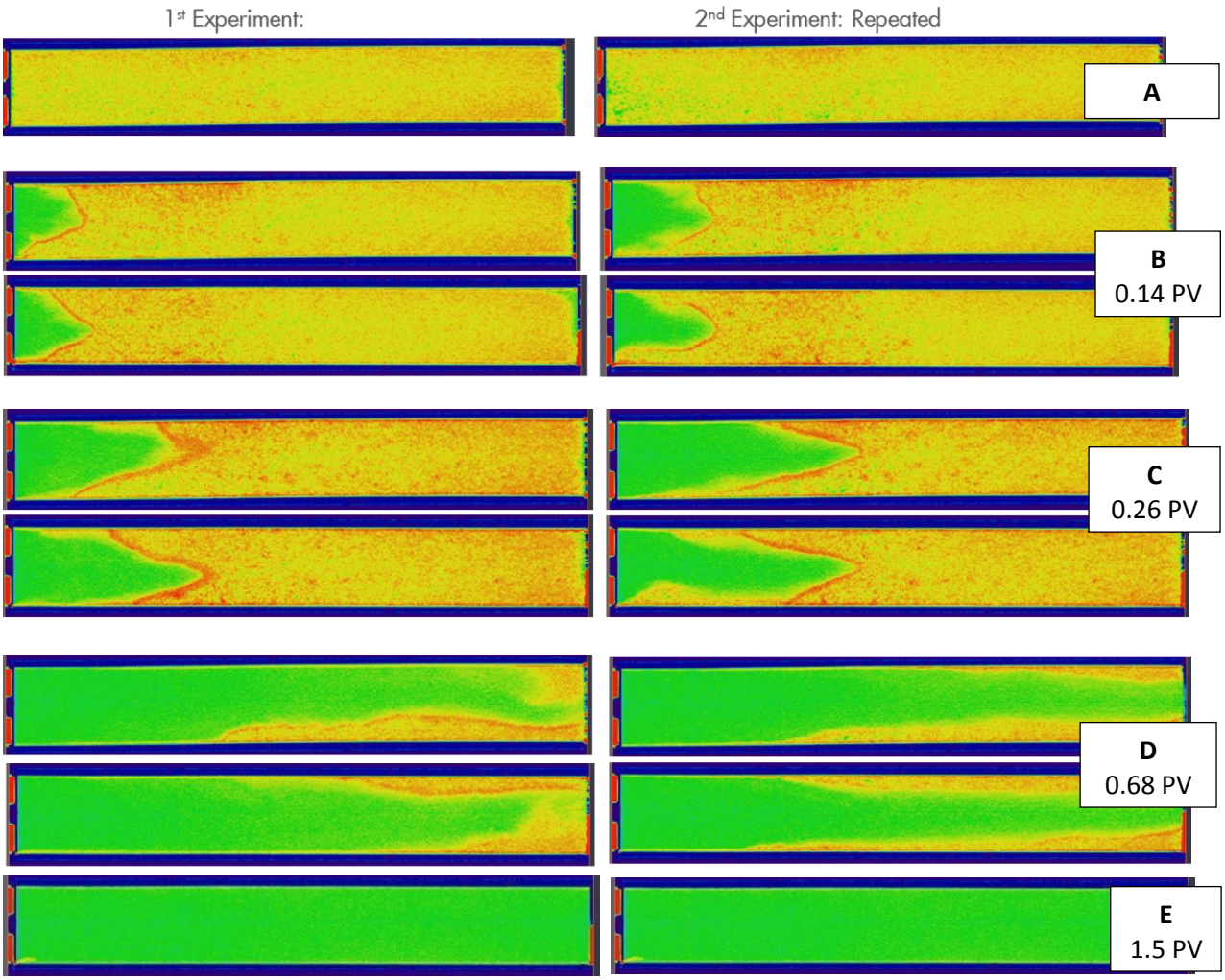

Figure 3.14: Synchronized CT scans at the same PV with chemical injection. The left-side images are the first experiments, the right side images represent the repeated experiments. Each PV is labelled from A to E. From each stage new phase injection stage we present a cross section in the horizontal and vertical cross-sections. Figure 3.14A present the residual oil status after waterflooding. Figure 14B, 14C show the surfactant movement and oil bank build up after 0.14 and 0.26 PV SP injected respectively. Figure 14D demonstrate the SP breakthrough after 0.68 PV. Figure 3.14E confirms that oil is swept after 1.5 PV.

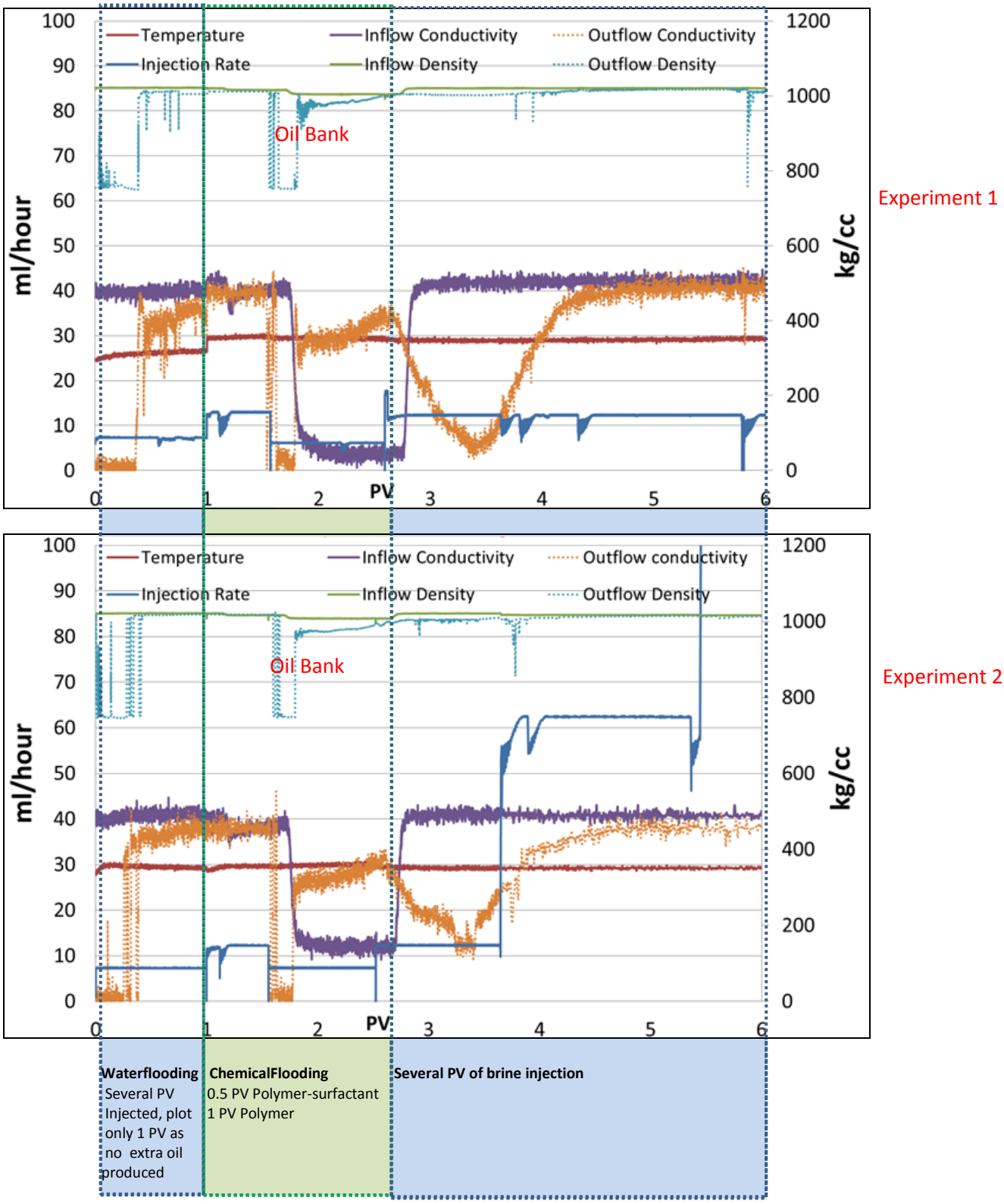

Figure 3.15: Two experiments repeated on the same core following the same experimental protocol to demonstrate the reproducibility of the experimental data. Oil Bank could be identified clearly at density of 750 kg/cc and conductivity of 0.

Summary of the reproducibility of coreflow experiments and variations in results:

Figure 3.16 and Table 3.3 presents the variance in the coreflow results in the same core samples at different stage of flood injection (initial oil saturation, residual oil saturation after wateflood and oil saturation after chemical flood). It could be observed that we got high initial oil saturation (>0.7) which is attributed to the effectiveness of the porous plate. On the reproducibility, we have a reasonable reproducible results within a variance of 3 saturation unit as shown in figure 3.16 and in table 3. In the sample 3 in table 4, which exhibits matrix heterogeneity as show in dry CT scan (figure 3.17), we observed a variation during repetitions of 11 saturation units. The flow in the porous media has been influenced and results could not be reproduced or predicted.

In other words, when the sample is homogenous the results are reproducible within the accepted range.

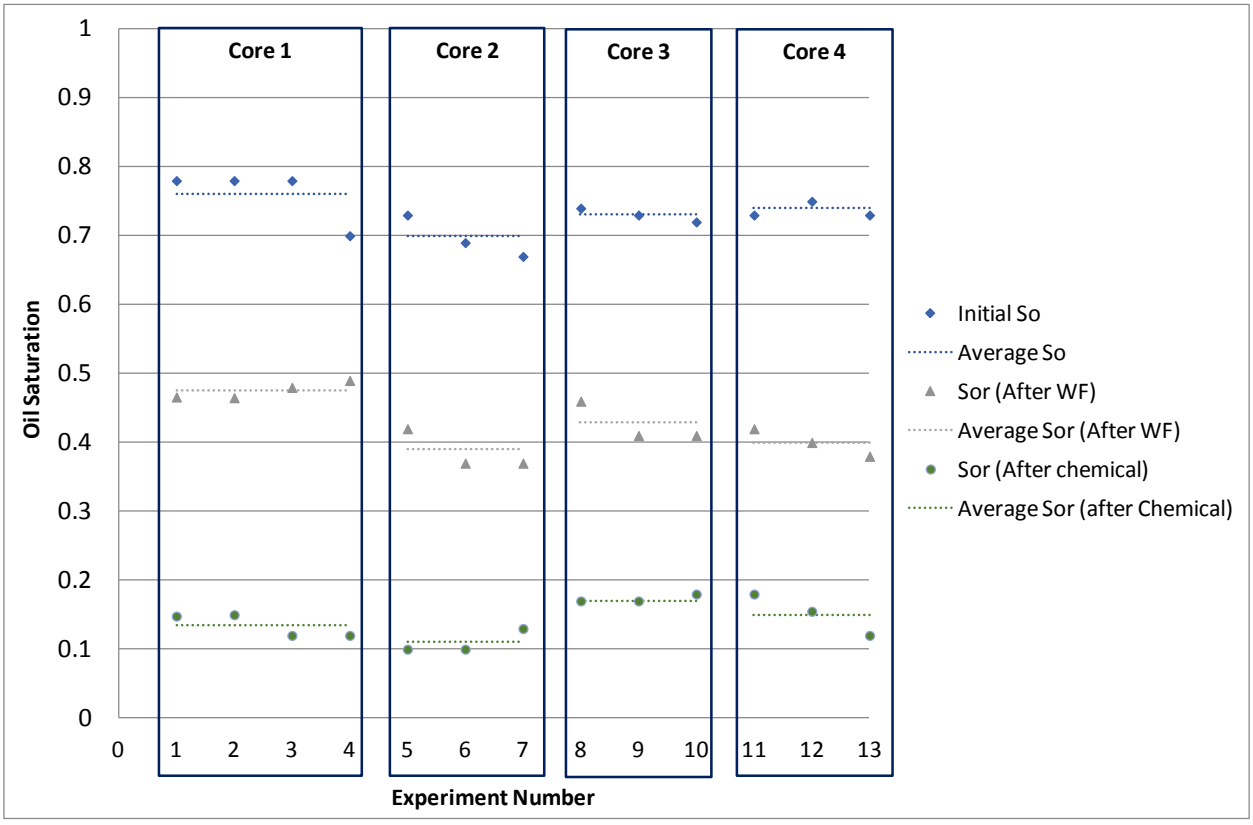

Figure 3.16: Oil Saturation profiles

Table 3: Examples of n experiments with three different samples.

Table with examples of n experiments with tow different samples.				
	Sample 1; 17 cm, permeability 70 mD			
3 repetitions in a cycle	Exp 1	Repetition 1	Repetition 2	Repetition 3
Initial Oil Saturation, S_{oi}	0.78	0.78	0.78	0.70
S_{or} Waterflood	0.47	0.48	0.47	0.49
S_{or} Chemical Flood	0.15	0.12	0.15	0.12

	Sample 2; 17 cm, Low permeability < 5 mD			
2 repetitions in a cycle	Exp 2	Repetition 1	Repetition 2	Repetition 3
Initial Oil Saturation, S_{oi}	0.73	0.67	0.69	0.74
S_{or} Waterflood	0.42	0.37	0.37	0.46
S_{or} Chemical Flood	0.1	0.13	0.1	0.12

Table 4: Example of variation in a core-flow experiment during repetition

	Sample 3; 39 cm, Heterogeneous		
2 repetitions in a cycle	Exp 1	Repetition 1	Repetition 2
Initial Oil Saturation, S_{oi}	0.66	0.66	0.66
S_{or} Waterflood	0.50	0.50	0.37
S_{or} Chemical Flood	0.05	0.16	0.13

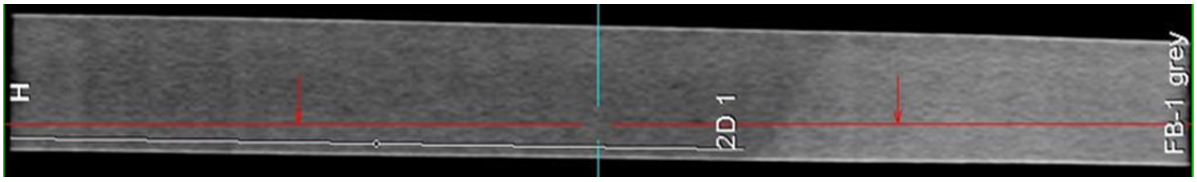

Figure 3.17: Dry CT scan of sample 3; variation in the density across the sample indicating the presence of heterogeneity.

5. Summary of results:

Two experimental setups have been developed to investigate the oil mobilization process in a porous system.

The microfluidic setup is capable to visualize the oil bank process at pore scale level (i.e. µm). It is designed with a path length of one meter with porous media geometry features. The results show:

- The three phases i.e. oil, brine and chemicals can be recognized by false color images. The separation of the phases by image quantification, during the process of building the oil bank, has been succeeded for the visualization of ganglion oil. However, for the other phases, the method must be improved by using higher resolution imaging and improvement of the phase-relevant grey-level pixel ranges and the corrections for optical effects.
- The continuous developing oil bank formation.
- The process of oil bank build-up where the residual oil is mobilized and started to coalescence. The oil bank is formed, stabilized and transported across the channels.

The coreflooding system combined with a CTS imaging system, visualizes the in-situ conditions of building the oil bank in the porous media of core samples with different lengths.

- The core samples properties (i.e. permeability and pore volume) have been calculated by using the differential pressure transducers.
- The phase composition of the effluent has been identified and quantified by using a Coriolis meter and conductivity measurements.
- A range of sample lengths, from 0.07 m to 1 m, can be accommodated in the setup. In this way we created an advanced experimental platform with various sizes of oil bank build-up through chemical enhanced oil recovery and associated effluent analysis.
- Porous plate gives a essential advantage and proven to be an effective tool as it gives high initial oil saturation in the range of 0.7 to 0.8.
- The experimental protocol and high resolution data-acquisition of the coreflow setup show that an efficient repetition of experiments with a good reproducibility has been achieved. This is an important requirement when performing complex multi-phase experiments. Hence, there are some experiments with less reproducibility where the matrix heterogeneity influence the fluid flows.
- The experimental results prove to have a high level of accuracy and resolution within a variance of 3 saturation units due to the designing and implementation of high quality measuring/monitoring devices.
- The improved instrumentation of the set-up has the ability to control the set-up remotely even with a smart phone.

Concluding remarks

A comprehensive set of experimental data for oil bank build-up has been produced for various experimental scales, lengths and volumes. In addition, the amount and distribution of residual oil left after waterflood and chemical slug injected and the salinity of the slugs, induce the process of building up of oil bank. In addition, the results show a positive correlation between sample size and oil bank characteristics, based on pore volume and matrix homogeneity.

The fully automated coreflow setup allows repetitive cleaning, saturation and displacement experiments without the need to disconnect the core and/or fluid system. It produces a quantitative measure of reproducibility and by that the accuracy of the experimental cycles.

The literature contains many studies based on the comparison of single experiments with varying conditions for each of the corefloods. Our experiments have shown that, even under the best of circumstances, there is variability for identical experiments on the same core. Without the repeatability, only the larger differences between different corefloods are significant. This is often overlooked in coreflood studies.

6. Acknowledgements:

The authors want to thank the TU Delft technical team (Karel Heller, Joost van Meel, Ellen de Koning and Jens van den Berg) for their contributions to the sample preparation, experimental work, CT scanning and image analysis discussions.

7. References:

1- Chatenever, A., and J.C. Calhoun, Jr. 1952. Visual examinations of fluid behavior in porous media: Part 1. J. Pet. Technol. 4:149–156. doi:10.2118/135-G.
2- Chen, J.-D., and D. Wilkinson. 1985. Pore-scale viscous fingering in porous media. Phys. Rev. Lett. 55:1892–1895. doi:10.1103/PhysRevLett.55.1892.
3- Lenormand, R., and C. Zarcone. 1985a. Invasion percolation in an etched network: Measurement of a fractal dimension. Phys. Rev. Lett. 54:2226. doi:10.1103/Phys-RevLett.54.2226.
4- Lenormand, R., and C. Zarcone. 1985b. Two-phase flow experiments in a two-dimensional permeable medium. Physicochem. Hydrodyn. 6:497–506.
5- Corapcioglu, M.Y., S. Chowdhury, and S.E. Roosevelt. 1997. Micromodel visualization and quantifi cation of solute transport in porous media. Water Resour. Res.33:2547–2558. doi:10.1029/97WR02115.
6- Blunt, M. J., M. D. Jackson, M. Piri, and P. H. Valvatne (2002), Detailed physics, predictive capabilities and macroscopic consequences for porenetwork models of multiphase flow, Adv. Water Resour., 25(8 – 12), 1069– 1089.
7- Unsal, E., Broens, M., & Armstrong, R. T. 2016. Pore Scale Dynamics of Microemulsion Formation. Langmuir 32(28): 7096–7108. Doi:10.1021.
8- Wegner, J., Hincapie, R.E., Foedisch, H. and Ganzer, L. (2015) Novel Visualisation of Chemical EOR Flooding Using a Lab-on-a-Chip Setup Supported by an Extensive Rheological Characterisation. Society of Petroleum Engineers, Kuala Lumpur. doi.org/10.2118/174648-MS.
9- Dullien F.A.L., Dhawan G.K., Gurak N., Babjak L. “A Relationship between Pore Structure and Residual Oil Saturation in Tertiary Surfactant Floods”, SPE J. 12, 4, 289-296. SPE-3040, 1972.
10- Stegemeier, G. L.: "Mechanisms of Entrapment and Mobilization of Oil in Porous Media", in Improved oil Recovery by Surfactant and Polymer Flooding, Shah, D. O. and Schechter, R. S. ed., Academic Press, New York, 1977.
11- Wardlaw, N. C., “The effects of geometry, wettability, viscosity, and interfacial tension on trapping in single pore-throat pairs”, J. Can. Pet. Technol., 213, 21–27, 1982.
12- Al Saadi F, Wolf KH and Kruijsdijk C.V. (2017) Characterization of Fontainebleau Sandstone: Quartz Overgrowth and its Impact on Pore-Throat Framework. J Pet Environ Biotechnol 7: 328. doi: 10.4172/2157-7463.1000328

13- J. Bruji´c, C. Song, P.Wang, C. Briscoe, G. Marty, and H.A. Makse. 2007. Measuring the coordination number and entropy of a 3d jammed emulsion packing by confocal microscopy. Physical review letters 98, 24 (2007), 248001
14- A. Datta, D. Mandal, S.K. Pal, and K. Bhattacharyya. 1997. Intramolecular charge transfer processes in confined systems. Nile red in reverse micelles. The Journal of Physical Chemistry B 101, 49 (1997), 10221–10225.
15- P. Greenspan, E.P. Mayer, and S.D. Fowler. 1985. Nile red: a selective fluorescent stain for intracellular lipid droplets. The Journal of cell biology 100, 3 (1985), 965–973.
16- Roof. J.G., "Snap-Off of Droplets in Water-Wet Cores," SPEJ (March 1970) 85-90; Trans .. AIME, 249.
17- Bear, J. Dynamics of Fluids in Porous Media; Courier Corporation: Chelmsford, MA, USA, 1972.
18- Bachmat, Y., & Bear, J., 1987. On the concept and size of a representative elementary volume (REV). In: Advances in transport phenomena in porous media. Springer Netherlands, 3-20.
19- Mills, R., Chalmerst, J., Desmond, J., Bartlesville, T., 1928. Oil Recovery Investigations of the Petroleum Experiment Station of the U. S. Bureau of Mines, Tulsa Meeting
20- Chalmerst, J., and Bartlesville, T., 1930. Recent Studies of the Recovery of Oil from Sands. New York Meeting
21- De Groot, I., "Flooding Process for Recovering Oil from Subterranean Oil-Bearing Strata," U.S. Patent No. 1.823.439 (1929).
22- Wyckoff, R. D., and H. G. Botset (1936), The flow of gas-liquid mixtures through unconsolidated sands, Physics, 7, 325–345.
23- Leverett, M. C., and W. B. Lewis (1941), Steady flow of gas-oil-water mixtures through unconsolidated sands, Trans. AIME, 142(1), 107–116, doi:10.2118/941107-G.
24- Eugene, B. R., Alvin, D. B. and Leonidas, W. P. 1952. Method for producing oil by means of carbon dioxide U.S. Patent No. 2,623,596
25- Teter, J. W., Friedman, B. S., 1954. Petroleum production process, U.S. Patent No 2,669,306.
26- Binder, G. G., 1955. Secondary oil recovery by self propelled solvent extraction, U.S. Patent No 2,718,262.
27- Binder, G. G., Edward J. F., 1956. Multiple solvent secondary recovery process, U.S. Patent No 2771139.
28- Holbrook, O. C., 1958 “Surfactant-Water Secondary Recovery Process,” U.S. PatentNo. 3,006,411.
29- Helm, L. W. and Bernard, G. G., 1959. “Secondary Recovery Waterflood Process,”U.S. PatentNo. 3,082,822.
30- Csaszar, A. K. 1961. “Solvent-Waterflood Recovery Process.”, U.S. Patent No. 3,163,214.

31- Saraf, D. N. and Fatt, I.: Three-Phase Relative Permeability Measurement Using a Nuclear Magnetic Resonance Technique for Estimating Fluid Saturation. SPEJ 7(3), 235-242 (1967)
32- Hounsfield GN (1973) Computerized transverse axial scanning (tomography)—part 1. Description of the system. British Journal of Radiology, 46, 1016–1022
33- Vinegar, H.J., Wellington, S.L., 1987. Tomographic imaging of three-phase flow experiments. Review of Scientific Instruments 58 (1), 96–107
34- Brown, K., Sheppard A., and Wildenschild D., 2014. On the challenges of measuring interfacial characteristics of three-phase fluid flow with x-ray microtomography.
35- Wang, S. Y. el al. 1984 “Reconstruction of Oil Saturation Distribution Histories During Immiscible Liquid-Liquid Displacement by . Computer-Assisted Tomography," AIChE J. 30, No.4, 642-46.
36- Wellington, S.L. and Vinegar, H.J. 1985 " CT Studies of Surfactant Induced C02 Mobility Control ," paper SPE 14393 presented at the 1985 SPE Annual Technical Conference and Exhibition, Las Vegas, Sept. 22-25.
37- Pancharoen, M., Kovscek, A.R., and Thiele, M.R.: “Inaccessible Pore Volume of Associative Polymer Floods,” paper SPE 129910 presented at the SPE Improved Oil Recovery Symposium, Tulsa, OK, 24-28 April 2010.
38- Constantinides, G. N. & Payatakes, A. C. 1991 A theoretical model of collision and coalescence of ganglia in porous media. J. Colloid Interface Sci. 141, 486–504.

Chapter 4

Conditions for building up an oil bank during surfactant polymer flooding

Authors: Faisal AL Saadi, Himanshu Sharma, Kishore K. Mohanty, Karl-Heinz Wolf, Cor Van Kruijsdijk

This chapter is based on article called “Conditions for building an oil bank during surfactant polymer flooding which has been sent to the journal for review and publication. It describes the process and requirements for building successful oil bank by chemical floods. It also demonstrates some of the aspects that influence the developments of a stable oil bank.

Abstract

Surfactant flooding is a technique in which surfactants are added to a reservoir to produce an ultra-low interfacial tension (IFT) with crude oil at optimum salinity, yielding high oil solubilisation in the microemulsion phase. This leads to mobilisation of micro-sized oil droplets trapped in the porous media due to capillary forces. Initially, the mobilised oil droplets start to move as discrete entities. Some mobilised oil droplets become re-trapped, while others continue to move and coalesce. These coalescing droplets start to form a continuous oil phase, which is called an oil bank. Our understanding of when, and under what conditions, an oil bank is formed and maintained is very limited. This is relevant for various steps of the interpretation and up-scaling of core flow experiments from centimetre scale to field scale.

Here, we investigated various factors that influence the development of a stable oil bank through an extensive core-flow experimental study with the aid of CT scanning. We evaluated the effects of the pore volume and heterogeneity of the porous media, the impacts of surfactant phase behaviour and microemulsion viscosity, and the polymer requirements for favourable mobility conditions. We demonstrated that because water relative permeability increases as IFT and residual oil saturation decrease, without mobility control (provided by the addition of polymer in our case), the low IFT front is not stable and the surfactant slug forms a finger through the generated oil bank. Furthermore, we visualise the process of building the oil bank at the microscopic (pore) scale, which provides insight into what occurs on a microscopic scale and how the oil droplets mobilise, coalesce and advance as a continuous phase in front of the chemical flood front during the displacement process.

Introduction

In oil fields, waterflooding is a secondary recovery mechanism that improves sweep efficiency, maintains the reservoir pressure, and increases ultimate oil recovery, in some field cases by up to 30–60% (Amyx, Bass and Whiting, 1962; Wu et al., 1989). Still, more than half of the oil is usually left behind as disconnected or isolated residual oil due to capillary forces, reservoir heterogeneity and/or viscous and gravity instabilities. Among tertiary mechanisms, a chemical enhanced oil recovery (EOR) process (in our research, the injection of a surfactant-polymer mixture) aims to coalesce the isolated oil drops, form an oil bank and enhance oil recovery (Sheng, 2013). At the field scale, the principles work under the right conditions (Denney, 2015, Al Shuaili et al., 2018). However, there is limited understanding of the build-up of the oil bank at the pore scale. Specifically, there is a lack of understanding of the mechanisms of reconnecting the remaining trapped oil (i.e., oil bank build-up) and its transport through the porous media. The challenge of increasing oil recovery is primarily related to poor connection of trapped oil after waterflooding.

In principle, the surfactant provides (ultra) low interfacial tension (IFT), which is the key parameter in releasing trapped oil, while the polymer is required for mobility control to prevent bypassing of oil and ensure interaction with all residual oil in the porous media. For successful recovery, these mobilised oil ganglia must reconnect and coalesce to form a stable, continuous oil bank. Coalescence (i.e. oil bank build-up) is important to avoid breakdown and re-entrapment of isolated oil ganglia (Payatakes et al., 1980) and to maintain and transport the oil bank through the porous media. Hence, the parameters that affect coalescence and oil bank build-up have a big influence on the efficiency of the chemical EOR process.

Chemical EOR mobilisation experiments are usually conducted in sandstone core samples or microfluidic chips and are assumed to be a good representation for field trials. However, no comprehensive attempt has been made to experimentally evaluate the effects of sample length and heterogeneity or oil type on coalescence and oil bank build-up. This evaluation will be of great value when upscaling these experiments to field scale.

Literature Review:

The investigation of the mobilisation of dispersed clusters of a non-wetting phase is not a new subject [see, for example Gardesu (1930) & Smith and Crane, 1930]. The original approach was basic and did not consider, among other factors, characteristics of oil bank build-up such as the coalescence and break up of displaced droplets, the spatial characteristics of ganglia, and coalescence time. Following the original studies, more detailed work (Stegemeier, 1977; Mohanty, 1987; Ng and Payatakes, 1980) was done on the mechanisms of oil-bank formation and development. It has been suggested that without the build-up of the oil bank, the process behaves more like the unstable injection of a surfactant solution alone, where the oil is produced in dispersed form or is emulsified in the flowing

surfactant stream (Wasan, 1979). A stabilised oil bank depends on the process of oil ganglia coalescence at the front, which continuously extends the length (volume) of the continuous oil phase. This coalescence is negatively impacted by the process of oil ganglia deterioration through break up (Payatakes, 1984). Recently, imaging of the pore-scale displacement process was conducted via X-ray computed micro-tomography, which provided further insight into the ganglion dynamics flow regimes (Iglauera et al., 2012; Berg et al., 2014). For field application, pore-scale modelling was proposed as a reservoir characterisation tool where the details of multiphase flow properties could be assigned to field geological models (Blunt et al., 2002).

Our hypothesis is that the oil ganglia start moving and coalescing as they are mobilised from their entrapments, but may break up and become re-trapped in the porous medium a short distance from where they were liberated. As more oil droplets coalesce and become a continuous oil phase, an oil bank is built up that dominates the flow regime (Figure 4.1, Figure 4.2). We attempt to investigate the transition from dispersed oil ganglia to continuous oil bank by evaluating the change in oil mobility at different core scales.

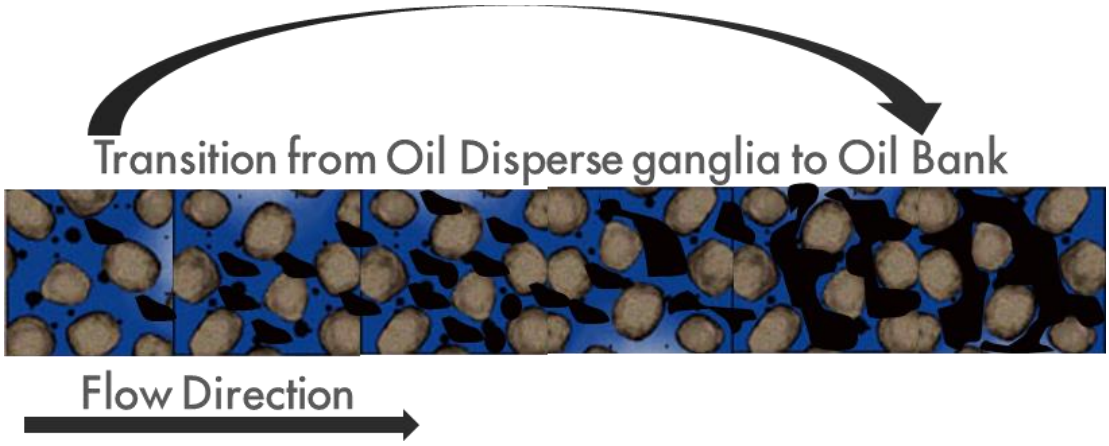

Figure 4.1: 2D Schematic of porous media; oil ganglia (black), brine (blue) and porous media grains (brown).

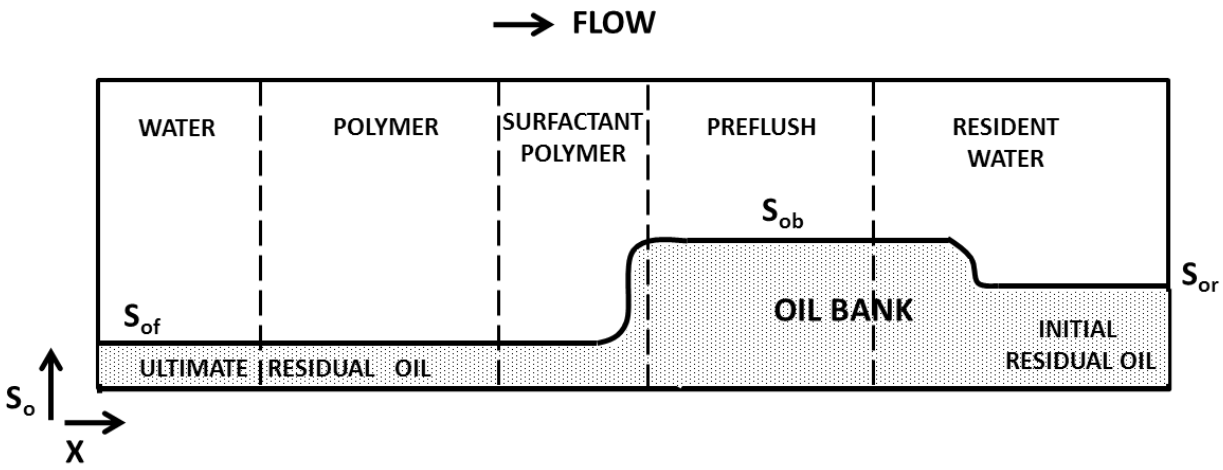

Figure 4.2: Distribution of oil saturation during the process of building an oil bank (modified from Reed and Healy, 1977, who used surfactant while we used surfactant polymer).

Materials and Methods

Materials

Fontainebleau sandstone cores, which consisted almost entirely of pure quartz (99.5%) without any clay, were used in the corefloods. A detailed characterisation of the core can be found elsewhere (Al Saadi et al., 2017). These cores were used to conduct highly reproducible corefloods, which can be compared quantitatively due to the use of a highly instrumented coreflood set-up (Al Saadi et al., 2019).

Table 4.1: Basic parameters of our core samples during the experiments.

Fontainebleau		**Set 1**	**Set 2**	**Set 3**	**Set 4**
Length	[cm]	7	17	39	60
Diameter	[cm]	3.9	3.9	3.9	3.9
Porosity	[%]	8–12	8–12	8–12	8–12
Brine permeability	[mD]	10–80	10–80	10–80	10–80

Dodecane and iododododecane were used as the oleic phases. Iododododecane was used in experiments conducted under the CT scanner.

Table 4.2: Properties of oleic phases during the experiments.

Name	**Formula**	**Density (kg/m^3)**	**Viscosity (Pa.s)**
Dodecane	$C_{12}H_{26}$	750	1.3
Iododododecane	$C_{12}H_{25}I$	1200	3

The aqueous solutions were prepared using laboratory-grade sodium chloride salt. The aqueous surfactant sample was prepared at the optimum salinity (determined as described below), which has been shown to promote the fastest coalescence (Payatakes 1981). Internal olefin sulphonate (IOS) surfactant was used in our experiments. It is an anionic surfactant produced by Shell Chemicals and part of ENRODET™ with carbon chain lengths of 20–24. Internal olefin sulfonates have twin hydrophobic tails that vary in individual lengths. It is a good EOR surfactant (Barnes, 2010) due to its low adsorption in sandstone. The surfactant formulation consisted of 1 wt% C20-24 IOS with 4 wt% 2-butanol. Secondary butanol was used as co-solvent. It was added to encourage the formation of

thermodynamically stable micro-emulsions with low viscosity (Fortenberry et al, 2014) and to obtain clear aqueous-phase solutions. It is a non-ionic co-solvent and not sensitive to salinity. It has a low tendency to attach to the rock. It reduces the formation of gels, liquid crystals and macro-emulsions and promotes rapid equilibration to low-viscosity microemulsions (Bera Mandal, 1989).

SNF Polymer Flopaam 3630 was also added to our surfactant solution to achieve favorable mobility conditions. Without the polymer, the low-IFT front is not stable and the surfactant slug will finger. The polymer drive reduces oil phase trapping, which helps to minimise surfactant retention (Sheng, 2013).

Methods

Surfactant phase behaviour

The optimal phase behaviour was determined by performing a salinity scan on the chosen surfactant formulation to identify ultralow IFT formulations for dodecane and iododododecane. Stock surfactant solution was prepared. Small quantities of solution were separated, and sodium chloride was added incrementally to produce separate samples with increasing salinity.

The first series covered a range of 1-5 wt% of sodium chloride in unit steps. Once properly mixed, 10 ml of each solution was added to a graduated test tube together with 10 ml of dodecane (1:1 volume ratio). The test tubes were shaken strongly for 60 seconds to accelerate microemulsion formation. The samples were placed in a rack and left to equilibrate under observation. A photo was taken and analysed to determine solubilisation ratios and determine optimum salinity. The test was repeated once an approximate optimum salinity was known. The increments in salinity were decreased (in steps of 0.25%) to obtain a more accurate measurement of the optimum. This procedure was carried out for both dodecane and iododododecane. After equilibration, solubilisation ratios were obtained based on the amount of oil (or brine) solubilised in the microemulsion phase. These ratios were used to estimate the IFT based on the Chun Huh correlation (Huh, 1979).

IFT measurements

IFT measurements were also performed using a spinning-drop tensiometer and the procedure described below. Although it is assumed that the optimum salinity also exhibits the lowest interfacial tension, this can be verified using a spinning-drop tensiometer. The model used was an SVT 20 produced by Dataphysics™. The method uses the density difference between the two phases and centrifugal force to determine the low IFT resulting from the surfactant. A capillary tube is filled with the denser phase (brine when using dodecane; oil when using iododododecane), and a drop of the less dense phase is added. By rotating at high RPMs, the drop will start to elongate due to the centrifugal force towards the tube walls, as seen in figure 4.3.

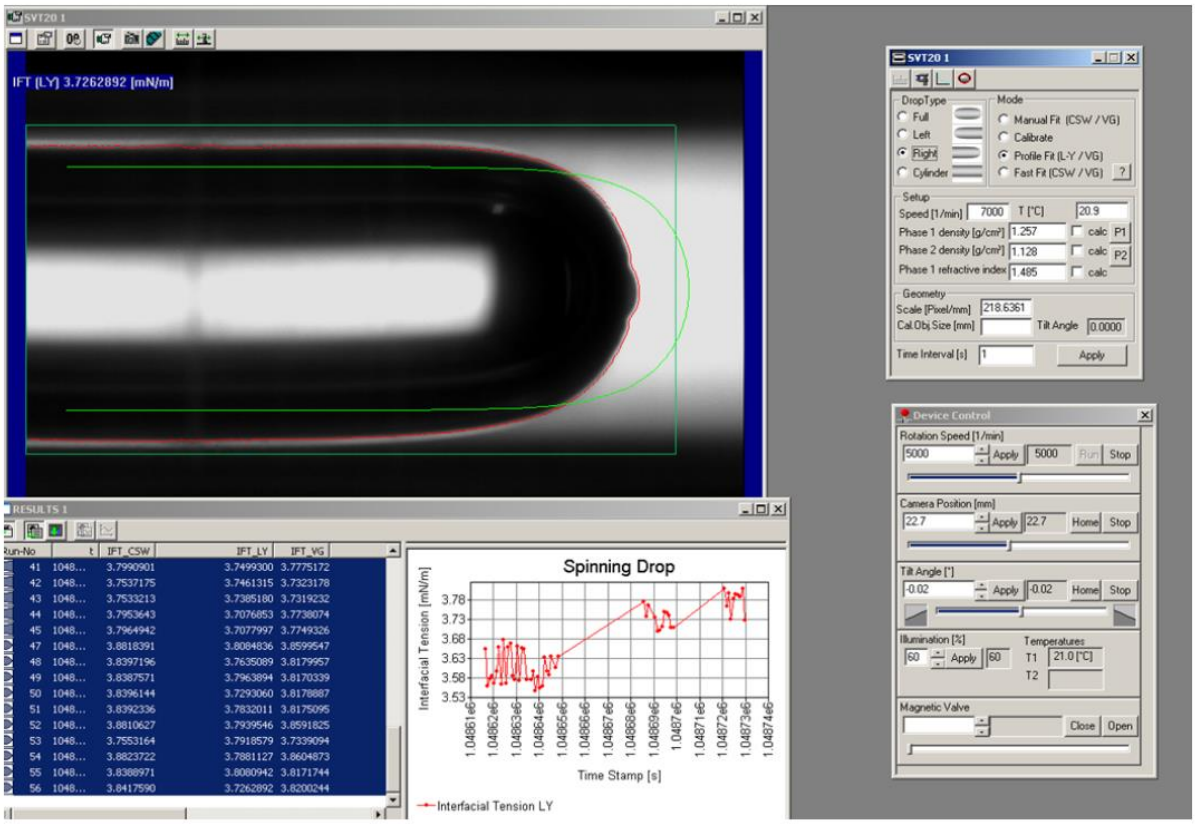

Figure 4.3: Screenshot showing the elongated oil droplet in the spinning drop tensiometer, as well the fitting software.

The deformation stops when the interfacial tension and centrifugal forces balance. The radius of the drop perpendicular to the axis of rotation is a function of the angular frequency, density difference and interfacial tension (Vonnegut, 1942). All of these are measured, and with the help of software, the dimensions of the drop are measured and the IFT calculated using the Young-Laplace method. The calculation was repeated 60 times and an average IFT determined.

Microemulsion viscosity measurements

Microemulsion rheology measurements were performed using a TA Instruments AR-G2 rheometer for the surfactant formulation which was used in corefloods. Samples were prepared similarly to those prepared during surfactant phase behaviour experiments; however, larger volumes were prepared. The samples were allowed to equilibrate at the desired temperature. The microemulsion phase was separated after the samples attained equilibrium for measurements (Humphry and van der Lee, 2013).

Coreflood experiments:(refer to chapter 3)

Experimental Results

Surfactant phase behaviour

For the dodecane/surfactant/brine system, the optimum salinity, which generates the required microemulsion phase, is in the range of 3.5–4 wt% as shown in Figure 4.4. Solubilisation ratios of oil and water in the microemulsion phase were calculated and are shown in Figure 4.5. Note from Figure 4.5 that the optimum salinity for the dodecane case (where oil and water solubilisation ratios are equal) was obtained at approx. 3.5 wt%. An optimum solubilisation ratio of approx. 8 (cc/cc) was obtained, corresponding to an IFT of approx. 0.003 mN/m. For iodododecane/surfactant/brine system, the optimum salinity is in the range of 4-5 wt% (figure 4.6, figure 4.8).

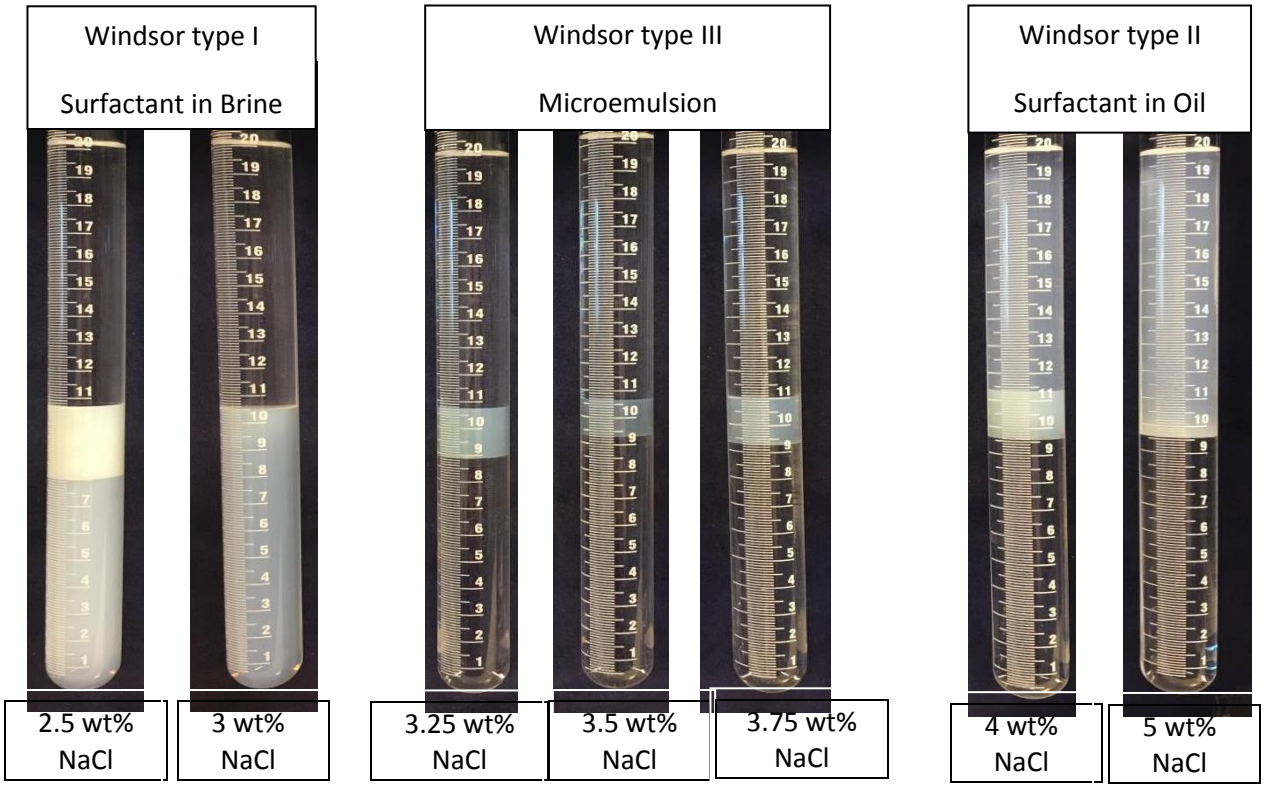

Figure 4.4: Visualisation of the phases during phase behaviour of a dodecane/surfactant/brine system at different salinities at ambient temperature.

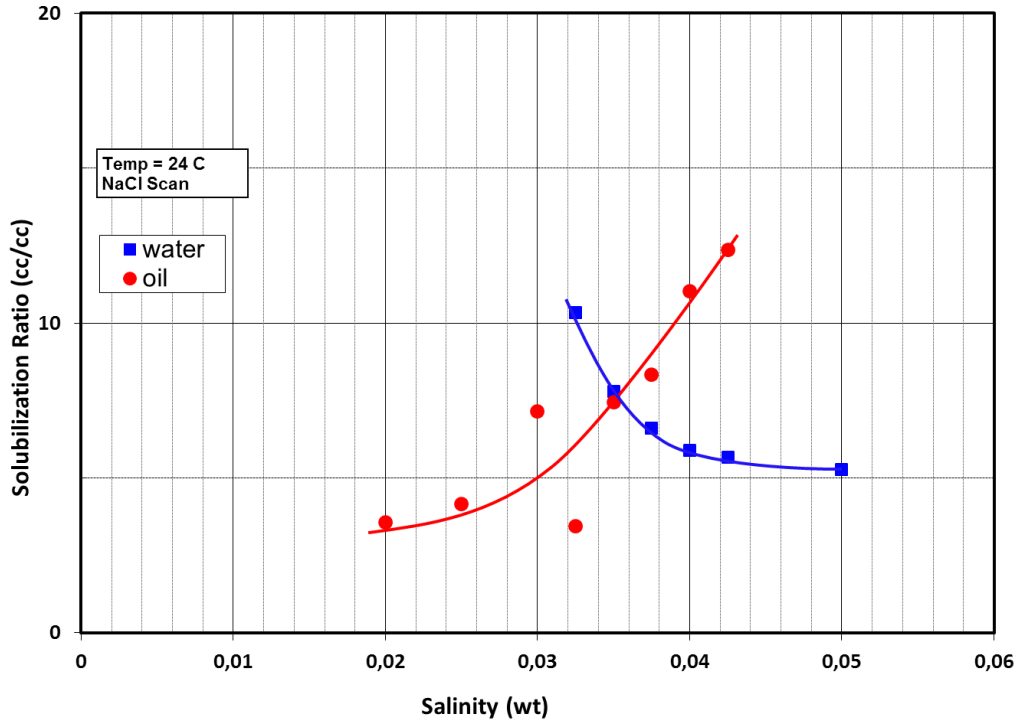

Figure 4.5: Solubilisation ratio of dodecane/surfactant system.

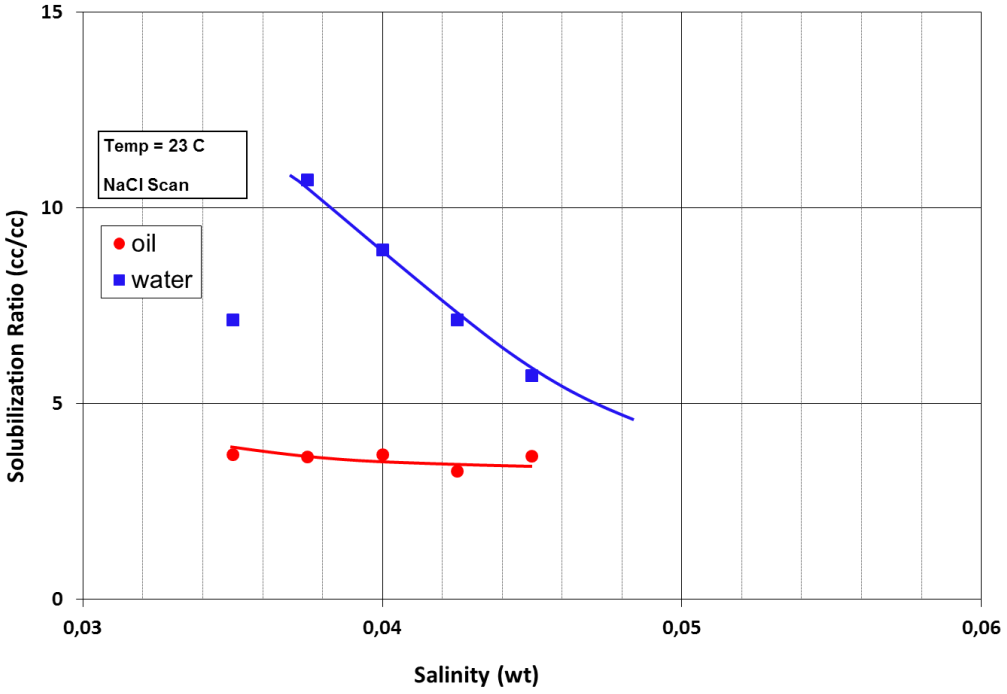

Figure 4.6: Solubilisation ratio of iodododecane/surfactant system.

IFT measurements

In addition to the phase behaviour results, we confirmed the IFT of being the Windsor type III using the spinning drop method with a tensiometer (Currie and Nieuwkoop, 1982). The IFT results (Figure 4.7) are in line with the phase behaviour tests; they show an ultra-low IFT at an optimum salinity of 3.5–4 wt%.

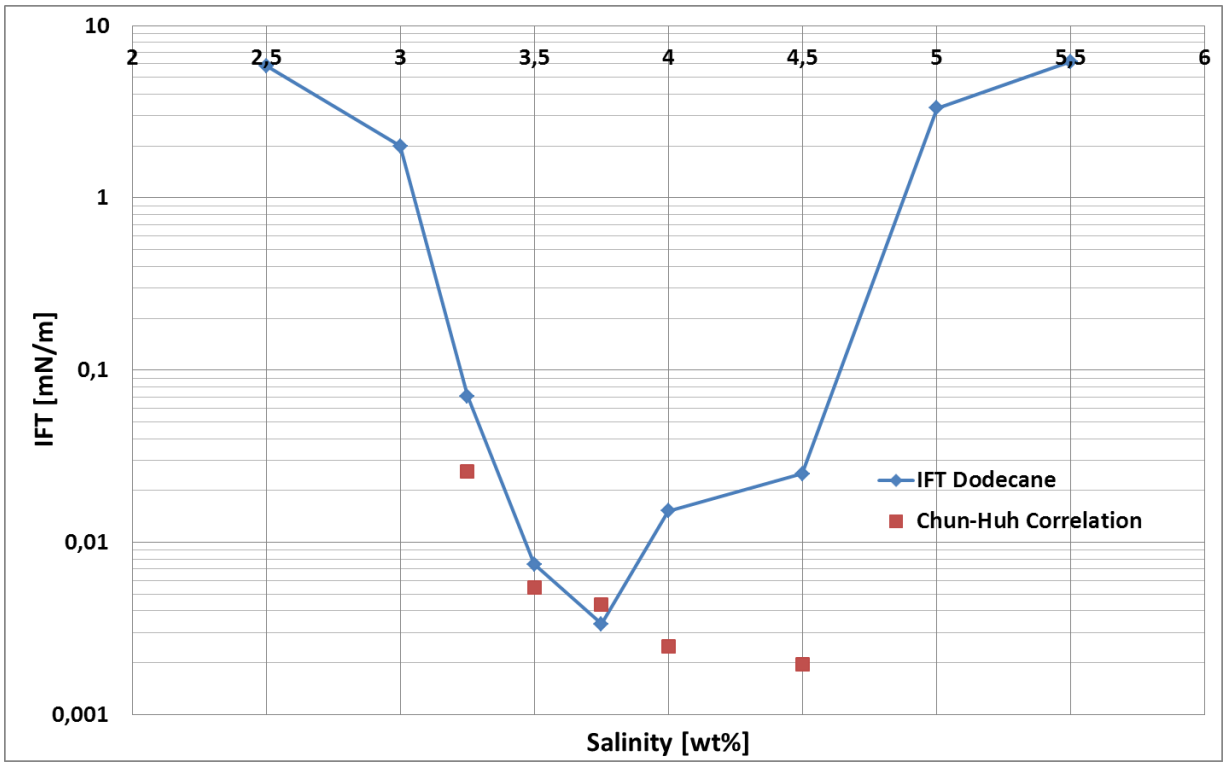

Figure 4.7: Spinning drop IFT measurements for dodecane/surfactant/brine system at different salinities and calculated IFTs based on solubilisation ratio and the Chun Huh correlation.

For the iododododecane/surfactant/brine system, similar tests and measurements show a clear shift to the right (i.e., higher salinity) to reach the microemulsion phase; this corresponds with the lowest IFT. Comparing the two systems shows an IFT 10 times higher for the latter system (Figures 4.7 and 4.8).

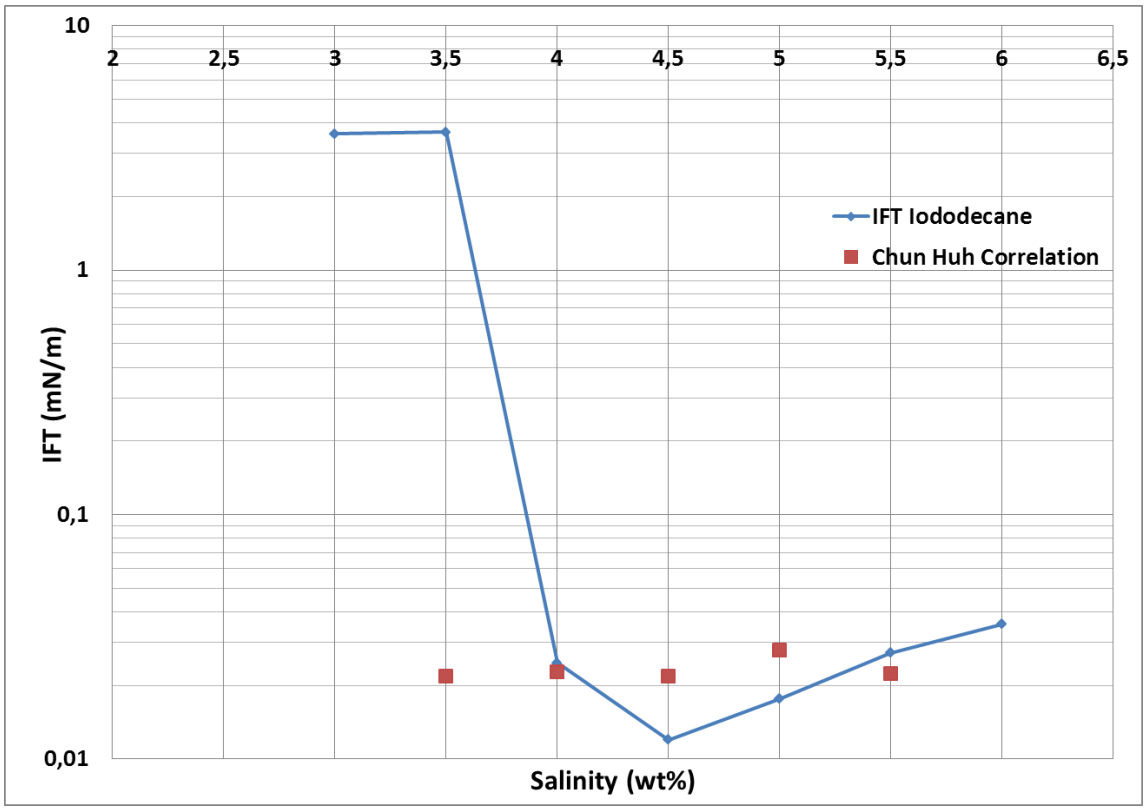

Figure 4.8: IFT measurements for iododododecane/surfactant/brine system at different salinities.

Coreflood experiments

We define the oil bank as the continuous mobilised oil phase that has been reconnected by the coalescence of the isolated oil ganglia. Once developed, it increases in volume during the transport through the porous media. If the oil bank is not formed, then the chemical process behaves more like the unstable injection of a surfactant solution alone. As a result, the oil is produced in dispersed or emulsified form in the flowing surfactant stream, leading to long and cost-ineffective oil recovery when applied under field conditions. We successfully created, visualised and reproduced the process of oil bank build-up, as shown in Figure 4.9. Details of the experimental protocol and visualisations of oil bank build-ups at different core lengths were previously published (Al Saadi et al., 2019). Van Batenburg et al. describe a series of experiments that used X-ray computer tomography (CT) to visualise the mobilisation of remaining oil by alkaline surfactant polymer flooding (van Batenberg et al., 2015).

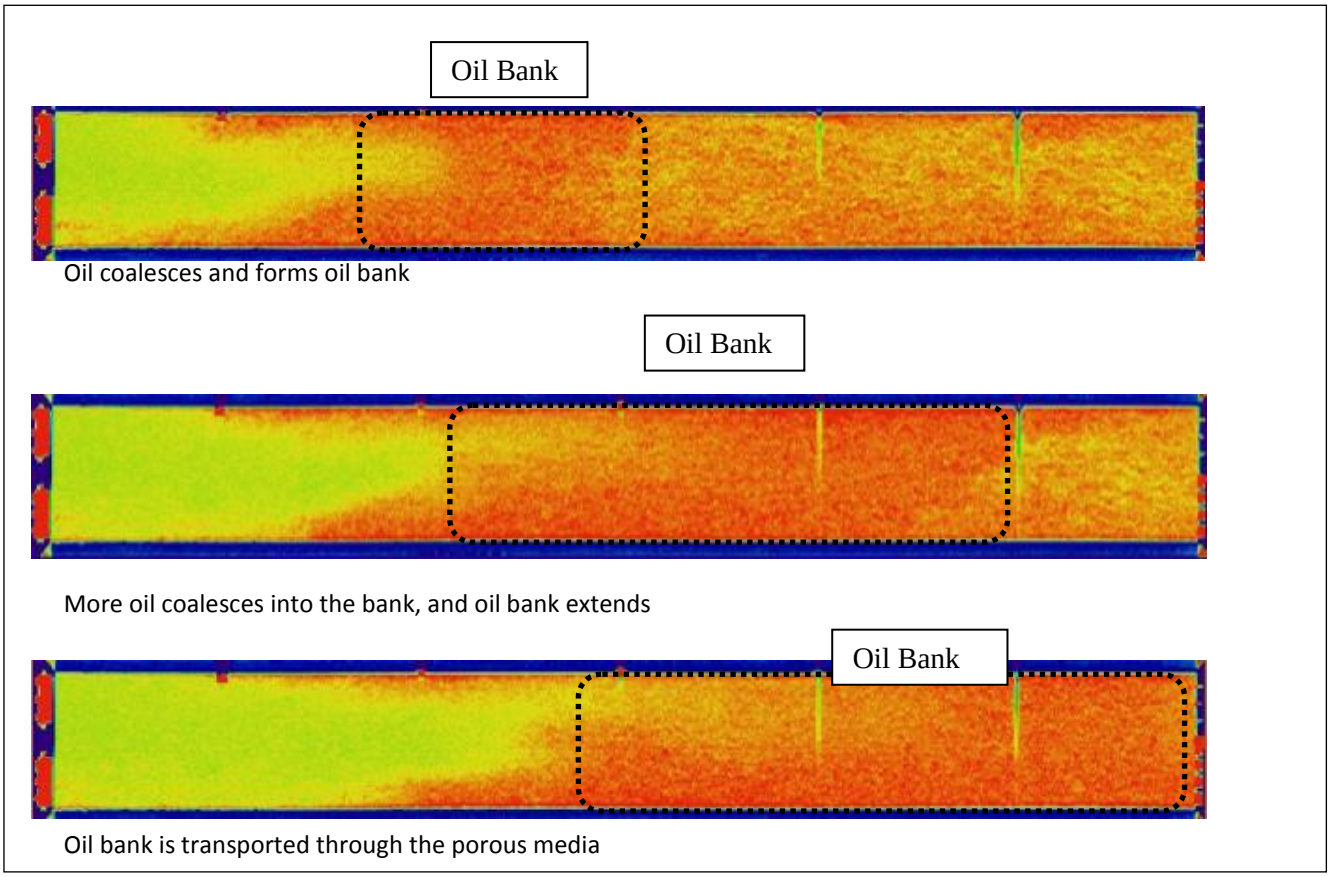

Figure 4.9: Oil Bank build up process in the core (Core Length is 38 cm, core diameter is 3.8 cm). Horizontal cross-sections from the X-ray CT data at the middle of the core. The injected volume increases from top to bottom. Red colour indicates larger oil volume fractions and green indicates the absence of oil.

Discussion

At the core scale, we observed the following processes that must occur to have a successful oil bank build up and accordingly a successful chemical EOR process.

1- Residual Oil Mobilisation:

After waterflooding, a considerable amount of oil (i.e. residual oil) is still trapped in the pores of the rock. The main reasons for this entrapment are microscopic features like pore geometry, wettability and capillary forces created by the oil/water interfacial tension (IFT). The residual/trapped oil ganglia can be mobilised if the displacing fluid (a surfactant polymer mixture in our case) reduces the IFT and overcomes the retaining capillary forces. The surfactant (IOS C_{20-24}) provides us the IFT in the range of 10^{-3} to 10^{-2} mN/m required to mobilise the oil ganglia. We visualised the process at the microscale level in (Al Saadi et al., 2018).

The stage of residual oil mobilisation is critical to freeing up and moving the trapped oil ganglia (droplets) but does not in itself guarantee an oil bank build-up.

2- Coalescence of the mobilised oil:

Once mobilised, the oil droplets must coalescence for efficient oil recovery. In this way, a continuous oil phase is formed ahead of the chemical flood front. Without coalescence, the mobilised oil may break up into small sizes and/or be re-trapped.

The continuous oil phase must move with a velocity higher than the velocity of the chemical front to form an effective oil bank. If so, it will tend to accumulate in front of the chemical flood. As result of collisions and coalescence between the continuous mobilised oil phases, an oil bank is formed. Consequently, it supports an efficient displacement of other mobilised oil encountered downstream. This process is influenced by the capillary number, the viscosity ratio, the contact angles and the size of the ganglia (Payatakes, 1991).

We observed that the coalescence process requires a certain minimum porous media pore volume (core length) to form a stable oil bank. Figure 4.10, here below, represents the oil cut of identical coreflow experiments with the same core materials at different core lengths (39 vs. 17 cm). It is quite evident that the oil bank (0.3 PV) is larger for the 39 cm core. For the 17 cm core, the oil bank (0.15 PV) is not significant. Berg et al. (2015) made similar observations. Hence, using too short a core, some researchers/operators might incorrectly exclude the chemical process and conclude that the reservoir is not favourable for chemical EOR. Note that there are many other aspects that must also be investigated prior to advocating for chemical EOR.

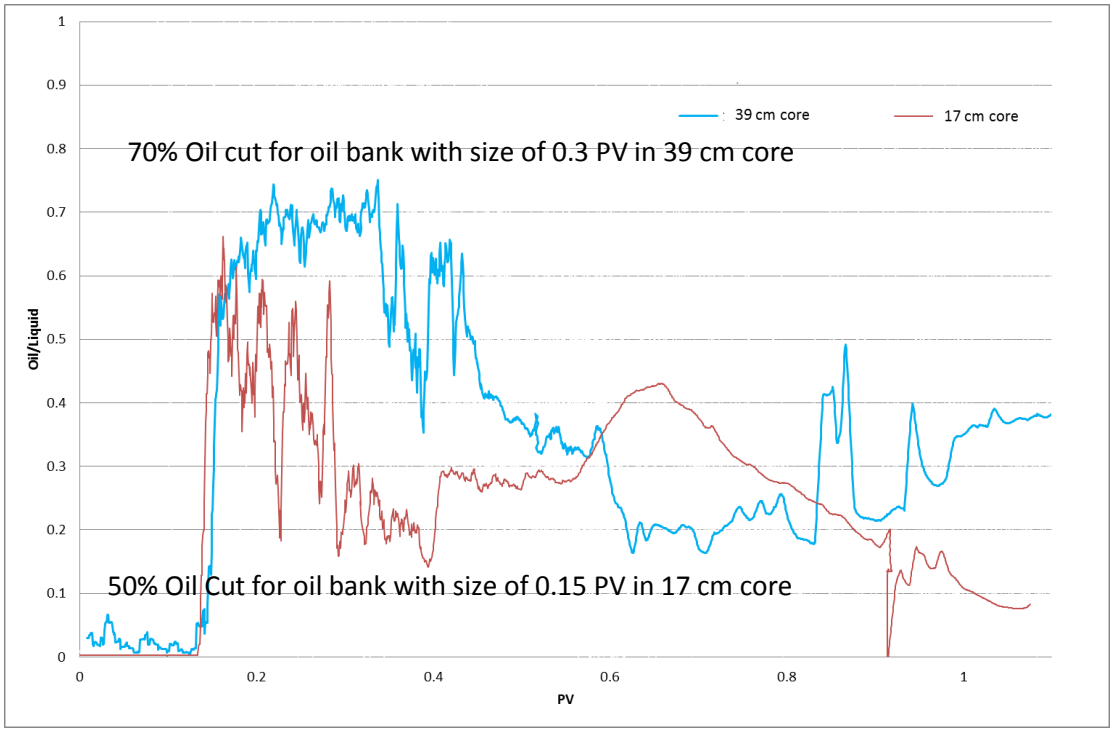

Figure 4.10: Oil cut profiles at the exit of the core for coreflow experiments with 17 and 39 cm core lengths.

3- Maintenance of the oil bank during displacement:

The coalescence of disjointed ganglia with each other and with the interface between the surfactant solution and the oil bank, contributes to the maintenance and propagation of the oil bank. Note that the oil bank, once formed, gathers up residual ganglia at its front, continually extending its length (volume). Thus, an important opportunity for improving surfactant/polymer system performance for oil-bank development exists in learning more about how the system affects the drop-interface and drop-drop coalescence behaviour and, hence, the stability of emulsions flowing through porous media. It would be highly desirable to be able to screen surfactants, co-surfactants, and other chemical additives for use in actual tests, based on emulsion stability experiments conducted in the laboratory.

Transportation of the oil bank through the porous media is the final stage for an efficient chemical EOR process in the laboratory. We observed two factors that influence the propagation of the oil bank in the porous media:

1- <u>Heterogeneity of the porous media:</u>

For low-permeability (5-10 mD) heterogeneous cores (CT scan), the oil bank was small (< 0.15 PV). This result may be improved by increasing the chemical slug size to 0.5 PV. Figure 4.12 presents results for a low-permeability sample where on the top we injected 0.3 PV of the chemical slug, resulting in a small oil bank. On the bottom is the experiment repeated on the same core but with an increased chemical slug size (0.5 PV). It can be seen that the oil bank build-up is bigger, resulting in a more efficient process. Hence, for more homogeneous sample at slightly higher permeability (80 mD), chemical slug of 0.3 PV is enough to build significant and comparable oil bank as it can be seen in figure 4.11.

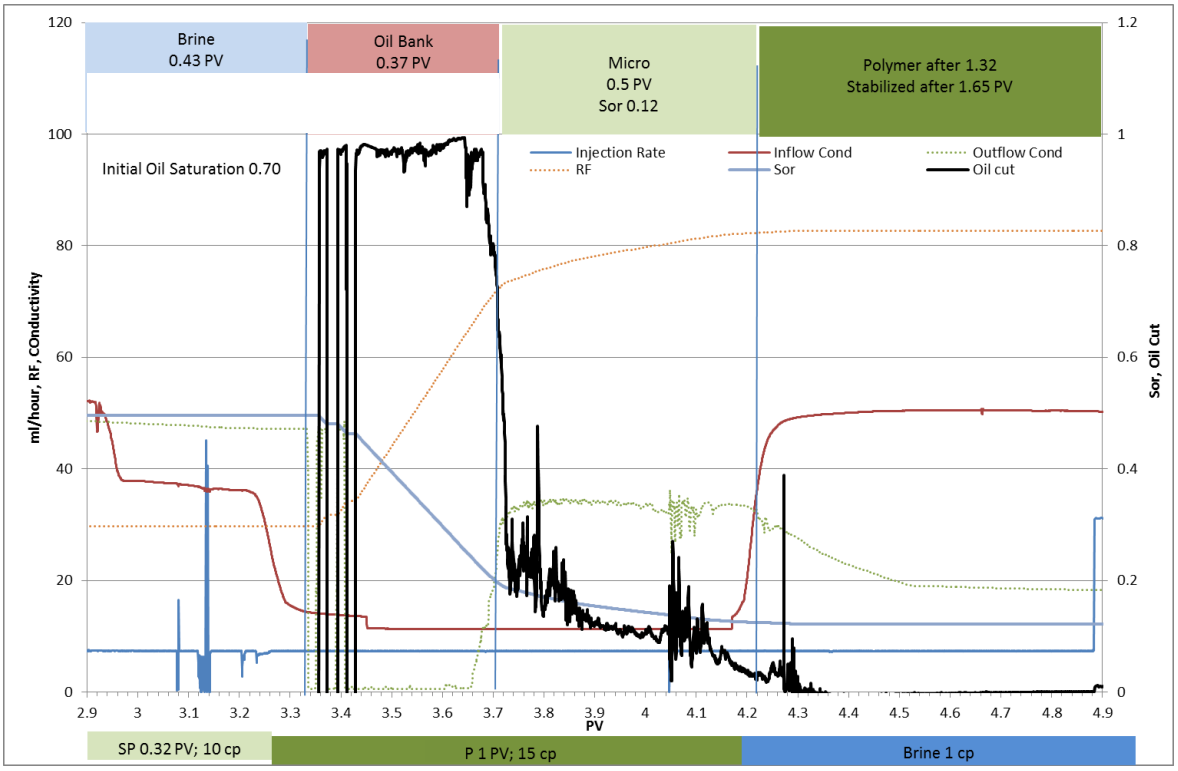

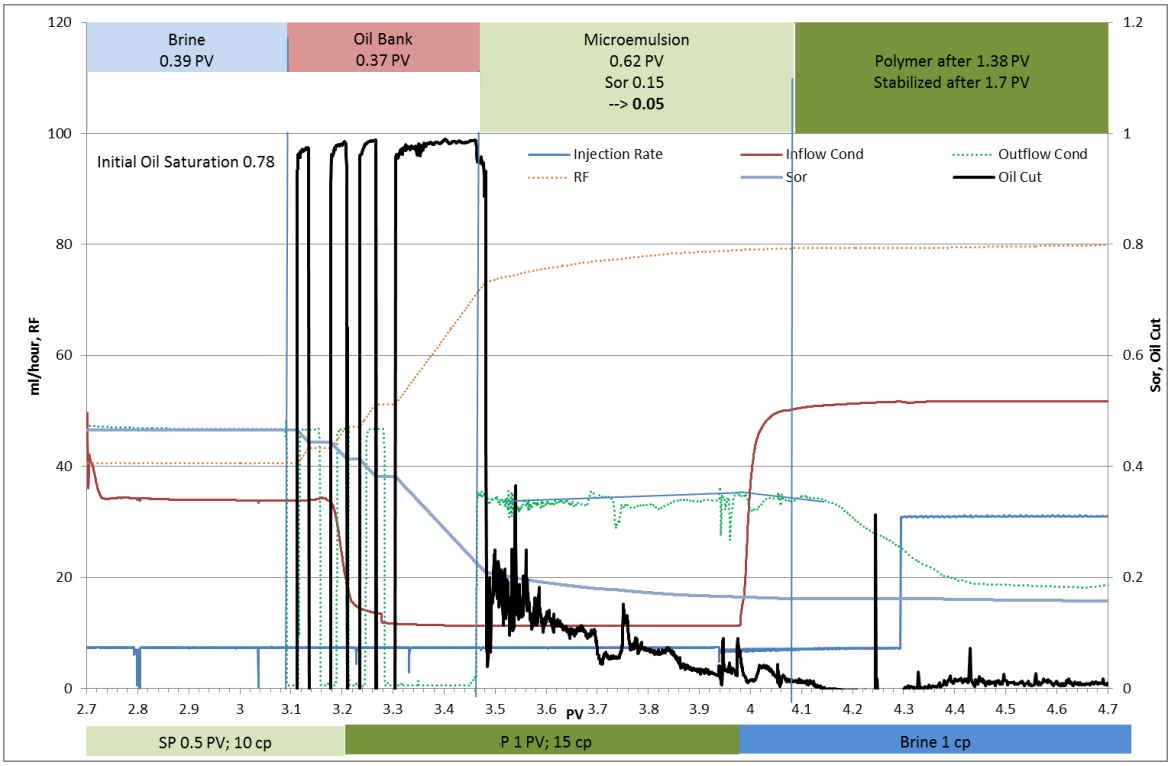

Figure 4.11: coreflow experiment in 80 mD sample; Top: chemical slug is 0.3 PV; bottom: chemical slug is 0.5 PV

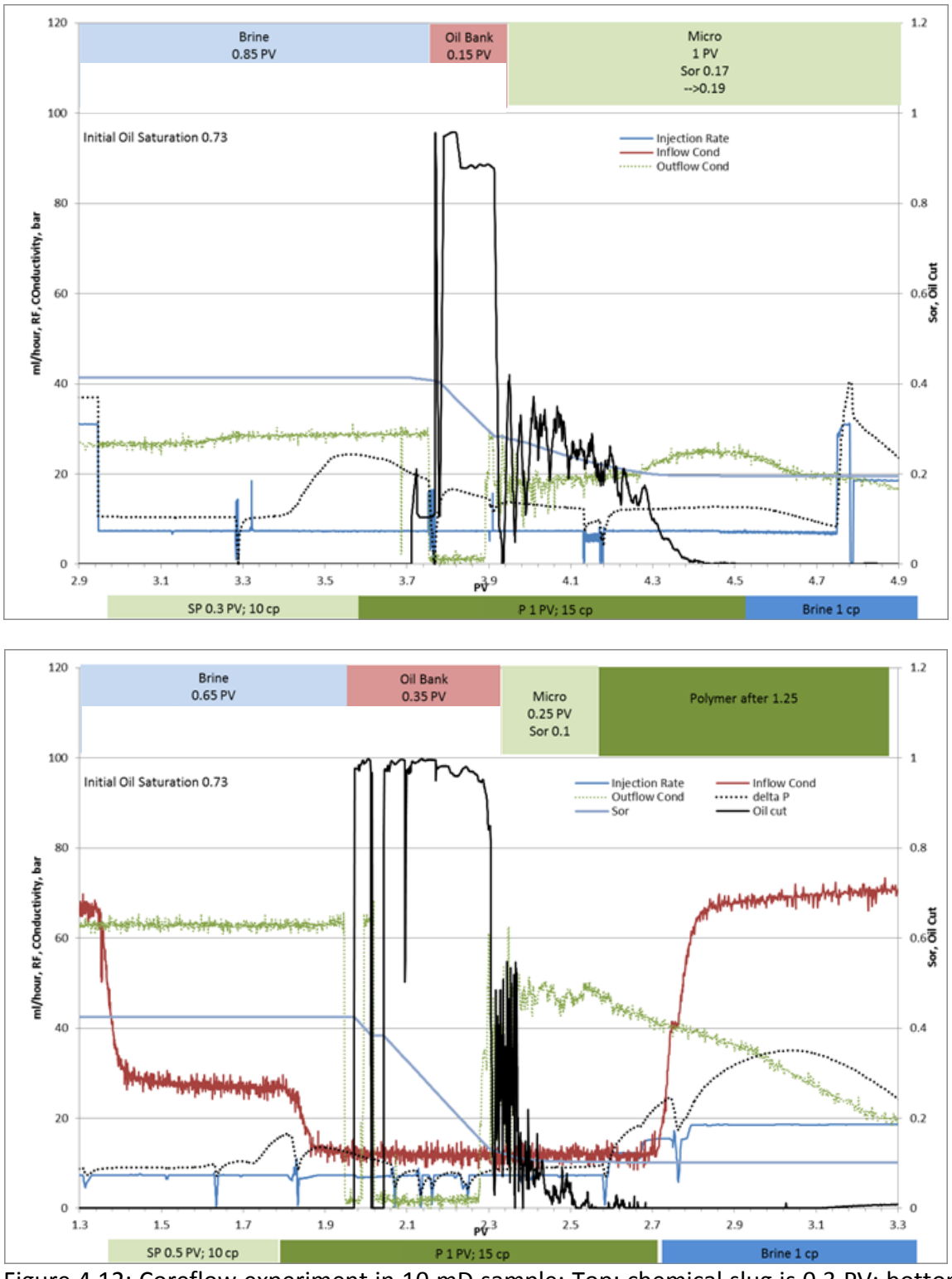

Figure 4.12: Coreflow experiment in 10 mD sample; Top: chemical slug is 0.3 PV; bottom: chemical slug is 0.5 PV

Reproducibility of the experimental data:

One of the main concerns on the experimental data is the summed measurement errors caused by the operator, the dead volume sensitivity, the calibration of the transducers, thermos couples, pumps, the external environment (temperature, humidity, air

pollution, etc.), the time elapsed between measurements, etc.. We reduce operator errors/variability by automating our setups through labview™. We define the reproducibility as repeatability of the experimental results under the same conditions, using the same core. As a consequence, in the experimental protocol, we repeat each experiment (including the cleaning and initialization/charging) more than once.

Table 4.3 presents the variance in the coreflow results in the same core samples at different stages of flood injection (initial oil saturation, residual oil saturation after wateflood and oil saturation after chemical flood) by changing the injected PV of SP. We have a reasonably reproducible results within a variance of 3 saturation unit for the homogeneous sample. In the third sample in table 4.4, which exhibits matrix heterogeneity as show in dry CT scan (figure 4.13), we observed a variation during repetitions of 11 saturation units. The flow in the porous media has been influenced by the heterogeneity of the sample and results could not be reproduced or predicted. In other words, when the sample is homogenous the results are reproducible within the accepted range.

Table 4.3: Examples of n experiments with 80 mD samples at two different SP PV slugs.

Table with examples of n experiments with same sample but different SP PV.				
	Sample 1; permeability 80 mD, 0.3 PV			
3 repetitions in a cycle	Exp 1	Repetition 1	Repetition 2	Repetition 3
Initial Oil Saturation, S_{oi}	0.70	0.71	0.70	0.65
S_{or} Waterflood	0.49	0.48	0.47	0.49
S_{or} Chemical Flood	0.12	0.11	0.13	0.12
	Sample 1; permeability 80mD, 0.5 PV			
3 repetitions in a cycle	Exp 2	Repetition 1	Repetition 2	Repetition 3
Initial Oil Saturation, S_{oi}	0.78	0.77	0.76	0.74
S_{or} Waterflood	0.50	0.47	0.47	0.46
S_{or} Chemical Flood	0.12	0.13	0.1	0.12

Table 4.4: Example of n experiments with heterogeneous samples at two different SP PV slugs.

	Sample 2; Heterogeneous sample, 0.3 PV		
2 repetitions in a cycle	Exp 1	Repetition 1	Repetition 2
Initial Oil Saturation, S_{oi}	0.73	0.66	0.60
S_{or} Waterflood	0.41	0.50	0.37
S_{or} Chemical Flood	0.2	0.16	0.23
	Sample 2; Heterogeneous sample, 0.5 PV		
2 repetitions in a cycle	Exp 1	Repetition 1	Repetition 2
Initial Oil Saturation, S_{oi}	0.78	0.70	0.66
S_{or} Waterflood	0.47	0.50	0.39
S_{or} Chemical Flood	0.15	0.10	0.14

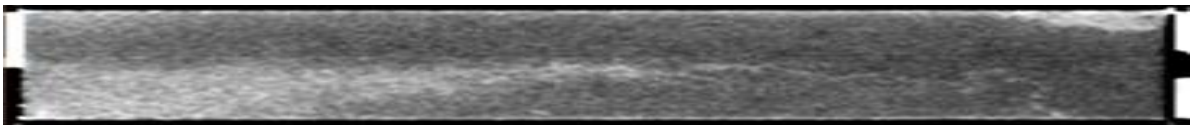

Figure 4.13: Dry CT scan of the heterogeneous sample; variation in the density across the sample indicating the presence of heterogeneity

2- *Front stability of the Chemical flood:*

The second issue that has been observed is on the chemical front stability. Figure 4.14 presents CT images of front instability. As a result of the front instability, some oil is left behind during the surfactant injection. The polymer slug eventually does recover this oil, however it thus took a longer time to produce and was produced with the emulsion phase. This issue is only observed in the iodododecane/surfactant system, whereas for the dodecane/surfactant system, the chemical front is stable. Increasing the chemical slug size did not help.

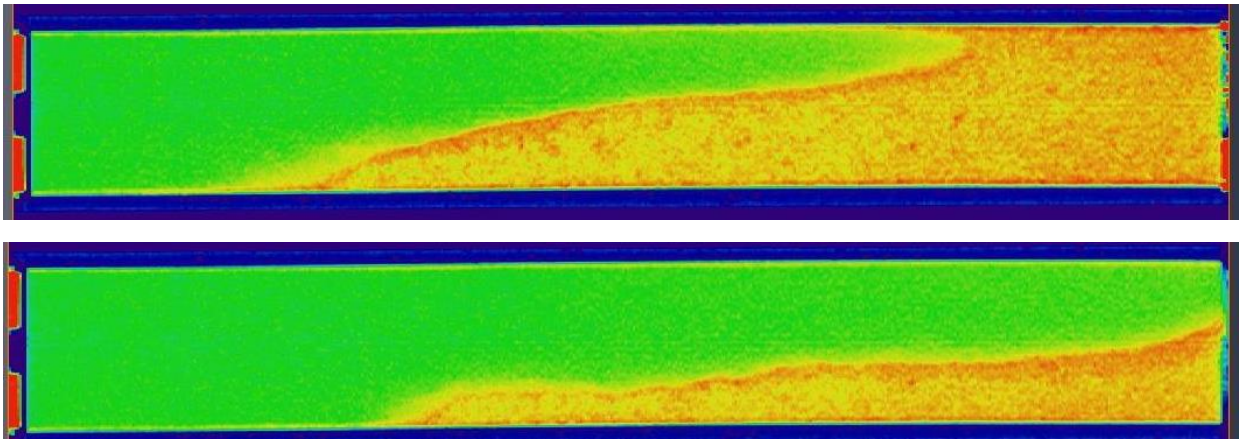

Figure 4.14: CT images of oil bank build up process in the core (core length is 39 cm, core diameter is 3.8 cm, red colour indicates oil, green is the surfactant polymer).

Figure 4.15 represents a schematic of the slug sequence in the porous media. The microemulsion phase appears in the front of the chemical slug and the tail of the oil bank. Literature showed that the viscosity of micro-emulsions at optimal salinity is greater than the oil viscosity (SPE 179672).

We measured the viscosity of the micro-emulsions for the dodecane/surfactant and iodododecane/surfactant systems at different salinities (Figure 4.16). It could be seen that for the dodecane/surfactant system, the microemulsion viscosity is approx. 7–10 cp. This has not caused any issue, as the polymer concentration (mobility control) is designed for a viscosity of 15 cp. For the iodododecane/surfactant system, we see higher viscosities for the microemulsion phase. The viscosities are in the range of 25–45 cp at different salinities.

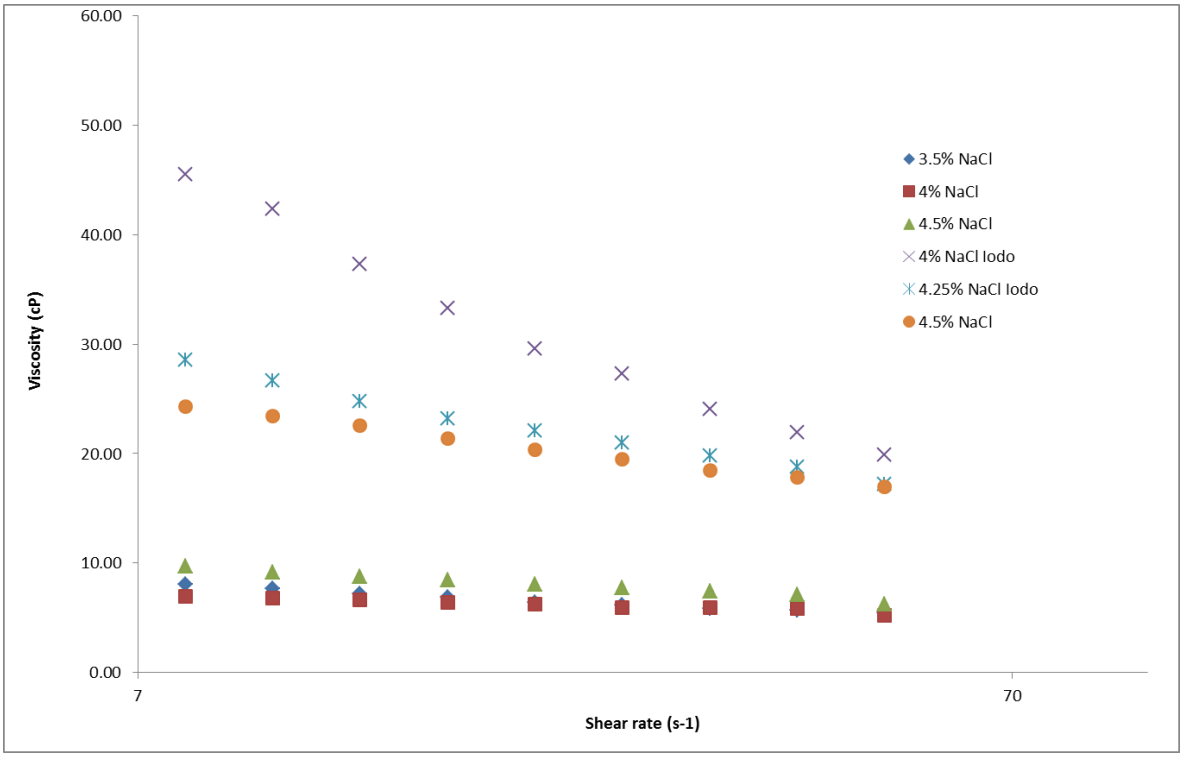

Figure 4.16: viscosity measurements for the dodecane/surfactant and iodododecane/surfactant systems.

Summary and Conclusions

The process of building an oil bank has been experimentally demonstrated for different length scales, i.e., µm, 7 cm, 17 cm, 30 cm, 39 cm. X-Ray CT images help to visualise the displacement process and give insight to the factors that influence the build-up of the oil bank. Our conclusions are as follows:

1- Building a stable oil bank supports the efficiency of the chemical EOR process, where
   a. Most of the residual oil is mobilised, reconnected and transported in front of the chemical flood. Oil is produced mostly with brine. Oil in the form of (micro)emulsion is minimised. This has big advantages for the surface facility in the producing field, as oil in emulsion form usually upsets the process facilities.
   b. The pseudo mobility of the oil is higher (i.e., oil production is accelerated) when it is produced as a connected oil bank in comparison with a dispersed

flow with emulsion. This has a positive impact on the revenue (net present value) of the chemical EOR process.

2- Successful build up and maintenance of an oil bank requires meeting four stages:
   a. Oil mobilisation: where the capillary forces holding the oil are reduced and oil ganglia are freed from their entrapments. The main factor influencing this stage is achieving an ultra-low IFT of 10^{-3} – 10^{-2} mN/m. This has proven to be sufficient to overcome the capillary forces in Fontainebleau sandstone.
   b. Coalescence of the mobilised oil: At this stage, there is a competition between the processes of oil droplet break-up/re-trapping and droplet collision, coalescence and merging to form a continuous oil phase. The influencing factor is the accessible pore volume, where the oil droplets require sufficient pore volume to coalescence and to build an oil bank. Our work in Fontainebleau sandstone recommends a minimum core length of 30 cm to have a successful coalescence process. The consequence of a shorter core would be producing the oil in a dispersed flow or developing a small oil bank where most of the oil production will be in an emulsified form. Another factor impacting coalescence is the amount of residual oil left after waterflooding. In Fontainebleau porous media with the given rock properties requires a minimum of 0.3 S_{or} to exhibit coalescence the formation of an oil bank.
   c. Maintenance and propagation of a stable oil bank: this is an often-ignored crucial stage. Once the oil bank has been formed (i.e., coalescence wins the competition with break-up and re-entrapment), it is transported through the porous medium. Two main factors influence this process: the porous media heterogeneity and bulk viscosity of the micro-emulsions. The latter may lead to unfavourable mobility control, and consequently the surfactant could finger through the microemulsion phase and break up the oil bank. In the case of the former, the oil bank can move through some high-permeablity streaks and bypass some of the trapped oil. For those circumstances, we demonstrated the value of introducing polymer into the surfactant EOR process to achieve favourable mobility conditions. Without the polymer, the low-IFT front is not stable and the surfactant slug will finger because the water relative permeability increases as the IFT and residual oil saturation decrease. The polymer drive reduces phase trapping, which helps to minimise surfactant retention. Hydrolysed polyacrylamide (HPAM) is a good candidate polymer at low salinities, but it is not recommended at high salinities. HPAM is water-soluble and has the capability to provide high viscosity at low concentrations.

References

1- C. Huh, “Interfacial Tensions and Solubilizing Ability of a Microemulsion Phase That Coexists with Oil and Brine,” Journal of Colloid and Interface Science, Vol. 71, No. 2, 1979, pp. 408-426.
2- Denney, D. “Progress and Effects of ASP Flooding,” Journal of Petroleum Technology, vol. 65, no. 01, pp. 77–81, 2015.

3- Al-Shuaili, K., Svec, Y., Guntupalli, S., Al-Amri, M., Al-Hinai, G., Al-Shidi, M., … Kruijf, S. de. (2018, March 26). Field Piloting of Alkaline Surfactant Polymer in Sultanate of Oman. Society of Petroleum Engineers. doi:10.2118/190392-MS.
4- Sheng JJ (2013). Modern chemical enhanced oil recovery: theory and practice. 1st Edition –Elsevier,
5- Humphry, K. J., van der Lee, M. (2013, April 16). Microemulsion Rheology and Alkaline-surfactant polymer Flooding. (Paper B14). EAGE 17th European Symposium on Improved Oil Recovery, St. Petersburg, Russia, April 16 - 18, 2013.
6- Blunt, M.J., Jackson, M.D., Piri, M.and Valvatne, P.H. (2002) 'Detailed physics, predictive capabilities and macroscopic consequences for pore-network models of multiphase flow' Advances in Water Resources 25, 1069-1089
7- Payatakes, C., NG, K. M. & Flumerfelrt., W (1980) "Oil ganglion dynamics during immiscible displacement: Model formulation". AZChE J. 26, 430.
8- Gardesu, I. 1 (1930). Behavior of Gas Bubbules in Capillary Spaces. Trans. AL\fE 86, 351-370.
9- Smith, W.O. , Crane, M.D. (1930). 'The Jamin effect in cylindrical tubes'. J. Am. Chem. Soc.. 52, 4, 1345-1349
10- Stegemeier, G. L (1977) "Mechanisms of Entrapment and Mobilization of Oil in Porous Media", in Improved oil Recovery by Surfactant and Polymer Flooding, Shah, D. O. and Schechter, R. S. ed., Academic Press, New York.
11- Mohanty, K. K, Davis, H.T., Scriven, L.E (1987) "Physics of Oil Entrapment in Water-Wet Rock". SPE Reservoir Engineering, SPE-9406.
12- Ng, K.M. , Payatakes, A.C. (1980). 'Stochastic simulation of the motion, breakup and stranding of oil ganglia in water-wet granular porous media during immiscible displacement'. American Institute of Chemical Engineers Journal. 26, 3, 419-420
13- Iglauera , S., Ferno, M. A., Shearing, P. and Blunt, M.J., (2012) Comparison of residual oil cluster size distribution, morphology and saturation in oil-wet and water-wet sandstone, Journal of Colloid and Interface Science 375 (2012) 187–192
14- Berg S et al. (2014) Multiphase flow in porous rock imaged under dynamic flow conditions with fast x-ray computed microtomography, Petrophysics, 55(04):304–312.
15- Payatakes, A.C., Ng, K.M. and Flumerfelt, R.W (1980).: "Oil Ganglion Dynamics During Immiscible Displacement: Model Formulation," AIChEJ., 26, 430-443.
16- Wasan, D. T., McNamara, J. J., Shah, S. M., Sampath, K., and Aderangi, N., J (1979) The Role of Coalescence Phenomena and Interfacial Rheological Properties in Enhanced Oil Recovery: An Overview, Journal of Rheology 23, 181, doi.org/10.1122/1.549524
17- Payatakes, A.C., Dias M. M., (1984) "Immiscible Microdisplacement and Ganglion Dynamics in Porous Media, doi.org/10.1515/REVCE.1984.2.2.85

18- Al Saadi F, Wolf KH and Kruijsdijk C.V. (2017) Characterization of Fontainebleau Sandstone: Quartz Overgrowth and its Impact on Pore-Throat Framework. J Pet Environ Biotechnol 7: 328. doi: 10.4172/2157-7463.1000328
19- Fortenberry, R., Kim, D. H., Nizamidin, N., Adkins, S., Arachchilage, G. W. P. P., Koh, H. S., Weerasooriya, U., Pope, G. A, (2014) Use of Co-Solvents to Improve Alkaline-Polymer Flooding, Society of Petroleum Engineers, doi: 10.2118/166478-MS
20- Currie, P. K., Nieuwkoop, J. V., (1982), "Buoyancy effects in the spinning-drop interfacial tensiometer", Journal of Colloid and Interface Science, Volume 87, Issue 2, Pages 301-316.
21- Johnson, E.F., Bossler D.P., and Naumann V.O, (1959), Calculation of Relative Permeability from Displacement Experiments, Transactions of the American Institute of Mining, Metallurgical and Petroleum Engineers. Vol. 216, 370-372
22- Vinegar, H.J., and Wellington, S.L., (1987). Tomographic imaging of three-phase flow experiments. Review of Scientific Instruments 58 (1), 96–107
23- Van Batenburg, D. W., Berg, S., Oedai, S., David, L. L., Siemens, A. O. N., and K., E. (2015). Visualization of light oil mobilization in asp core floods using x-ray ct imaging. In Proceedings SPE Enhanced Oil Recovery Conference, number SPE 174660. Society of Petroleum Engineers, Society of Petroleum Engineers.
24- King, G. R., Ertekin, T., Stahl, C.D., Jones, J. H., Nagarajan, R. and Yarzumbeck, A.J. (1981) 'Physicochemical Mechanics of the Propagation of the Stabilized Oil Bank Formed During Di!ute Surfactant Flooding' SPE 10371
25- Gillard JH, Antoun NM, Burnet NG, Pickard JD (2001). Reproducibility of quantitative CT perfusion imaging. Br J Radiol 2001;74:552–555
26- Berg, S., Oedai, S., van Batenburg, D. W., Elewaut, K., Boersma, D. M., and Ineke, E. M. (2015). Visualization of ASP core flood experiments using X-ray CT imaging. In Proceedings IOR-2015 – 18th European Symposium on Improved Oil Recovery, Dresden, Germany.

Chapter 5

Oil Bank Dynamics Discussions and Conclusions

1- Framework for chemical Core-flow Experiments:

Core-flow experiments are considered a low-cost and manageable platform to evaluate and test new chemical concepts or to get dynamic insights on the fundamentals of the chemical process during rock-fluid interaction. However, meaningful core-flow experiments are more than injecting liquid volumes in a porous medium and measuring the effluents at the output of the core. It is also more than designing a proper procedure and validating hypothesis. It is an art of understanding all parameters that might influence the chemical process. For example, the characteristics of the porous medium and the fluids, the errors and faults during conducting experiments. It is crucial for the scientist to distinguish between genuine/true science and artefacts, errors of the system, before starting to draw conclusions.

Figure 5.1 shows our framework to conduct a meaningful core-flow experiments.

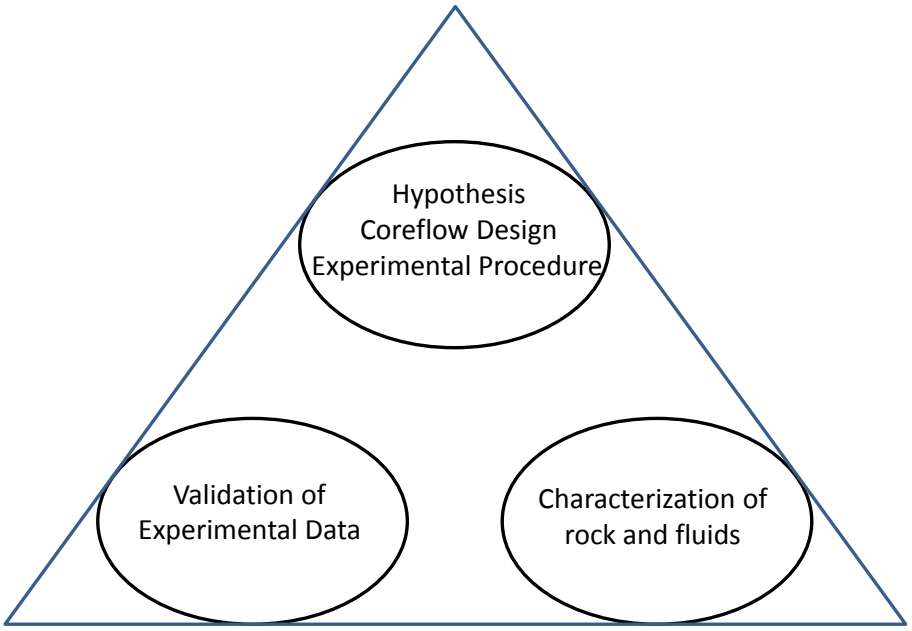

Figure 5.1: Coreflow Experimental framework

Experimental conditions and protocols:

In our experimental approach we avoid changing many parameters in all our experiments and the only change was in core length. During repetition of any experiment, it

was conducted at same conditions as 1st experiment. The experimental protocol was explained in chapter 3 and it has not been repeated in this chapter. Appendix 1 contains the information of each experiment.

1.1. Characterization of rock and fluids:

In our framework, we have chosen for a wider range of petrographical and petrophysical characterization of the used porous media in order to understand the petrophysical and electrical transport properties, mineralogy, chemical composition and spatial attributes of the grain- and pore framework.

The characterization varies from pore scale where spatial attributes of the grain and pore's matrix is measured by Computed Tomography (CT) image analysis, thin sections, Scanning Electron Microscopy (SEM) to conventional methods of measuring porosity and fluid permeability with a pycnometer and Ruska permeameter. The nature of the rock minerals, their chemical composition and surface electrical properties are essential for understanding the geochemical reaction and interaction between the fluids and the grains of the rocks.

The results, as presented in chapter 2 indicated a compositional homogeneity of an almost pure quartz grain packing of the Fontainebleau sandstone. It showed to be the preferred reference rock regarding porosity-permeability relations, capillarity and wettability for oil bank build up.

We concluded that the cementation in Fontainebleau occurred via quartz overgrowth, which plays a central role in the pore-throat geometry and impacts both permeability and porosity by reducing the diameter of the pore throats (i.e. coordination number and capillary pressure). This elimination of pore-throats created higher tortuosity value (figure 5.2) and by that lower permeabilities. This means that:

- Porosity defines permeability through pore morphology.
- Porosity/permeability linked to heterogeneity. Lower porosity changes porous medium to lower coordination number creating larger (than pore size) length scales, As a result, increased dispersion and higher S_{or}.
- Fontainebleau is strongly water wet (99.5 % quartz) before potential changes during EOR flooding. Hence, polymer and/or surfactant adsorbtion on rock but not the oil component directly.

Overall, the choice of Fontainebleau had positive characteristics (simple structure, mostly quartz) and negative characteristics (heterogeneity, low porosity, low perm, availability where quarry is interested on consolidated rock with low porosity). We decided to pick Fontainebleau due to its pure composition and absence of clay minerals. Its porous

meduim has no impact on the fluid flow behavior during core-flow experiments. This will ensure maximal reproducibility and comparable fluid flow experimental results.

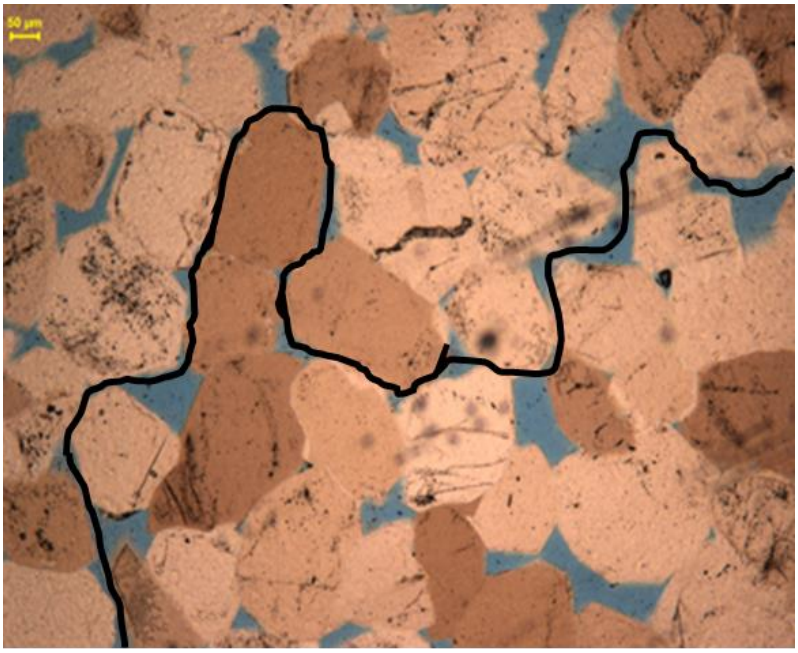

Figure 5.2: 2D thin section of Fontainebleau. Black line shows schematic flow path in 2D.

In cases of low porosity ($\varphi < 0.08 - 0.09$), the permeability reduced from 300 mD to 10 mD. As a result, various sandstone samples with different permeabilities could be used for oil bank mobilization, to study the impact of quartz overgrowth on oil bank build up. Figure 3.12 in chapter 3 shows the magnitude of the oil bank in low porosity/perm sample ($\varphi < 0.08$, K=10 mD) at different SP slug size for the same core.

We observed that more SP volume is required to build a bigger oil bank. It is attributed to the pore-throats framework where the aspect ratio (i.e. pore body/pore-throat ratio) is high and more volume will be required to include all accessible pores. This is based on core-flow experiments presented in Figure 5.3 and Figure 5.4.

We also observed that the reduction in pore throats, and by that coordination number and high aspect ratio, decreased the waterflood efficiency (sweep efficiency as some pore throats are completely blocked). Thus, this is permeability and capillary pressure related. The waterflood recovered up to 40% of the mobile oil, which is on the low side.

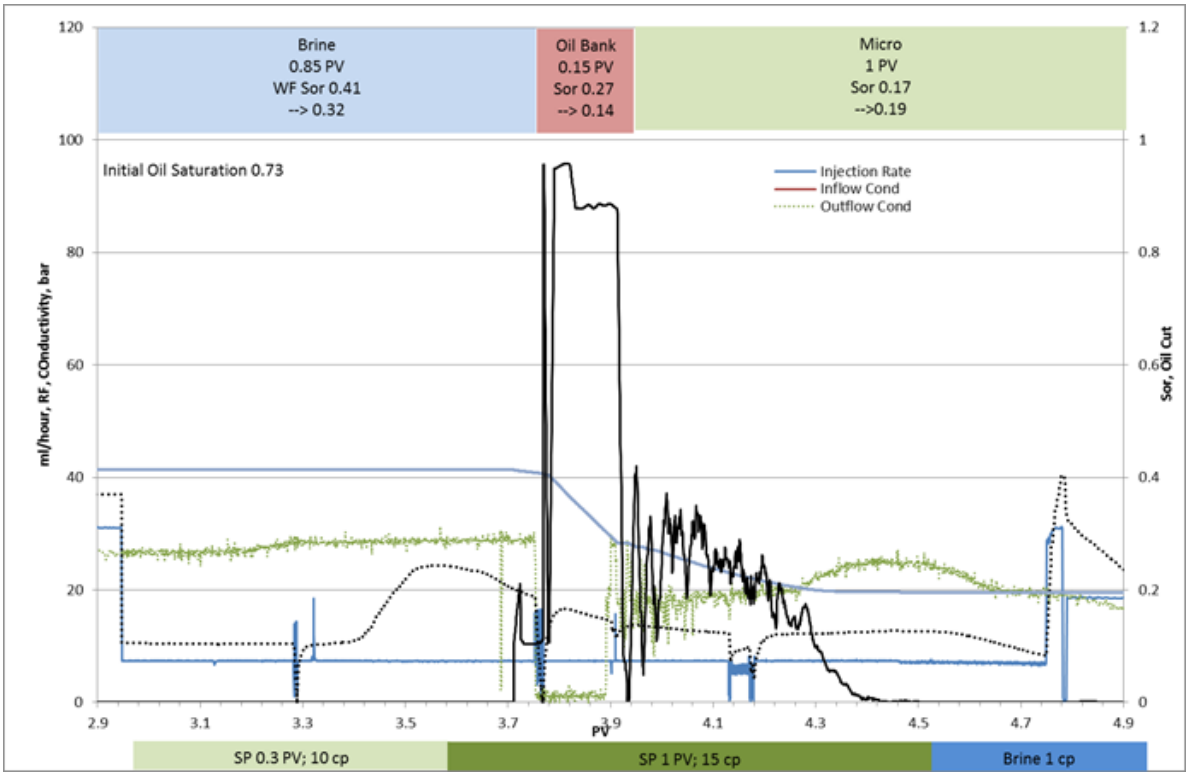

Figure 5.3: coreflow experiment in 10 mD sample; chemical slug is 0.3 PV

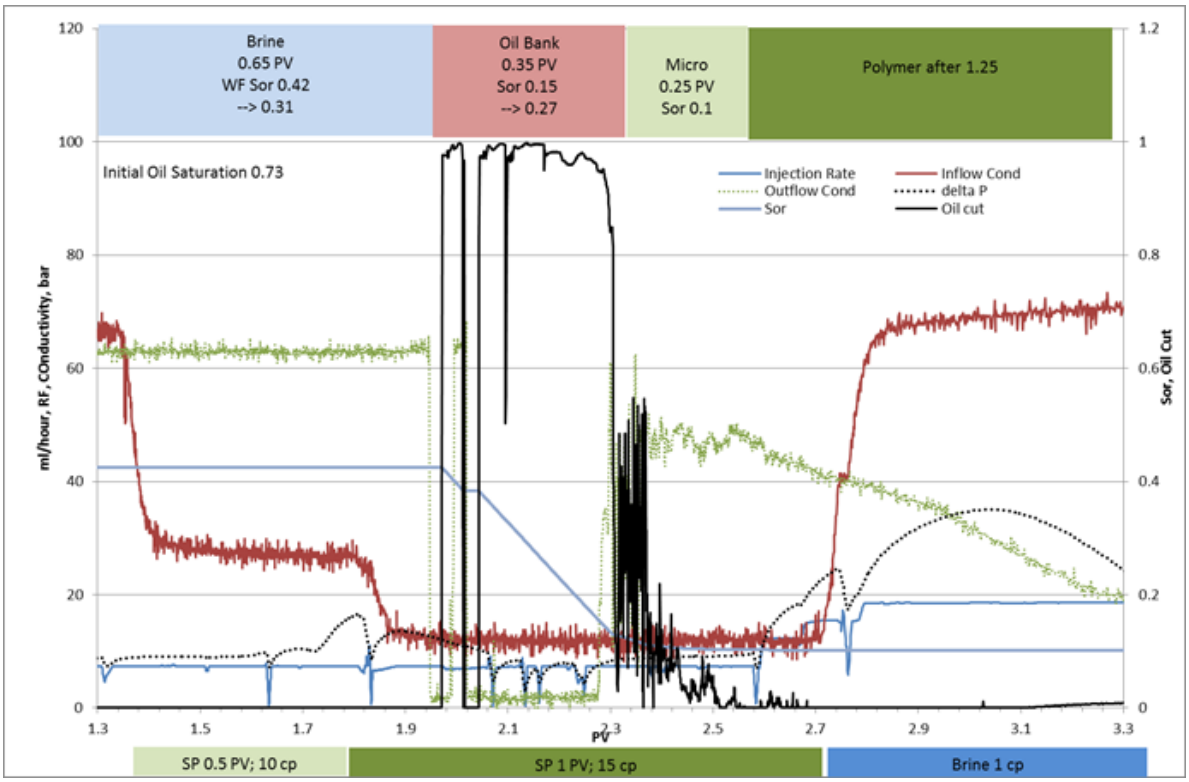

Figure 5.4: coreflow experiment in 10 mD sample; chemical slug is 0.5 PV

From the experimental work in chapter 3 and CTS-imaging, it was concluded that during the waterflood displacement process, the oil occupies the larger pores while the water moves faster in small pores. Hence, oil is trapped in those relatively large pore bodies by the bypassing mechanism and another amount of oil is trapped by snap-off that occurs in pore bodies of high aspect ratio. Figure 5.5 visualizes the distribution of residual oil after waterflood in our 2D-micromodel, where the structure of oil ganglia could be defined as:

1. Moderately big blobs involving several pore bodies
2. Minor blobs formed by two to three relatively large pore bodies
3. Oil in single pore bodies.

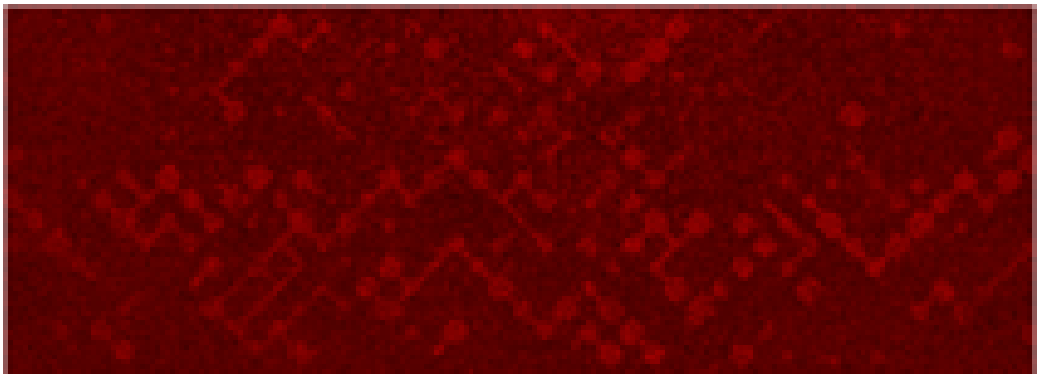

Figure 5.5: oil distribution in a micromodel

We also learnt from the microfluidic experiments that the mobilized oil moves with a velocity larger than the velocity of the chemical front. It will tend to accumulate in the front of the flood. Because of collisions and coalescence between the mobilized oil a denser zone of mostly connected oil (i.e. oil bank) is formed. Consequently, it supports an efficient sweep of other mobilized oil seen downstream. This process is influenced by many factors like the capillary number and the size of the ganglia. As the oil ganglia coalesce with other ganglia, they merge and size increase, velocity reduces and starts to form a stable displacement. Without coalescence, the mobilized oil droplet may be break up to small sizes, increases its velocity and move as a disperse flood.

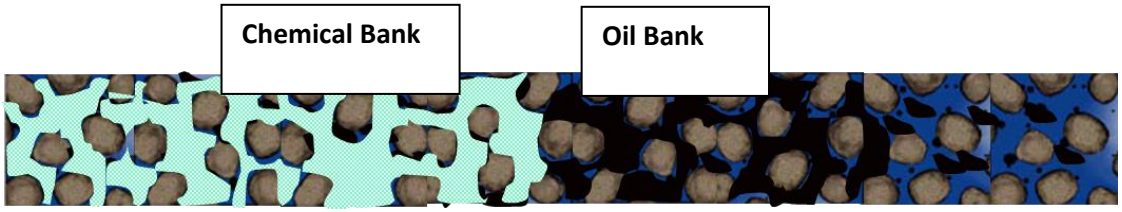

Figure 5.6: schematic of Oil Bank build up in 2D model

2. Validation of Experimental Data and Importance of Data reproducibility:

In our experimental approach, we use duplo's or triplo's to confirm whether an entire experiment can be completely reproduced, providing the same results by using the

same experimental protocols. Reproducibility is important to understand the value of the experiments. It demonstrates that our scientific findings are not expected to change over time and can be repeated by others. Hence, if the results differed significantly, then we would probably conclude that the results were erroneous or the experiment was not the same, leading us on to further investigations. As such, reproducibility gives comparable research findings a degree of confidence. It helps to draw the same conclusions from either an independent replication of a study or a reanalysis of the original study.

We got reasonable degree (within a variance of 3 saturation unit) of reproducible results but it was not constant across all experiments as sometimes the variance reached 11 saturation units. Here the main potential reasons for factors that influence the reproducibility in our experimental data are:

1- Influence of repetition on the core properties:

In our experimental protocol, we repeat the chemical experiment in the same core two times and determine data reproducibility. We observed that there is a good matching (within 3 saturation units) between the 2nd and 3rd experiment where the 1st experiment slightly differs. Furthermore, we observed that the chemical flooding movement is faster in 2nd and 3rd experiments in comparison with 1st experiment. Most likely there are changes in the surface and/or pore properties of the porous media. We think it is due to two reasons:

A- Isopro- Propanol Alcohol (IPA), which is a solvent agent, is used to clean the core after completing each experiment. During the repetition of the experiment on the same core materials, IPA does not bring the porous medium to 100% initial situation. From tracer analysis, we observed that there is still a tiny amount of oil left behind that could not be washed out or cleaned. Also, IPA influences the surface (i.e. wettability) of the porous media (Lake et al, 2014) and most likely makes the system not as strongly water wet as it was initially.

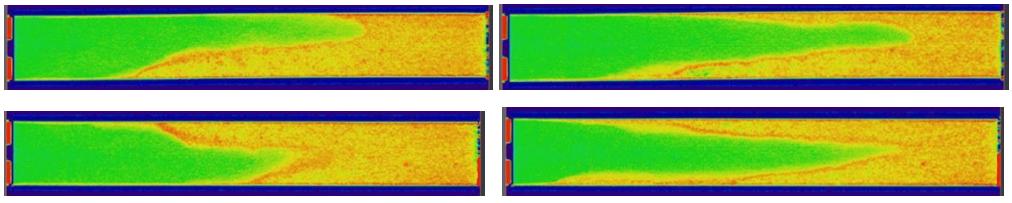

Figure 5.7: chemical movement in the pore space; Left is 1st experiment; right is the second experiment.

B- Polymer is injected to improve the conformance during as well as after the SP flooding. Despite all cleaning efforts, the polymer does not always completely come out of the pore space and therefore will influence the surface properties (Sorbie, 2013, Dang et al 2014). Figure 5.8 presents some of the entrapment mechanisms of the polymer in a porous medium (Sorbie, 2013).

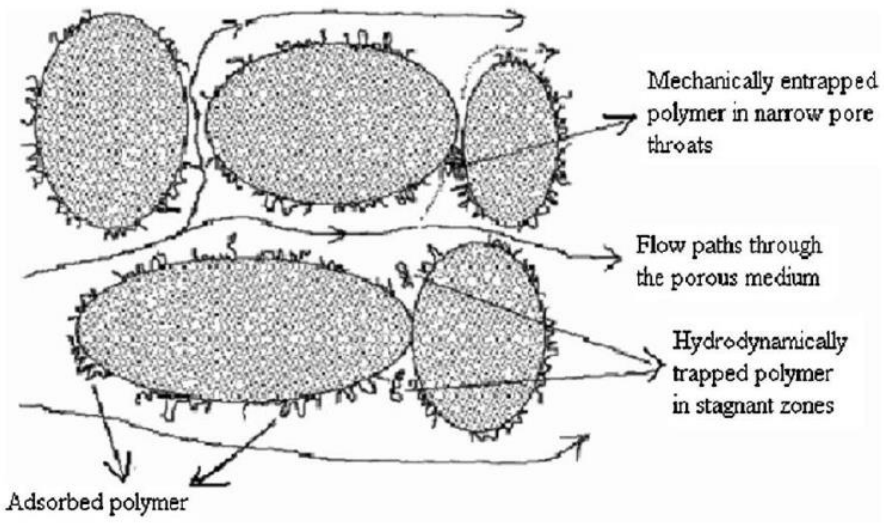

Figure 5.8: Polymer entrapment mechanisms in porous medium (Sorbie, 2014)

2- Change of the properties of Chemical Formulation over time/product:

The Surfactant polymer chemical formulation is sensitive to salinity, temperature, chemical substitutions, equilibrium, etc. It was observed that the chemical mixture starts to degrade over time and influences the experimental data reproducibility, giving undesirable results. Also, the surfactant-polymer and polymer chemical batches are not identical and alter the results if the chemical batch is changed during repetition the experiments. Figure 5.9 A shows the results of the 1st coreflow experiment which we could not reproduce in the two repeat experiments in Figure 5.9 B & 5.9 C. After further investigation, we identified the reason as the change of chemical formulation over time. By preparing a new chemical formulation we managed to reproduce the results as seen in Figure 5.9 D.

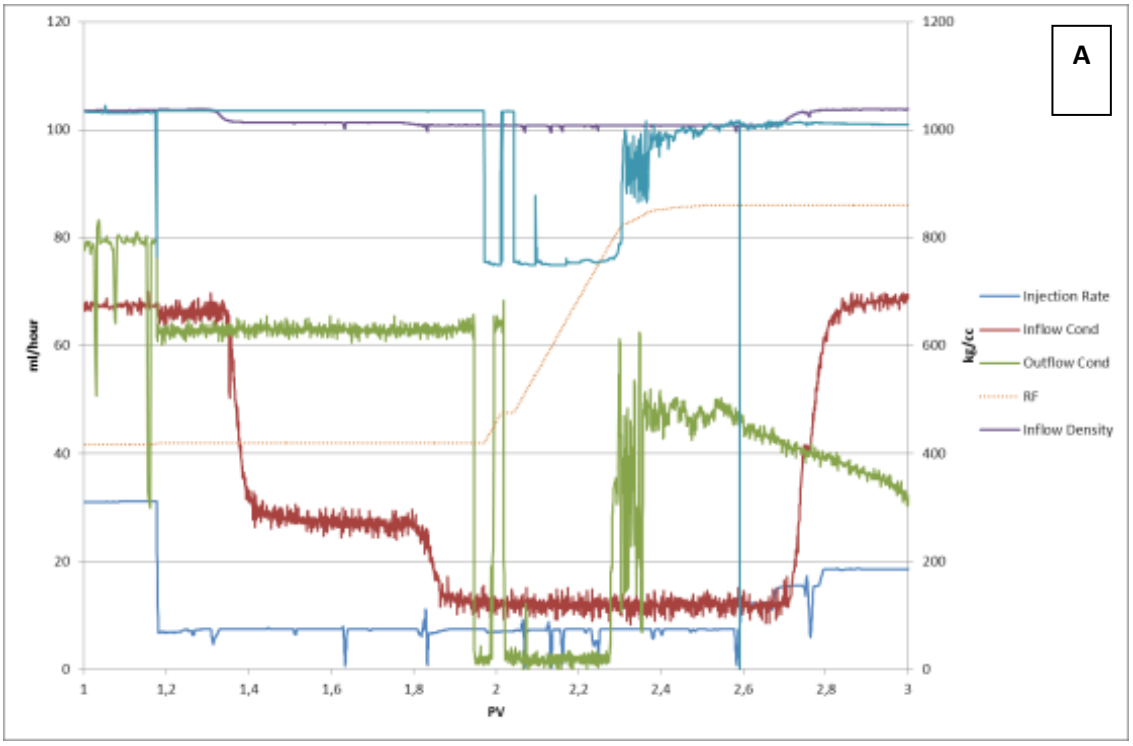
A
120
100
80
60
40
20
0
1200
1000
800
600
400
200
0
1
1,2
1,4
1,6
1,8
2
2,2
2,4
2,6
2,8
3
PV
ml/hour
kg/cc
Injection Rate
Inflow Cond
Outflow Cond
RF
Inflow Density

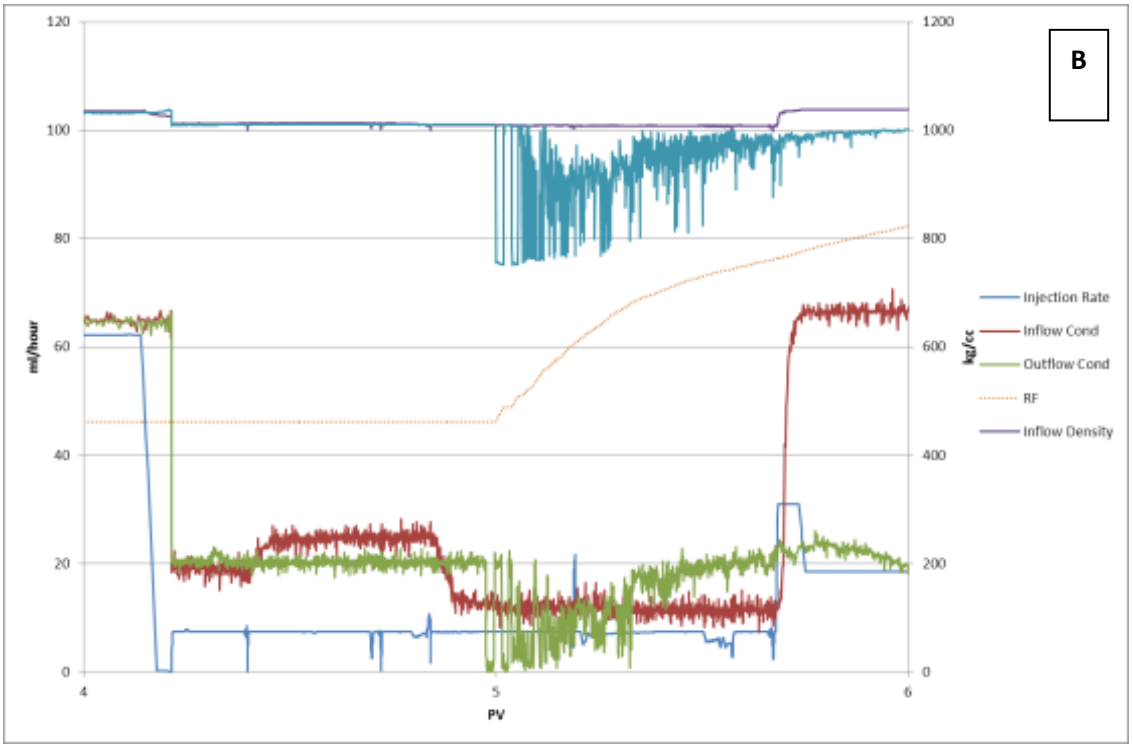
B
120
100
80
60
40
20
0
1200
1000
800
600
400
200
0
4
5
6
PV
ml/hour
kg/cc
Injection Rate
Inflow Cond
Outflow Cond
RF
Inflow Density

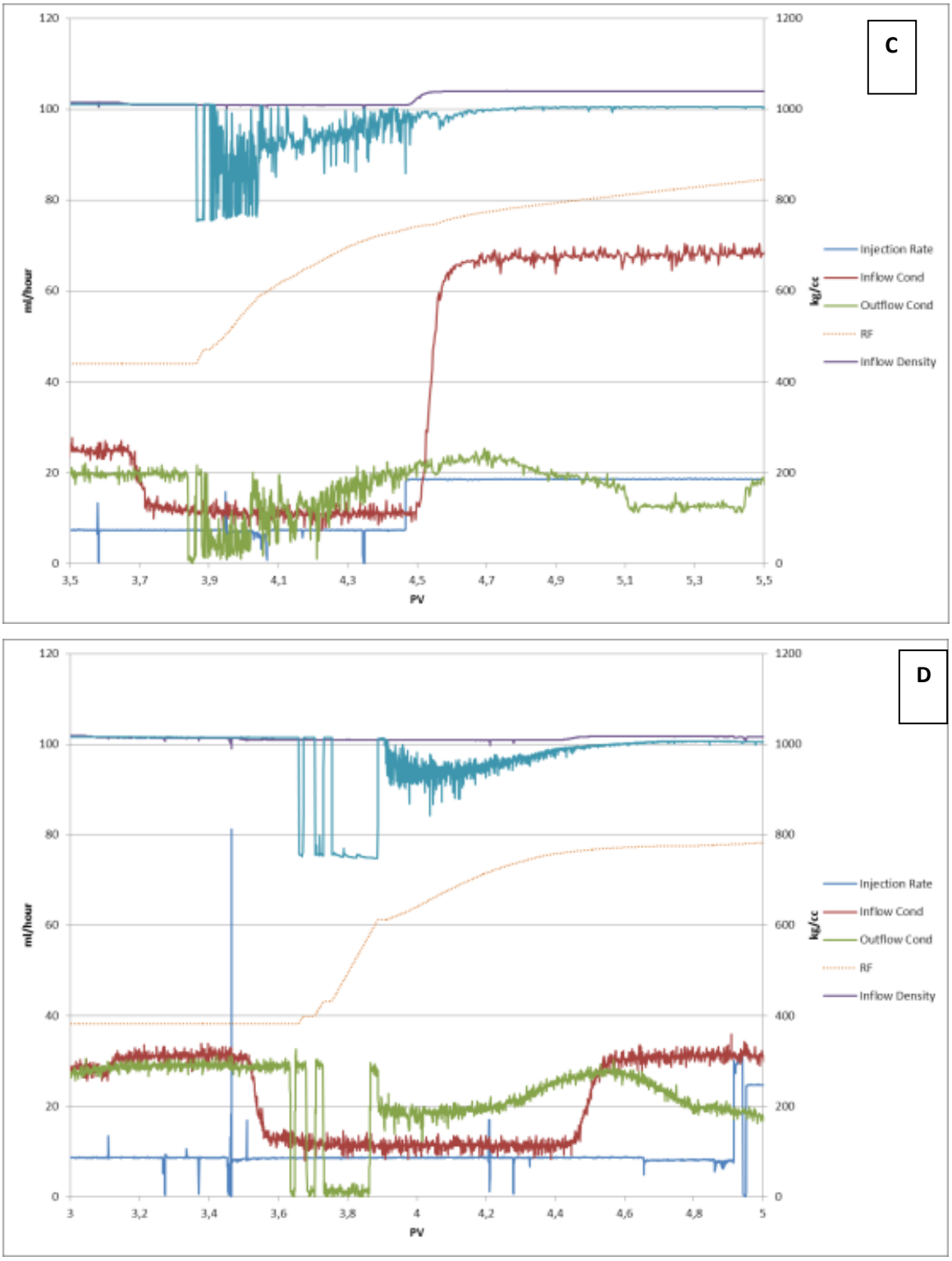

Figure 5.9: Core flow results on the same core. Figure 5.9 A shows the results of the 1st coreflow experiment. Figure 5.9 B 5.9 C presents two repeated experiments where we could reproduce same results as in the 1st experiment. After further investigation, we identified the reason as the change of chemical formulation over time. By preparing a new chemical formulation we managed to reproduce the results as seen in Figure 5.9 D.

3- Rock properties:

Although the Fontainebleau samples appeared at a block scale to have homogenous properties and consistent grain framework structure, we observed in various samples some fine-scale complexities. The complexity arises from spatial distribution of the heterogeneities of the microstructure pore space (i.e., connectivity, tortuosity, shape, etc.) which has a significant effect on bulk physical properties such as permeability, electrical conductivity... etc, for low-permeable samples (5 mD). It influences the flow and transport characteristics and hence affects the core-flow data reproducibility in both the duplos and between different cores. The main reason is the fine-scale complexities (cementations, pore-throats eliminations) which affects the accessible pore volume during different core-flow experiments.

Another rock property that influences the reproducibility is the layering, which usually occurs on a varied range of length scales varying from a few grain diameters to tens or even hundreds of meters. In some of our samples we observed small-scale periodic structure layers, which affect the reproducibility of core-flow experiments in the same core materials. Figure 5.10 shows the CT scans for three reproducible experiments on the same sample. It could be observed that this sample has two layers not fully separated, as seen in figure 5.10, and the flow behaves differently at each experiment and is therefore not reproducible. Figure 5.10: CT scan presents the chemical flow in two-layer samples

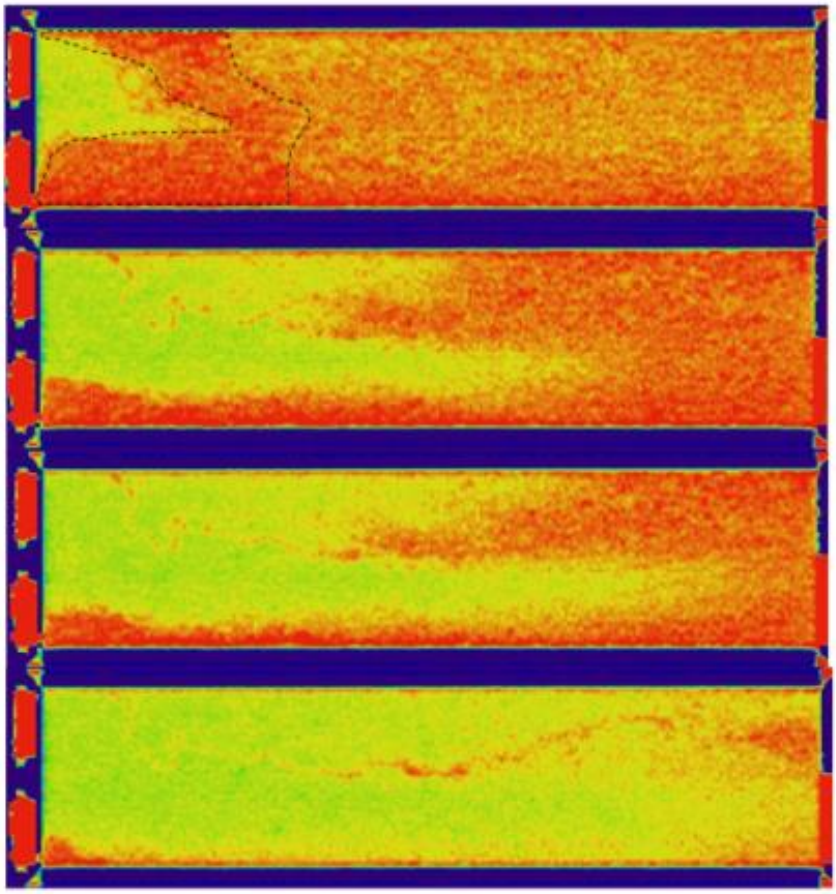

4- Chemical flood instability:

In some of our core-flow experiments we observed an instable flood front due to an unfavorable mobility contrast between the microemulsion phase and surfactant polymer phase. Viscous fingering occurs in the interface region between the microemulsion and SP phase when the highly viscous microemulsion phase is displaced by SP fluid with relatively low viscosity. Those fingers become unstable and grow rapidly in an unpredictable mode.

The experimental data reproducibility was a challenge as the characterization of viscous fingering in SP displacement is not straightforward or well understood. Different fingering patterns occur during repetition of the experiments and the formation of patterns is morphologically unstable (Homsy, 1987). The explanation for not having a reproducible fingering pattern is as follows: the porous medium has a distribution of pore sizes. The front flood at the interface will flow at different velocities and consequently the size and shape of the finger patterns will depend on the pore-size distribution of the porous medium and the balance between viscous and capillary forces, which will vary each time we repeat the experiment. Another component is the local variations in porosity and permeability which will have much more impact on the reproducibility of the unstable displacements than the stable displacements. Furthermore, unstable flow is very sensitive to small changes such as, e.g., slightly different initial oil distribution and/or small changes in surface chemistry due, e.g., to adsorbed polymer.

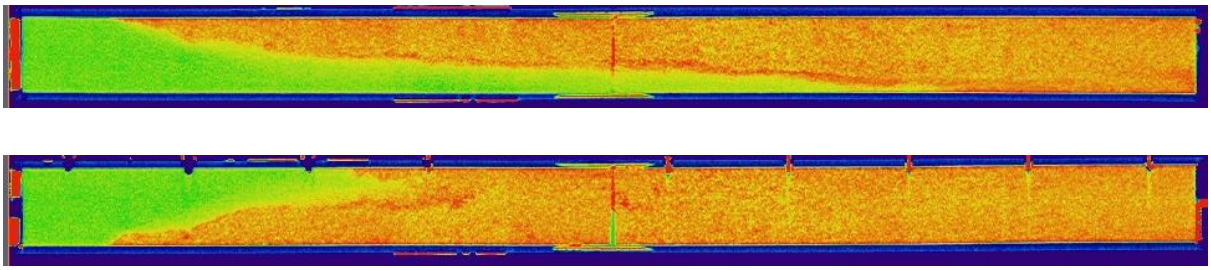

Figure 5.11: CT scans for instable displacement; reproducibility is not guaranteed.

3- Oil Bank Build up:

The oil bank is mobilized oil, which has been reconnected by coalescence of isolated oil ganglia and has been transported via a stabilized displacement in the porous media. The process of building an oil bank requires:

- Mobilizing the trapped oil by reducing the capillary forces
- Coalescence of the mobilized oil, avoiding break up, and re-trapping.
- Maintenance and transport of a stable oil bank in the porous media.

We studied the build-up of oil banks by conducting more than 80 core-flood experiments using the Fontainebleau sandstone cores of varying lengths. In chapter 3 we demonstrated the effects of certain parameters on the oil bank behaviour like rock properties such as permeability and core length, to fluid properties such as optimality of the surfactant to viscosity of the surfactant-polymer and polymer. In the coming examples we will discuss some parameters that influence the process of building an oil bank.

1- Effect of IFT on Mobilizing the trapped oil

The effect of IFT on the process of building the oil bank was evaluated. We concluded that the required IFT to mobilize oil and build an oil bank is 10^{-3} mN/m. In Figure 5.12, we present two examples of two core-flow experiments of different IFT in the chemical cocktail. Experiment 2 demonstrates a successful oil mobilization with an oil cut of 0.7 in the oil bank at IFT of 10^{-3} mN/m. Experiment 1 presents lower amount in the oil bank with an oil cut of around 30%, as a result of an increase of IFT to around 0.1 mN/m in the chemical cocktail injected where only small amount of trapped oil is being mobilized. Hence, still an amount of residual oil is left behind. Even with an increasing polymer viscosity with the same IFT does not help the process.

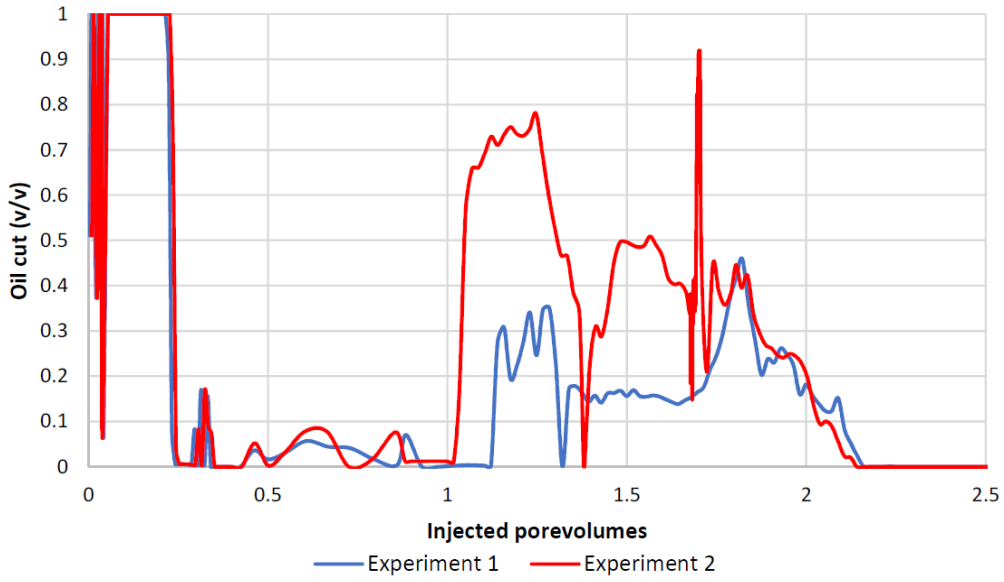

Figure 5.12: Oil cut for two different experiments at different IFT.

2- Effect of the porous media on coalescence and the transport process

- Oil Bank break up due to heterogeneous/discontinuous boundary:

We introduced an artificial boundary effect by stacking two 30 cm samples to obtain a longer 60 cm core. Stacking experimental protocol is explained in appendix 2. The capillary contrast at the boundary between the two samples was minimized by filling the space with packed sand grains of the same grain size distribution. The core-flow experiment was conducted following the experimental protocol.

Despite all the efforts, the boundary between the two stacked cores always shows a degree of discontinuity, resulting in a piston-type displacement till the slug passes through the discontinuity. After the slug passes through the interference zone, the oil bank is broken up, fingering is initiated and there is unstable displacement.

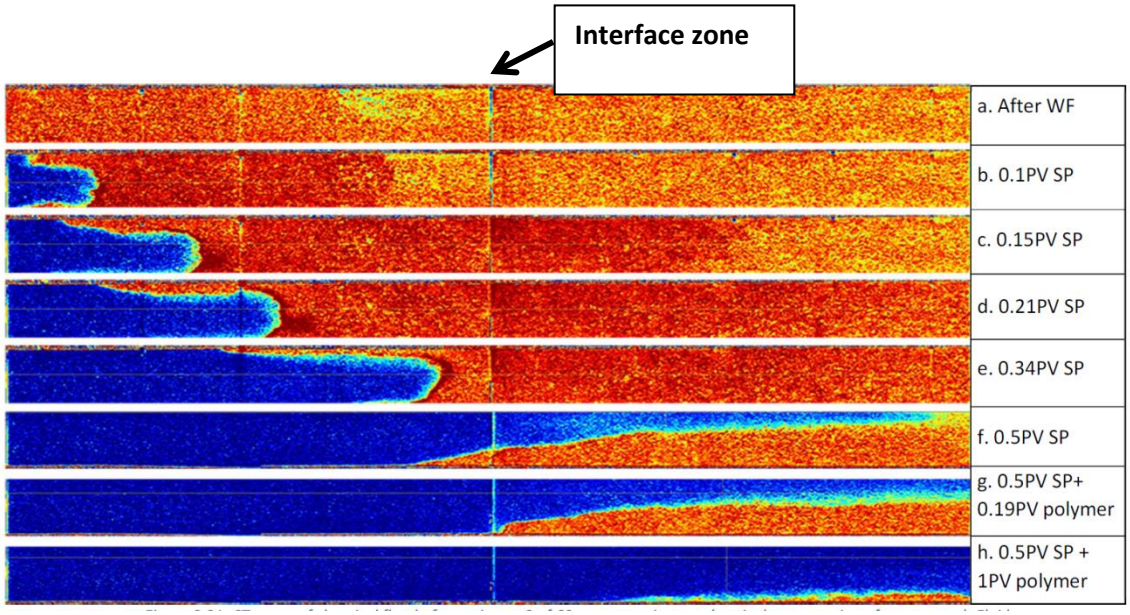

Figure 5.13: CT scans for 60 cm stacked core Fontainebleau. Same experimental protocol as explained in chapter 3 was used.

To address this issue further, we conducted the same experiment on a 1m Bentheimer core (Figure 5.14). This core has two distinctly different high permeability zones. The permeabilities values across the core have been determined by pressure differentials (via pressure tranducers) and darcy law applied as explained in chapter 3. At the interface zone, we observed that fingering has not occurred, and the oil bank does not break up and the process is successful.

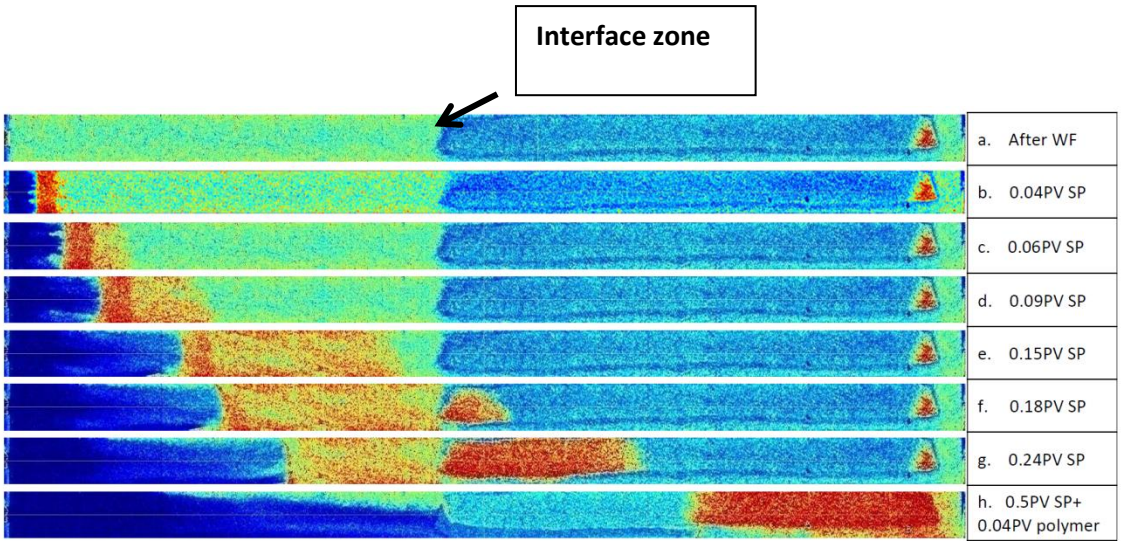

Figure 5.14: CT scans for 1 m Bentheimer core.

CT-scans show that the boundary between the stacked cores, acts as a heterogeneous capillary boundary with strongly contrasting permeabilities, playing a relevant role in the unstable displacement. For continuous porous media in a 1 m Bentheimer core, we observed a stable displacement (Figure 5.15).

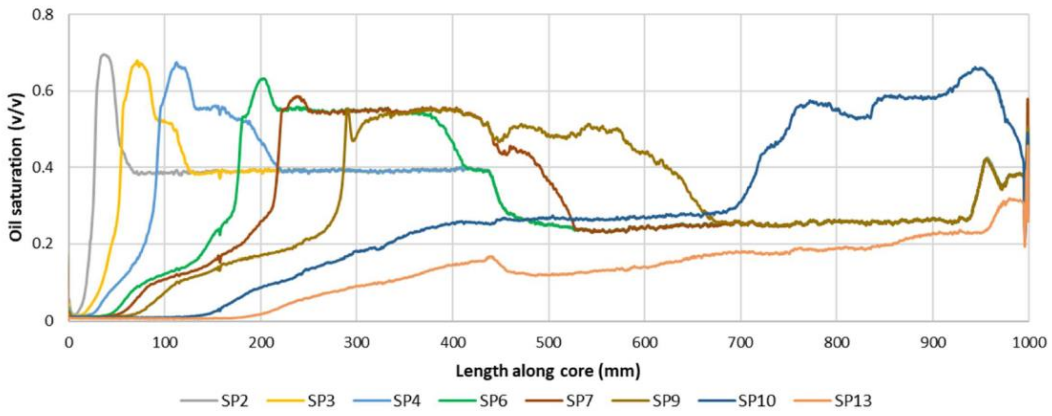

Figure 5.15: Oil Saturation across 1 m Bentheimer core. The saturation profiles composed from the CT-scans labelled as SP1-13. Scan SP1-13 show that the highest oil saturation is directly ahead of the SP-slug and the oil bank volume increases across the core.

3- Effect of core Length and initial saturation on oil bank build up

Figure 5.16 shows the oil bank build up for more than 75 experiments. For each experiment we calculate the initial oil saturation (blue line), the residual oil saturation after waterflood (orange line), the oil saturation after oil bank (yellow line), and the oil saturation

after chemicals (pink line). The coreflow experiments are organized as per their sample length.

Figure 5.16: Demonstrations of Reproducible Coreflow experimental data for 78 coreflow experiments. X-axis represents the Number of experiments and the core length of the core used in each experiment. Y-Axis represents the remaining average oil saturation after each flooding step (Initial S_{or} is the initial oil saturation after oil filling, WF S_{or} is the oil saturation after waterflooding, OB S_{or} is the oil saturation after oil bank, Polymer S_{or} is the residual oil saturation after polymer flooding). The dotted lines represents the 1st and 2nd repeations of the experiments on the same core.

A. Effect of initial oil saturation:

The comparison between core-flow experiments with different initial saturations show that a lower residual oil, unsurprisingly, yields a smaller oil bank. This can be seen in experiment No 25 and 26. For Fontainebleau sandstone at low permeability of 10 mD we could not build an oil bank if the residual oil saturation is less than 0.3.

B. Effect of Core Length:

There is a clear proportional relationship between the porous media length versus the size of the oil bank. At 100 – 60 cm core length, the oil bank size is in the range of 0.3 –

0.2 PV. As core length is reduced to 17 – 7 cm, the oil bank size reduces to 0.05 PV. So, core length matters in building the oil bank.

C. Effect of polymer slug:

The polymer does not increase the amount of produced oil. As we see clearly, there is no further increase in S_{or} due to polymer. However, the polymer improves the conformance and speeds up the mobilization process.

4- Influence of the Oil Mobility on oil bank build up

The combined Buckley-Leverett (Buckley and Leverett, 1942) and JBN (Johnson et al, 1959) (pseudo) relative permeability data give an insight as to how certain parameters affect oil mobility. The comparison between the short cores (7 cm – 17 cm) with longer cores (39 cm – 100 cm) show that the cores length has a positive influence on the oil mobility. A larger core length gives more time and space for coalescence of the oil droplets into the oil bank.

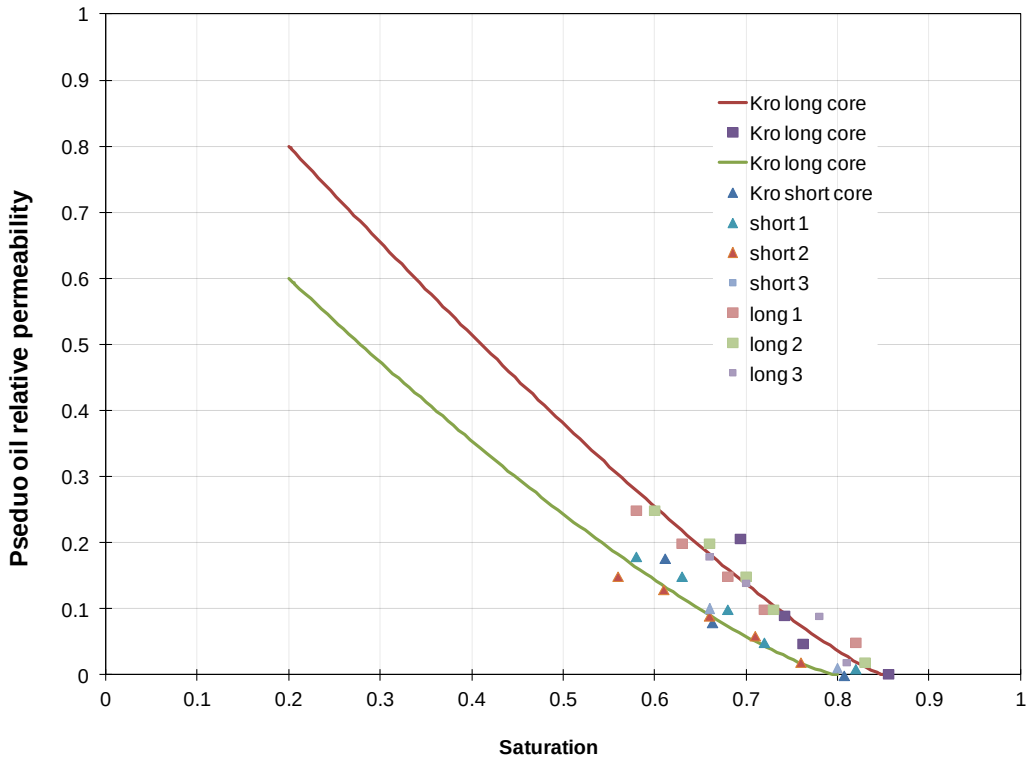

Figure 5.17: oil mobility for different core lengths. (Y-axis: Pseudo relative permeability)

References:

1- Lake, L. W., Johns, R. T., Rossen, B., and Pope, G., (2014) Fundamentals of Enhanced Oil Recovery, Society of Petroleum Engineers.

2- Dang, T.Q.C.; Chen, Z.; Nguyen, T.B.N.; Bae, W. Investigation of isotherm polymer adsorption in porous media. Pet. Sci. Technol. 2014, 32, 1626–1640.

3- Sorbie, K.S. Polymer-Improved Oil Recovery; Springer Science & BusinessMedia: Berlin/Heidelberg, Germany, 2013.

4- G.M. Homsy, Viscous fingering in porous media, Annu. Rev. Fluid Mech. 19 (1987) 271–311.

5- Buckley, S. E., and M. C. Leverett (1942), Mechanism of fluid displacement in sands, Trans. Am. Inst. Min. Metall. Eng., 146, SPE-942107-G(01), 107–116, doi:10.2118/942107-G.

6- Johnson, E. F., D. P. Bossler, and V. O. N. Bossler (1959), Calculation of relative permeability from displacement experiments, SPE-1023-G, Petroleum Transactions, AIME, 216, 370–372.

Chapter 6

Final Results and Conclusions

In our research, we selected Fontainebleau sandstone to conduct a series of core-flow experiments to study the mobilization and displacement of residual oil by means of chemical enhanced oil recovery processes. We demonstrated via extensive characterization programme that Fontainebleau has pure composition and constant grain size distributions. Clay minerals are almost non-existent. It allows us to study the fluid flow behaviour in core samples independently of other parameters. This ensured maximal reproducibility and comparison of fluid flow experimental results.

Repeatability and experimental data reproducibility were ensured while conducting the experimental core-flow series in this research to distinguish between data that provide meaningful insights into the dynamics of the build-up of oil banks and those that represent statistical anomalies or flaws in an experimental design. Hence, the literature contains many studies based on the comparison of single experiments with varying conditions for each of the core-flows. Our experiments have shown that, even under the best of circumstances, there is variability for identical experiments on the same core. Without the repeatability and experimental data reproducibility, only the larger differences (around 10%) between different core-flow are significant. This is often overlooked in core-flow studies. The fully automated core-flow setup allows repetitive cleaning, saturation and displacement experiments without the need to disconnect the core and/or fluid system. It produces a quantitative measure of reproducibility and by that the accuracy of the experimental cycles.

Despite the purity of Fontainebleau sandstone, it was observed that at low permeability (<10 md) and porosity (< 0.08), the quartz overgrowth (i.e. cementation) mostly affects the pore-throat geometry and impacts both permeability and porosity by closing the pore-throats (i.e. coordination number). This microstructure property (i.e. quartz overgrowth) has significant impact on fluid flow. The tortuosity is higher, and it influences the path of the fluid during the transport.

Experimental setups (microfluidic and core-flow with aid of CTs) enables us to visualized the process of building an oil bank from pore scale (i.e. μm) to 1 metre scale. We define the oil bank as a continuous volume of mobilized oil that forms from the coalescence of mobilised oil ganglia. Once developed, the dimensions of the oil bank extend during its movement through a porous medium.

The microfluidic chip mimics 3D Fontainebleau porous media by using geometry features (pores, grains, tubes and throats) of the porous media. For this chip, the same wettability (i.e. water wet) is maintained. It is designed with a path length of one meter. The three phases, i.e. oil, brine and chemicals, can be recognized by false color images. The separation of the phases by image quantification, during the process of building the oil bank, has been successful for the visualization of ganglion oil and continuous developing oil bank formation.

The core-flow system combined with a CTs imaging system visualizes the in-situ conditions of building the oil bank in the porous media of core samples with different lengths. The core samples properties (i.e. permeability and pore volume) have been calculated by using the differential pressure transducers. The phase composition of the effluent has been identified and quantified by using a Coriolis meter and conductivity measurements. A range of sample lengths, from 0.07 m to 1 m, can be accommodated in the setup. In this way we created an advanced experimental platform with various sizes of oil bank build-up through chemical enhanced oil recovery and associated effluent analysis. Porous plate gives an essential advantage and proven to be an effective tool as it gives high initial oil saturation in the range of 0.7 to 0.8. The experimental protocol and high-resolution data-acquisition of the coreflow setup shows that an efficient repetition of experiments with a good reproducibility has been achieved. This is an important requirement when performing complex multi-phase experiments. There are a few experiments with less reproducibility where the matrix heterogeneity influence the fluid flows. The experimental results prove to have a high level of accuracy and resolution due to the design and implementation of high-quality measuring/monitoring devices. The improved instrumentation of the set-up has the ability to control the set-up remotely even with a smart phone.

Following the extensive and detailed experimental programme, a comprehensive set of experimental data for oil bank build-up has been produced for various experimental

scales, lengths and volumes. In addition, the amount and distribution of residual oil left after waterflood and injection of the chemical slug and the salinity and sizes of the chemical slugs, induce the process of building up of oil bank. The results show a positive correlation between sample size and oil-bank characteristics, based on pore volume and matrix homogeneity.

Additionally, building a stable oil bank supports the efficiency of the chemical EOR process where most of the residual oil is mobilized, reconnected and transported in front of chemical flood. Oil is produced mostly with brine. Oil in microemulsion is minimized. This has big advantage to the surface facility in the field, as oil in emulsions usually upsets the facility process. The pseudo-mobility of the oil is higher (i.e. oil production is accelerated) when it is produced as a connected oil bank in comparison with dispersed flow as an emulsion. This has positive impact on the revenue (net present value) of the chemical EOR process.

We also concluded that successful build-up and maintenance of an oil bank requires meeting three stages as follow:

Stage 1 → Oil Mobilization: where the capillary forces holding the oil are reduced and oil moves from its entrapments. Main factor influencing this stage is achieving ultra IFT. 10-3 – 10-2 mN/m is proven to be sufficient to overcome the capillary forces in Fontainebleau sandstone.

Stage 2 → Coalescence of the mobilized oil: at this stage there is a competition between the oil droplets break up, re-trapped again and oil drops collide, coalesce and merge together. The influencing factor is the accessible pore volume where the oil droplets requires sufficient pore volume to coalesce and build an oil bank. Our work in Fontainebleau sandstone recommends a minimum 30 cm core length to have successful coalescence process. Consequence of having short cores (less than 30 cm) would be producing the oil in dispersed flow or a small oil bank, while most of the production in microemulsion phase. Another factor impacting the coalescence is the amount of residual oil left after waterflooding. For Fontainebleau porous media descried properties, it requires minimum 0.3 Sor to have coalescence and form an oil bank for surfactant polymer flood.

Stage 3 → Maintenance and transport of a stable oil bank: this is a crucial stage that often is ignored. Once the oil bank formed (i.e. coalescence wins the competition over break up and re-trapement) it transported in the porous media. Mainly two factors influence this process; the porous media heterogeneity and bulk viscosity of the microemulsions, where it

leads to unfavorable mobility control and hence the surfactant fingers through the microemulsion phase and break up the oil bank or the oil bank goes through some high-permeablity streaks and bypasses some oil. For those circumstances we demonstrated the value of introducing the polymers in the surfactant EOR process to achieve favorable mobility conditions. Without the polymer, the low IFT front is not stable and the surfactant slug will finger because the water relative permeability increases as the IFT and residual oil saturation decreases. The polymer drive reduces the phase trapping which helps to minimize surfactant retention. Hydrolysed polyacrylamide, HPAM, is a good candidate at low salinities, but not recommended at high salinities. It is water-soluble and has the capability to give high viscosity at low concentration.

List of Figures

List of tables

Nomenclature:

CT	Computerized axial tomography
PV	Pore Volume
EOR	Enhanced Oil Recovery
MICP	Mercury Injection Capillary Pressure
SEM	Scanning Electron Microscope
2D	2-Dimensional
3D	3-Dimensional
Peek	PolyEtherEtherKerone
NaCl	Sodium Chloride
KI	Potassium Iodide
REV	Representative Elementary Volume
SP	Surfactant Polymer
CO_2	Carbon Dioxide
NMR	Nuclear Magnetic Resonance
X-Ray	Electromagnetic Radiation

About the author

Faisal Al Saadi was born on September 8, 1979 in Rustaq, Sultanate of Oman. He is holding Bsc in Control Engineering from Sheffield university in England and Msc in Petroleum Engineering from Herriot-Watt university in Scotland. In 2015, he started his Phd in Delft university of technology in collaboration with Shell Global Solutions International.

Faisal worked in Petroleum Development of Oman (PDO) as a Reservoir Engineer for more than 10 years in different teams , study team, Development Planning team and Well and reservoir management team. After that, he worked as Polymer project manager leading the execution of the polymer in Marmul field south of Oman. Currently, Faisal is the development planning team leader in the largest cluster in the south of Oman.

Faisal is married and has five children. His hobbies are reading, travelling and (still) playing football!!

List of Publications

1- Phd Related Publications:

Peer-reviewed journal papers:

Characterization of Fontainebleau Sandstone: Quartz Overgrowth and its Impact on Pore-Throat Framework.
Al Saadi F, Wolf KH and Kruijsdijk C.V. (2017), J Pet Environ Biotechnol 7: 328. doi: 10.4172/2157-7463.1000328

Developments in Coreflow and Microfluidic Experimental Setups for Oil Mobilization in Porous Media.
F. AL Saadi, M. Slob, K-H. Wolf, and C. Van Kruijsdijk, submitted to the journal "Review of scientific instruments", under review.

Conditions for building up an oil bank during surfactant polymer flooding
Faisal AL Saadi, Himanshu Sharma, Kishore K. Mohanty, Karl-Heinz Wolf, Cor Van Kruijsdijk, to be submitted to SPE Journal.

Conference proceedings:

A Revised Workflow for Spatial and Petrophysical Rock Characterization: The Fontainebleau Case Study *Faisal Al Saadi (Shell Global Solutions International B.V./TU Delft), Karl-Heinz Wolf (TU Delft), Cor van Kruijsdijk (Shell Global Solutions International B.V./ TU Delft), Nederlands Aardwetenschappelijk Congres, 7 – 8 th April 2016, Eindhoven, Netherlands*

Comparison of the Petrography and Petrophysical Parameters of Fontainebleau Sandstone: Measurements and Literature *Faisal Al Saadi (Shell/TU Delft), Karl-Heinz Wolf (TU Delft), Cor van Kruijsdijk (Shell/ TU Delft), 78th EAGE Conference & Exhibition 2016, Vienna, Austria, 30 May – 2 June 2016*

Dielectric properties of Natural porous media, *Faisal AL Saadi (Shell Global Solutions International B.V./TU Delft), Karl-Heinz Wolf (TU Delft), 9th International Conference on Porous Media & Annual Meeting, Rotterdam 2017, Submission 545*

Fontainebleau Porous Media: Visualization of Oil Bank in MicroModels
Faisal Al Saadi (Shell Global Solutions International B.V./TU Delft), Martijn Hurksman (TU Delft), Karl-Heinz Wolf (TU Delft), Cor van Kruijsdijk (Shell Global Solutions International B.V./ TU Delft), 9th International Conference on Porous Media & Annual Meeting, Rotterdam 2017, Submission 545

Characterization of Enhanced Oil Bank Build Up through Relative Permeability Analysis
F. Al Saadi, M. Wijsman, K. Wolf, C. Van Kruijsdijk, 80th EAGE Conference & Exhibition 2018, Copenhagen, Denmark, 11 - 14 June 2018.

2- Work Related Publications:

Polymer Flooding in a Large Field in South Oman - Initial Results and Future Plans (Document ID SPE-154665-PP)
Faisal Saadi, Badr Amri, Sami Nofli, John Van Wunnik, Henri Jaspers, Said Harthi, Khalfan Shuaili, Pradeep Cherukupalli, Chakravathi Ravula
SPE EOR Conference at Oil and Gas West Asia, scheduled 16-18 April 2012 in Muscat, Oman.

Recovery Factor Estimation in EOR polymerflood project: Field case (Document ID SPE-169694-MS)
F.S. Al-Saadi (Petroleum Development Oman) | H.A. Al-Subhi (Petroleum Development Oman) | H. Al-Siyabi (Petroleum Development Oman)
SPE EOR Conference at Oil and Gas West Asia, 31 March-2 April 2014, Muscat, Oman

Fracture Growth Monitoring in Polymer Injectors - Field Examples (Document ID 160967-MS)
Al-shuaili, Khalfan H., Cherukupalli, Pradeep Kumar, Saadi, Faisal, Al-hashmi, Khalid Hamad, Jaspers, Henri F., Sen, Subrata, SPE Conference Paper - 2012

Planning for Increased Production Through Integrated Well and Reservoir Surveillance in the Oman EOR Developments. (Document ID 144164-MS)
Marcel Zwaan, Rob Hartmans, Jasmeet Saluja, Stan Schoofs, Guillermo Rocco, Rashid Adawi, Faisal Saadi, Jorge Lopez, Joel Ita, Hassan Mahani, Yuan Qiu, Johannes Rehling, SPE Enhanced Oil Recovery Conference, 19-21 July 2011, Kuala Lumpur, Malaysia

Integrated Well and Reservoir Surveillance in the PDO EOR projects. (Document ID 141649-MS)
Marcel Zwaan, Rob Hartmans, Jasmeet Saluja, Stan Schoofs, Guillermo Rocco, Faisal Saadi, Jorge Lopez, Joel Ita, Tibi Sorop, SPE Middle East Oil and Gas Show and Conference, 25-28 September 2011, Manama, Bahrain

Developing a Layered Heterogeneous Precambrian Reservoir by Polymer Flooding (Document ID SPE-154465-PP)
Robbert A Nieuwenhuijs, Ryan Ross, Gary Lanier, Abdulaziz Belushi, Faisal Saadi, Sami Nofli, Vipin Gupta, John Van Wunnik, SPE EOR Conference at Oil and Gas West Asia, scheduled 16-18 April 2012 in Muscat, Oman.

Application of Injection Fall-Off Analysis in Polymer flooding
P. J. van den Hoek, H. Mahani, T. G. Sorop, A. D. Brooks, M. Zwaan, S. Sen, K. Shuaili, F. Saadi
74th EAGE Conference & Exhibition incorporating SPE EUROPEC 4 – 7 June 2012 in Copenhagen, Denmark

An Integrated Approach to Efficiently Unlock the Resource Potential in a Large Cluster of Fields
Faisal Saadi, Martin A. Kraaijveld, Jon B Hognestad, Ajay Samantray, Pius Udeh, Waleed Bulushi, Andres E. Cerutti, Madelon P.Y. Nijman, Zaher Al Kindy, Ayman Ibrahim, Norbert Janusz (Petroleum Development Oman, Regional RE-PP Conference Muscat, 12-16 May 2007

Active WF (Pattern) Management Through Modern Online Production Data Base Systems Using Classical Techniques : A Case Study On Heavy Oil Fields In South Oman. (Document ID 13569-MS)
Vipin Gupta,Faisal Saad ; Abdul Aziz Belushi, Petroleum development of Oman, International Petroleum Technology Conference, 7-9 December 2009, Doha, Qatar.

AKNOWLEDGEMENTS

At the end of this Thesis, I would like to express my gratitude to people and institutions have largely contributed to my project with their help, support and guidance.

First of all, I would like to thank my promotors Prof Cor van kruijsdijk who provided to me unlimited support, large degree of freedom and empowered me to conduct the research. Dr Karl-Heinz Wolf for his time, discussions, guidance and full access and support in the laboratory of Geoscience and Engineering.

I also gratefully acknowledge MDC members of Petroleum Development Oman, Dr Ali Ghaithi, Dr Suleiman Tobi, Dr Badr Kharusi, Khamis Saadi, Dr Sultan Shidani for their support and yearly review of my project. Nasser Azri, Hamed Subhi, Junaid Ghulam and Hisham Syiabi for giving me the opportunity to work on EOR research. I also Acknowledge Shell Global Solutions for their unlimited support, Dr Boresma, Roelien Bross, Dr van Wunnik, Dr van Batenburg and colleagues in Shell EOR team in Amsterdam for their support and discussions. I am also grateful to committee members of this thesis Dr.ir. D.W. van Batenburg, Prof.dr.ir. T.J. Heimovaara, Prof.dr. C.J. Spiers, Prof.dr.ir. H.E.J.G. Schlangen, Prof.Dr. K.K. Mohanty, Prof.dr. W.R. Rossen, thank you for all your efforts and feedback.

The experimental work of this research would not have been possible without support of technicians at the laboratory of TU Delft. I would like to thank Micheil Slob for his support in the development of the experimental setups and his assistance with the experiments. Mark Friebel, Karl Heller, Jolanda van Haagen and Paul for their efforts, knowledges and helps. Ellen Meijvogel-de Koning, Wim Verwaal and Joost van Meel for their help and support during CT scanning and processing of the images. Dirk Delforterie and Jens van den Berg for their unlimted support with rocks and samples. Cutting 1 meter sample was not an easy exercise, attaching 30 meter samples was also a challenge, thank you Laboratory team, we made it!! A special thank to the staff of Geoscience and Engineering team; Anke, Hannie, Ralf, Marlijn, Lydia, Margot, Claudia and Marja. Also, I would like to thanks my friends and fellow PhD's Nikita Lenchenkov, Anna Peksa, Mohammed Chahardowli, Bander ALQuaimi, Seyed Mojtaba Hosseini Nasab, Negar Khoshnevis, Narjes Shojaei Kaved, Siavash Kahrobaei, Jaikun Gong, Matteo Cusini, Ahmed Hussain, Swej Shah, Sin Jones and rest of colleagues. I would like also to thank my Omani friends in Netherlands; Khalid Jahwari, Hamed Mahrouqi, Hamood Alawi, Qahtan Yarubi, Ali Nasri, Khalid Ghilani, Salim Rahbi, Ali

Alawi, Yahya Amri, Abdulraheem Huqani, Mosa Jahdhami, Abdulaziz Shahri, I truly enjoyed your company.

During my PhD, I had a great opportunity to work as visiting researcher in UT Austin in USA. I would like to thank Prof Mohanty for hosting me as well as for the many fruitful discussions we had together and his support during my stay in USA. Also I would like to thank Dr Sharma for his daily supervision and support in conducting some experiments in the lab in UT Austin.

I would like also to thank Bsc and Msc students that I supervised during my PhD; Bsc students Jan Bot, Rachid Arbib, Hamza Tatar, Zakaria Aab and Mohammed Sealiti. Msc students Athanasios Tzanavaris, Martijn Hurkmans, Maxim Wijsman and Mohamed Sealiti. Thank you for hard working and excellent results.

Last but not least, thanks to all those close to my hears, my family, without your love, encouragements, support and understanding, this research would not have finished.

Appendix 1:

Core			Oil Saturation			
No	Length	Experiment No	Initial	after WF	after Oil Bank	Residual
Core 1	100 cm	1st Experiment	0.7	0.49	0.18	0.06
		Repeated Experiment (Duplo)	0.71	0.48	0.19	0.07
		Repeated Experiment (Triplo)	0.69	0.47	0.16	0.05
Core 2	100 cm	1st Experiment	0.78	0.48	0.17	0.05
		Repeated Experiment (Duplo)	0.78	0.45	0.18	0.07
		Repeated Experiment (Triplo)	0.76	0.45	0.18	0.06
Core 3	100 cm	1st Experiment	0.73	0.42	0.15	0.1
		Repeated Experiment (Duplo)	0.7	0.38	0.11	0.12
		Repeated Experiment (Triplo)	0.71	0.36	0.17	0.09
Core 4	100 cm (CT Scanned)	1st Experiment	0.75	0.54	0.27	0.08
		Repeated Experiment (Duplo)	0.75	0.52	0.25	0.1
		Repeated Experiment (Triplo)	0.73	0.5	0.23	0.11
Core 5	60 cm	1st Experiment	0.78	0.47	0.2	0.15
		Repeated Experiment (Duplo)	0.75	0.44	0.24	0.13
		Repeated Experiment (Triplo)	0.76	0.42	0.22	0.16
Core 6	60 cm	1st Experiment	0.78	0.47	0.2	0.15
		Repeated Experiment (Duplo)	0.75	0.45	0.188	0.14
		Repeated Experiment (Triplo)	0.74	0.43	0.22	0.16
Core 7	60 cm (CT Scanned)	1st Experiment	0.87	0.57	0.32	0.1
		Repeated Experiment (Duplo)	0.88	0.54	0.35	0.12
		Repeated Experiment (Triplo)	0.85	0.55	0.35	0.13
Core 8	60 cm	1st Experiment	0.66	0.5	0.27	0.09
		Repeated Experiment (Duplo)	0.66	0.47	0.32	0.1
		Repeated Experiment (Triplo)	0.64	0.47	0.27	0.11
Core 9	39 cm (CT Scanned)	1st Experiment	0.75	0.58	0.38	0.16
		Repeated Experiment (Duplo)	0.72	0.55	0.35	0.18
		Repeated Experiment (Triplo)	0.71	0.56	0.36	0.15
Core 10	39 cm	1st Experiment	0.8	0.51	0.32	0.15
		Repeated Experiment (Duplo)	0.78	0.5	0.29	0.16

		Repeated Experiment (Triplo)	0.75	0.5	0.34	0.18
Core 11	39 cm	1st Experiment	0.78	0.42	0.24	0.14
		Repeated Experiment (Duplo)	0.79	0.39	0.21	0.12
		Repeated Experiment (Triplo)	0.76	0.38	0.24	0.13
Core 12	39 cm	1st Experiment	0.66	0.5	0.32	0.19
		Repeated Experiment (Duplo)	0.65	0.47	0.35	0.17
		Repeated Experiment (Triplo)	0.64	0.47	0.28	0.15
Core 13	30 cm	1st Experiment	0.74	0.46	0.29	0.17
		Repeated Experiment (Duplo)	0.71	0.44	0.27	0.19
		Repeated Experiment (Triplo)	0.71	0.43	0.26	0.16
Core 14	30 cm	1st Experiment	0.78	0.52	0.35	0.2
		Repeated Experiment (Duplo)	0.77	0.49	0.32	0.17
		Repeated Experiment (Triplo)	0.75	0.47	0.34	0.18
Core 15	30 cm (CT Scanned)	1st Experiment	0.78	0.5	0.28	0.22
		Repeated Experiment (Duplo)	0.78	0.48	0.33	0.19
		Repeated Experiment (Triplo)	0.76	0.48	0.33	0.18
Core 16	30 cm	1st Experiment	0.75	0.43	0.27	0.1
		Repeated Experiment (Duplo)	0.74	0.4	0.24	0.11
		Repeated Experiment (Triplo)	0.72	0.39	0.31	0.09
Core 17	17 cm	1st Experiment	0.69	0.37	0.22	0.1
		Repeated Experiment (Duplo)	0.69	0.34	0.19	0.12
		Repeated Experiment (Triplo)	0.67	0.35	0.2	0.11
Core 18	17 cm	1st Experiment	0.7	0.48	0.33	0.12
		Repeated Experiment (Duplo)	0.67	0.46	0.37	0.09
		Repeated Experiment (Triplo)	0.65	0.46	0.32	0.1
Core 19	17 cm (CT Scanned)	1st Experiment	0.73	0.41	0.27	0.17
		Repeated Experiment (Duplo)	0.73	0.38	0.24	0.15
		Repeated Experiment (Triplo)	0.7	0.39	0.31	0.16
Core 20	17 cm	1st Experiment	0.72	0.41	0.28	0.18
		Repeated Experiment (Duplo)	0.7	0.38	0.31	0.16
		Repeated Experiment (Triplo)	0.69	0.37	0.3	0.15
Core 21	17 cm	1st Experiment	0.7	0.44	0.33	0.25
		Repeated Experiment (Duplo)	0.69	0.45	0.34	0.23
		Repeated Experiment (Triplo)	0.69	0.43	0.32	0.22

Core 22	17 cm	1st Experiment	0.67	0.37	0.29	0.13
		Repeated Experiment (Duplo)	0.67	0.35	0.27	0.12
		Repeated Experiment (Triplo)	0.66	0.35	0.27	0.15
Core 23	7 cm	1st Experiment	0.7	0.33	0.26	0.08
		Repeated Experiment (Duplo)	0.67	0.3	0.29	0.06
		Repeated Experiment (Triplo)	0.67	0.31	0.3	0.05
Core 24	7 cm	1st Experiment	0.7	0.34	0.29	0.07
		Repeated Experiment (Duplo)	0.7	0.32	0.27	0.09
		Repeated Experiment (Triplo)	0.69	0.32	0.32	0.1
Core 25	7 cm	1st Experiment	0.66	0.37	0.33	0.17
		Repeated Experiment (Duplo)	0.65	0.34	0.36	0.15
		Repeated Experiment (Triplo)	0.65	0.35	0.3	0.2
Core 26	7 cm	1st Experiment	0.78	0.27		0.1
		Repeated Experiment (Duplo)	0.77	0.24		0.11
		Repeated Experiment (Triplo)	0.75	0.23		0.13
Core 27	17 cm Assessment of reproducibility and Homogeneity Chemical Slug size 0.3 PV	1st Experiment	0.70	0.49		0.12
		Repeated Experiment (Duplo)	0.71	0.48		0.11
		Repeated Experiment (Triplo)	0.70	0.47		0.13
	17 cm Assessment of reproducibility and Homogeneity Chemical Slug size 0.5 PV	1st Experiment	0.78	0.50		0.12
		Repeated Experiment (Duplo)	0.77	0.47		0.13
		Repeated Experiment (Triplo)	0.76	0.47		0.1
Core 28	17 cm Assessment of reproducibility and heterogeneity Chemical Slug size 0.3 PV	1st Experiment	0.73	0.41		0.2
		Repeated Experiment (Duplo)	0.66	0.50		0.16
		Repeated Experiment (Triplo)	0.60	0.37		0.23
	17 cm Assessment of reproducibility and heterogeneity Chemical Slug size 0.5 PV	1st Experiment	0.78	0.47		0.15
		Repeated Experiment (Duplo)	0.70	0.50		0.10
		Repeated Experiment (Triplo)	0.66	0.39		0.14

Appendix 2:

This appendix chapter describes the steps taking in stacking two 30cm cores into a composite 60cm one. There are several factors to be considered to ensure the transition from one core to the other is as continuous as possible. First consideration is minimising capillary forces at the boundary between the two cores. In this project this issue was tackled by filling the space between the two cores with a piece of one of the cores. The piece was ground up and the resulting sand was filtered down to the dominant grain size of the cores, a grain size determined in (Al Saadi et al, 2017).

Another issue is that cores had to be aligned adequately enough to minimise distortion of the flow path and to ensure that the composite core would fit in a core holder. This challenge was tackled by placing a 10cm long aluminium tube around the boundary between the two cores. The tube's inner diameter must match the outer diameter of the cores, as is depicted in Figure App1. To keep the stacked cores aligned in the Perspex tube when they are cast in glue, a support made of dried glue is placed around the aluminium tube. Small supporting blocks made of dried glue are stuck to the aluminium tube to support it against the Perspex tube.

Figure App1: Core to be stacked with guiding aluminium tube.

In summary the stacking of two cores is done by taking the following steps

- Cut the cores to 1cm bigger the required size and save a piece of about 2cm from one of the two cores.
- Apply the thin layer of glue onto both cores.
- Cut the excess 1cm of both cores to expose the sides that'll be connected.
- On the side of the exposed core ends, mill the outer diameter of both cores down to a diameter of 4.1cm over a length of 5cm.

- Crush the saved 2cm and sieve the resulting sand to the dominant grain size.
- Glue on the aluminium tube support blocks that are big enough to occupy the void between the aluminium tube and the Perspex tube and insert one core into the aluminium tube.
- Pour the sieved sand into the aluminium tube and onto the core end. Make sure that the sand is distributed evenly over the entire core end.
- Insert the second core into the aluminium tube and press and hold them closely together.
- Cast the whole in glue via the conventional core casting procedure while making sure that the cores remain as close together as possible, by placing a weight on top of the composite core for example.

Figure App2: Stacked cores before being cast in glue